

CRANFIELD UNIVERSITY

Gang Zhao

Individual Research Project Report

School of Applied Science
Advanced Bearing System for Ultra Precision Plastic Electronics
Production Systems

Academic Year: 2013 - 2014

Supervisor: Paul Shore & Paul Morantz
September 2014

CRANFIELD UNIVERSITY

School of Applied Science

Advanced Bearing System for Ultra Precision Plastic Electronics
Production Systems

Academic Year 2013 - 2014

Gang Zhao

Individual Research Project Report

Supervisor: Paul Shore & Paul Morantz
September 2014

© Cranfield University 2014. All rights reserved. No part of this publication may be reproduced without the written permission of the copyright owner.

ABSTRACT

The aims of this MSc research project are to investigate the application of aluminium for the main components of an ultra-precision spindle defined for use in R2R production systems and to produce a reel to reel rotary aluminium hydrostatic bearing system of high accuracy to meet the demand of manufacturing the flexible displays with an effective production capability for this special kind of film-based product.

The original concept design was already finished to manufacture the bearing components and the objective of this project was to test the functionality of this new hydrostatic bearing system. Firstly, theoretical were performed to work out the output responses, including temperature rise, flow rate, load capacity etc., of the hydrostatic bearing system under different input design parameters, including supply pressure, fluid viscosity, the rotational speed etc. Then ANSYS software was used to build a FEA model to simulate the actual working conditions of the hydrostatic bearing system and to obtain the theoretical output parameters, especially the deflection conditions of the bearing shaft. Finally the experimental validation tests were conducted to verify the actual output responses to check correlation with the modelled results.

Keywords: R2R production systems, hydrostatic bearing systems, input parameters, output responses, FEA modelling, deflection conditions of the bearing shaft.

ACKNOWLEDGEMENTS

Many sincere thanks to the valuable mentorship from my two supervisors, Professor Paul Shore and Mr Paul Morantz as well as the instructions from the Subject adviser, Dr Xavier Tonnellier.

Many thanks to the help and assistance from Mr Rodger Read, Mr Keith Carlisle, Mr Renaud Jourdain, and all the technicians in the Ultra-precision laboratory, Mr Alan Heaume, Mr Adam Kerr, Mr Kevin Howard and Mr John Hedge.

TABLE OF CONTENTS

ABSTRACT	i
ACKNOWLEDGEMENTS.....	iii
LIST OF FIGURES.....	vii
LIST OF TABLES	xii
LIST OF EQUATIONS.....	xvi
LIST OF ABBREVIATIONS.....	xviii
1 INTRODUCTION.....	1
1.1 BACKGROUND	1
1.1.1 INTRODUCTION TO PLASTIC ELECTRONICS PRODUCTION SYSTEMS.....	1
1.1.2 THE CHARACTERISTICS OF THE HYDROSTATIC BEARINGS	1
1.1.3 THE APPLICATIONS OF THE HYDROSTATIC BEARINGS.....	1
1.2 THE PROJECT PLAN.....	1
1.3 GANTT CHART OF THE IRP PLAN.....	1
1.4 AIMS AND OBJECTIVES	3
2 LITERATURE REVIEW.....	5
2.1 ASSUMPTIONS.....	5
2.2 REVIEW OF THE THEORETICAL DESIGN APPLIED TO ULTRA- PRECISION SPINDLE.....	9
3 DESIGN OF SPINDLE SYSTEM.....	25
3.1 THE INITIAL DESIGN OF THE SYSTEM.....	25
3.2 THE COMPARISON ANALYSIS BETWEEN THE MATERIALS OF STEEL AND ALUMINIUM.....	28
3.2.1 THE MATERIAL PROPERTIES COMPARISON.....	30
3.2.2 THE COST ANALYSIS.....	33
4 THEORETICAL CALCULATION OF HYDROSTATIC BEARINGS	37
4.1 CALCULATION FOR THE JOURNAL BEARING	37
4.2 CALCULATION FOR THE THRUST BEARING	42
5 FEA OF BEARING COMPONENTS.....	46
5.1 MODELLING OF THE BEARING SHAFT AND THRUST PLATES	47
5.2 THE FEA DEFORMATION ANALYSIS FOR THE HYDROSTATIC BEARING SYSTEM.....	53
6 EXPERIMENTAL PROCEDURES	69
6.1 THE EXPERIMENTAL INPUT PARAMETERS SELECTIONS BASED ON THE THEORETICAL CALCULATIONS AND FINITE ELEMENT ANALYSIS	69
6.1.1 THE OIL TYPE.....	69
6.1.2 THE SUPPLY PRESSURE	69
6.1.3 THE BEARING CLEARANCE	70
6.1.4 THE EXPERIMENTAL INPUT PARAMETERS COMBINATION.....	72

6.1.5 THE POWER CONSUMPTION CONDITION UNDER THE RECOMMENDED COMBINATION	73
6.1.6 THE REYNOLDS NUMBER CONDITION UNDER THE RECOMMENDED INPUT COMBINATION	74
6.2 THE MEASUREMENT AND MACHINING PROCESS OF THE HYDROSTATIC BEARINGS.....	76
6.2.1 THE MEASUREMENT OF THE BEARING COMPONENTS.....	76
6.2.2 THE DIMENSIONS OF THE EXPERIMENTAL COMPONENTS.....	82
6.2.3 THE MACHINING PROCESS OF THE BEARING COMPONENTS	84
6.3 THE PARAMETERS MEASUREMENT AND THE TEST EQUIPMENT .	86
6.3.1 THE INPUT PARAMETERS AND THE EQUIPMENT.....	86
6.3.2 THE OUTPUT RESPONSES	93
6.4 ALUMINIUM HYDROSTATIC BEARING PERFORMANCE	103
6.4.1 THE ASSEMBLING AND DISASSEMBLING PROCESS.....	103
6.4.2 THE EXPERIMENT PROCESS	110
6.4.3 THE EXPERIMENT RESULTS	114
7 RESULTS AND DISCUSSION	139
8 CONCLUSIONS AND FURTHER WORKS.....	143
APPENDICES	145
Appendix A THE CODES FOR AUTOMATIC CALCULATION EXCEL SPREADSHEET	145
Appendix B THE TABLES OF MATERIALS TO BE TURNED BY DIAMOND.....	149
Appendix C THE SPECIFICATIONS FOR SJ100 INVERTER.....	151
Appendix D THE SPECIFICATIONS FOR ABB M2AA 090 L-4 MOTOR....	153
Appendix E THE SPECIFICATIONS FOR MILLIMAR 1200 IC COMPACT AMPLIFIER.....	154
Appendix F THE SPECIFICATIONS FOR NI 9217 RTD ANALOG INPUT C SERIES MODULE.....	155
Appendix G THE SPECIFICATIONS FOR HAAKE PHOENIX II SYSTEMS.	155
Appendix H THE SPECIFICATIONS FOR LEMO FGG.00 TEMPERATURE MEASURING CONNECTOR.....	158
Appendix I THE SPECIFICATIONS FOR TAYLOR-HOBSON FORM TALYSURF-120L.....	159

LIST OF FIGURES

Figure 1 Gantt chart of the IRP plan by Gang Zhao	1
Figure 2 The parameter input and output window of the calculations of hydrostatic journal bearings in the Excel spreadsheet.....	13
Figure 3 The interrelationships between the input and output parameters of the Excel spreadsheet.....	15
Figure 4 The relationship between the supply pressure and the temperature change for a specific kind of hydrostatic bearing	16
Figure 5 The relationship between the supply pressure and the flow for a specific kind of hydrostatic bearing.....	17
Figure 6 The relationship between the radial clearance and the temperature change for a specific kind of hydrostatic bearing	18
Figure 7 The relationship between the radial clearance and the radial stiffness for a specific kind of hydrostatic bearing.....	18
Figure 8 The relationship between the radial clearance and the flow for a specific kind of hydrostatic bearing.....	19
Figure 9 The relationship between the viscosity of the fluid and the temperature change for a specific kind of hydrostatic bearing	20
Figure 10 The relationship between the viscosity of the fluid and the flow for a specific kind of hydrostatic bearing.....	21
Figure 11 The relationship between the rotational speed and the temperature change for a specific kind of hydrostatic bearing	22
Figure 12 The initial design of the shaft of the hydrostatic bearing system for the ultra-precision plastic electronics production systems (Separated)	47
Figure 13 The initial design of the shaft of the hydrostatic bearing system for the ultra-precision plastic electronics production systems (Bolted together) ...	48
Figure 14 0.001m element size meshing.....	49
Figure 15 0.01m element size meshing.....	49
Figure 16 The FEA results with element size of 0.01m	50
Figure 17 0.005m element size meshing.....	50
Figure 18 The FEA results with element size of 0.005m	51
Figure 19 The fixed support face of the bearing spindle.....	52
Figure 20 The journal bearing area under the pressure of 3MPa.....	54

Figure 21 The total deformation of the journal bearing under the pressure of 3MPa	55
Figure 22 The thrust bearing area under the pocket area pressure of 2MPa and the average land area pressure of 1MPa.....	56
Figure 23 The total deformation of the thrust bearing under the pocket area pressure of 2MPa and the average land area pressure of 1MPa	57
Figure 24 The overall pressure condition for the combination of journal bearing pressure 3MPa, thrust plate pocket area pressure 2MPa, and the thrust plate land area pressure 1MPa.....	58
Figure 25 The total deformation for the combination of journal bearing pressure 3MPa, thrust plate pocket area pressure 2MPa, and the thrust plate land area pressure 1MPa	59
Figure 26 The overall pressure condition for the combination of journal bearing pressure 1.5MPa, thrust plate pocket area pressure 0.3MPa, and the thrust plate land area pressure 0.15MPa.....	60
Figure 27 The total deformation for the combination of journal bearing pressure 1.5MPa, thrust plate pocket area pressure 0.3MPa, and the thrust plate land area pressure 0.15MPa	61
Figure 28 Three deformation analysis points.....	62
Figure 29 The pressure condition for Set 1 analysis	63
Figure 30 The deformation solution for Set 1 analysis	64
Figure 31 The bearing shaft after being coated and before the second diamond turning process	77
Figure 32 The thrust plate after being coated and before the second diamond turning process	77
Figure 33 The bearing house after being coated and before the second diamond turning process	78
Figure 34 TESA IMICRO with analogue indication 90-100.....	78
Figure 35 The Moore & Wright depth gauge micrometer	79
Figure 36 The Moore & Wright outside micrometer.....	79
Figure 37 The Mitutoyo caliper digital absolute IP67	80
Figure 38 Leitz PMM-F 1000 CMM	80
Figure 39 The bearing house is being measured by the Leitz CMM	81
Figure 40 The important dimensions of the experimental components	83

Figure 41 The CUPE nanocentre in the EPSRC Centre at Cranfield University	85
Figure 42 The re-machined bearing house after the coating process	85
Figure 43 The experimental inverter.....	86
Figure 44 HITACHI SJ100 Series Inverter	87
Figure 45 The ABB M2AA 090 L-4 motor	87
Figure 46 The pressure gauge for pressure from 10MPa to 69MPa	88
Figure 47 Pressure gauge to measure the pocket pressure.....	89
Figure 48 Hole on the bearing housing to insert the pressure gauge	89
Figure 49 Dial Reading Viscometer.....	90
Figure 50 The physical and chemical properties of Kristol M10	92
Figure 51 NI 9217 RTD Analog input C Series module	94
Figure 52 LEMO FGG.00 temperature measuring connector and sensor	95
Figure 53 The positions of the four temperature sensors	95
Figure 54 Temperature sensor Tai0 to measure one oil outflow pipe.....	96
Figure 55 Temperature sensor Tai1 and Tai2 to measure the oil flowing out from the pump	96
Figure 56 Temperature Tai3 to measure one oil outflow pipe	96
Figure 57 HAAKE Phoenix II systems	97
Figure 58 The connection of the HAAKE Phoenix II systems.....	97
Figure 59 The workbench for the R2R hydrostatic bearing system	98
Figure 60 The edge of measuring the x displacement.....	100
Figure 61 Mahr Millimar 1200 IC Compact Amplifier	100
Figure 62 The probe of the Millimar 1200 IC Amplifier	101
Figure 63 The clean view of the journal bearing restrictor	103
Figure 64 The clean view of the thrust bearing restrictor.....	103
Figure 65 The burs on the top of an unclean thrust bearing restrictor tube	104
Figure 66 Testing before the bearing shaft being put on	104
Figure 67 The bearing spindle being put into the housing.....	105
Figure 68 The bearing thrust plate being bolted on the bearing spindle.....	105

Figure 69 The debris inside the bearing housing.....	106
Figure 70 The microscope image of the coating debris inside the bearing housing.....	107
Figure 71 The delamination and scratches condition on the surface of the thrust plate.....	108
Figure 72 Taylor-Hobson Form Talysurf-120L.....	109
Figure 73 The surface roughness of the surface of the thrust bearing pad	109
Figure 74 The depth of the scratches on the thrust bearing pad	110
Figure 75 Seven pocket pressure measuring screws.....	115
Figure 76 The pipes and connections for the hydraulic system.....	116
Figure 77 The schematic diagram of the oil supply system.....	116
Figure 78 The start rotating force of the bearing spindle under uneven journal bearing pocket pressures	117
Figure 79 The start rotating force of the bearing spindle under even journal bearing pocket pressures	119
Figure 80 The container used to measure the flow rate	121
Figure 81 Lying down the bearing housing to measure the axial stiffness	122
Figure 82 The sensor of the clock fixed on the top face of the bearing housing	123
Figure 83 The schematic diagram of the axial stiffness testing system.....	123
Figure 84 The figure of axial stiffness test 1 of the bearing system ($P_{journal1}=9bar$, $P_{journal2}=17bar$, $P_{journal3}=13bar$, $P_{journal4}=18bar$, $P_{journal5}=12bar$, $P_{thrustfront}=5bar$, $P_{thrustrear}=5bar$)	124
Figure 85 The experimental tools used to measure the radial stiffness.....	126
Figure 86 The schematic diagram of the radial stiffness testing system	127
Figure 87 The weights used to load the system	127
Figure 88 Stack same weights on both sides of the rod at the same time.....	128
Figure 89 The figure of radial stiffness test 1.....	130
Figure 90 The temperature rise condition under stationary pumping condition and lower pocket pressure.....	134
Figure 91 The temperature rise condition under stationary pumping condition and higher pocket pressure	136

Figure C-1 The specifications for HITACHI SJ100 inverter	151
Figure D-1 The specifications for the ABB M2AA 090 L-4 motor.....	153
Figure E-1 The specifications for Millimar 1200 IC compact amplifier	154
Figure G-1 Specifications for HAAKE Phoenix II systems	157

LIST OF TABLES

Table 1 Abbreviations for journal bearings	xviii
Table 2 Abbreviations for thrust bearings	xix
Table 3 Formulas for journal bearings calculations (Stansfield, 1970, Page 123-163)	10
Table 4 Formulas for thrust bearings calculations (Stansfield, 1970, Page 164-191)	11
Table 5 Reasons for choosing the four specific parameters as the input parameters	14
Table 6 The relationship between the supply pressure and some output parameters	16
Table 7 The relationship between the radial clearance and some output parameters	17
Table 8 The relationship between the viscosity of the fluid and some output parameters	19
Table 9 The relationship between the rotational speed and some output parameters	21
Table 10 The relationship within the parameters of the hydrostatic bearings ...	22
Table 11 The material property analysis of steel and aluminium.....	30
Table 12 The cost analysis of materials of steel and aluminium.....	33
Table 13 The initial theoretical calculation of the journal bearing of the R2R hydrostatic bearing system ($h_{L(av)}=20\mu\text{m}$, $p=1.5\text{MPa}$, $N=0\text{rpm}$, $\eta=10.00\text{cSt}$)	37
Table 14 The theoretical relationship between the rotational speed and the temperature rise for the journal bearing of the R2R hydrostatic bearing system ($h_{L(av)}=20\mu\text{m}$, $p=1.5\text{MPa}$, $\eta=10.00\text{cSt}$).....	38
Table 15 The appropriate combinations of the parameters to meet the demand of the journal bearing system ($h_{L(av)}=20\mu\text{m}$, $N=300\text{rpm}$, temperature rise $<3^{\circ}\text{C}$)	40
Table 16 The theoretical relationship between the rotational speed and the temperature rise for the journal bearing of the R2R hydrostatic bearing system ($h_{L(av)}=30\mu\text{m}$, $p=1.5\text{MPa}$, $\eta=10.00\text{cSt}$).....	40
Table 17 The appropriate combinations of the parameters to meet the demand of the journal bearing system ($h_{L(av)}=30\mu\text{m}$, $N=300\text{rpm}$, temperature rise $<3^{\circ}\text{C}$)	40

Table 18 The initial theoretical calculation of the thrust bearings of the R2R hydrostatic bearing system ($h_{L(av)}=20\mu\text{m}$, $p=0.3\text{MPa}$, $N=0\text{rpm}$, $\eta=10.00\text{cSt}$)	42
Table 19 The theoretical relationship between the rotational speed and the temperature rise for the thrust bearings of the R2R hydrostatic bearing system ($h_d=20\mu\text{m}$, $p=0.3\text{MPa}$, $\eta=10.00\text{cSt}$)	43
Table 20 The appropriate combinations of the parameters to meet the demand of the thrust bearing system ($h_d=20\mu\text{m}$, $N=300\text{rpm}$, temperature rise $<3^\circ\text{C}$)	44
Table 21 The theoretical relationship between the rotational speed and the temperature rise for the thrust bearings of the R2R hydrostatic bearing system ($h_d=30\mu\text{m}$, $p=0.3\text{MPa}$, $\eta=10.00\text{cSt}$)	44
Table 22 The appropriate combinations of the parameters to meet the demand of the thrust bearing system ($h_d=30\mu\text{m}$, $N=300\text{rpm}$, temperature rise $<3^\circ\text{C}$)	45
Table 23 The FEA results table for set 1 analysis	63
Table 24 The FEA analysis results	65
Table 25 The comparison between the influences on the temperature rise by increasing bearing clearance at different initial bearing clearance	66
Table 26 The flow rate and temperature rise conditions at low supply pressure and high oil viscosity	68
Table 27 The relationship between the radial clearance, radial stiffness and temperature rise of the journal bearing ($p=3\text{MPa}$, $\eta=10.00\text{cSt}$, $N=300\text{rpm}$)	70
Table 28 The relationship between the thrust bearing clearance, stiffness and temperature rise of the thrust bearing ($p=1\text{MPa}$, $\eta=10.00\text{cSt}$, $N=300\text{rpm}$)	70
Table 29 The theoretical calculation table when the clearance is $25\mu\text{m}$	71
Table 30 One of the suitable experimental input parameters combinations	72
Table 31 The power consumption condition under the recommended combination ($h=25\mu\text{m}$, $N=300\text{rpm}$, $\eta=10\text{cSt}$, $P_{\text{journal}}=3\text{MPa}$, $P_{\text{thrust}}=1\text{MPa}$)	73
Table 32 The power consumption condition under the recommended combination ($h=30\mu\text{m}$, $N=300\text{rpm}$, $\eta=10\text{cSt}$, $P_{\text{journal}}=3\text{MPa}$, $P_{\text{thrust}}=1\text{MPa}$)	73
Table 33 The power consumption condition under the recommended combination after ANSYS modelling ($h=25\mu\text{m}$, $h'_{\text{journal}}=27.952\mu\text{m}$, $h'_{\text{thrust}}=28.691\mu\text{m}$, $N=300\text{rpm}$, $\eta=10\text{cSt}$, $P_{\text{journal}}=3\text{MPa}$, $P_{\text{thrust}}=1\text{MPa}$) .	73
Table 34 The power consumption condition under the recommended combination after ANSYS modelling ($h=30\mu\text{m}$, $h'_{\text{journal}}=32.952\mu\text{m}$, $h'_{\text{thrust}}=33.691\mu\text{m}$, $N=300\text{rpm}$, $\eta=10\text{cSt}$, $P_{\text{journal}}=3\text{MPa}$, $P_{\text{thrust}}=1\text{MPa}$)	74

Table 35 The Reynolds number condition under the recommended combination before and after ANSYS modelling ($h=25\mu\text{m}$, $h'_{\text{journal}}=27.952\mu\text{m}$, $h'_{\text{thrust}}=28.691\mu\text{m}$, $N=300\text{rpm}$, $\eta=10\text{cSt}$, $P_{\text{journal}}=3\text{MPa}$, $P_{\text{thrust}}=1\text{MPa}$)	75
Table 36 The Reynolds numbers under the recommended combination before and after ANSYS modelling ($h=30\mu\text{m}$, $h'_{\text{journal}}=32.952\mu\text{m}$, $h'_{\text{thrust}}=33.691\mu\text{m}$, $N=300\text{rpm}$, $\eta=10\text{cSt}$, $P_{\text{journal}}=3\text{MPa}$, $P_{\text{thrust}}=1\text{MPa}$).....	75
Table 37 The dimensions of the experimental components	82
Table 38 Effect of the change of the viscosity of the oil.....	91
Table 39 The products table of different mineral oil products from Millers Oils Ltd.	92
Table 40 The journal bearing parameters under the testing conditions.....	110
Table 41 The thrust bearing parameters under the testing conditions.....	111
Table 42 The journal bearing parameters under the specified testing conditions	112
Table 43 The thrust bearing parameters under the specified testing conditions	113
Table 44 The table of axial stiffness test 1 of the bearing system ($P_{\text{journal1}}=9\text{bar}$, $P_{\text{journal2}}=17\text{bar}$, $P_{\text{journal3}}=13\text{bar}$, $P_{\text{journal4}}=18\text{bar}$, $P_{\text{journal5}}=12\text{bar}$, $P_{\text{thrustfront}}=5\text{bar}$, $P_{\text{thrustrear}}=5\text{bar}$)	124
Table 45 The table of axial stiffness test 2 of the bearing system ($P_{\text{journal1}}=9\text{bar}$, $P_{\text{journal2}}=17\text{bar}$, $P_{\text{journal3}}=13\text{bar}$, $P_{\text{journal4}}=18\text{bar}$, $P_{\text{journal5}}=12\text{bar}$, $P_{\text{thrustfront}}=5\text{bar}$, $P_{\text{thrustrear}}=5\text{bar}$)	125
Table 46 The figure of axial stiffness test 2 of the bearing system ($P_{\text{journal1}}=9\text{bar}$, $P_{\text{journal2}}=17\text{bar}$, $P_{\text{journal3}}=13\text{bar}$, $P_{\text{journal4}}=18\text{bar}$, $P_{\text{journal5}}=12\text{bar}$, $P_{\text{thrustfront}}=5\text{bar}$, $P_{\text{thrustrear}}=5\text{bar}$)	125
Table 47 Front thrust plate displacement measurement	128
Table 48 Rear thrust plate displacement measurement	129
Table 49 Radial stiffness test 1	129
Table 50 Radial stiffness test 2	130
Table 51 The figure of radial stiffness test 2.....	131
Table 52 Radial stiffness test 3	131
Table 53 The figure of radial stiffness test 3.....	132
Table 54 The temperature rise condition under stationary pumping condition and lower pocket pressure.....	133

Table 55 The temperature rise condition under stationary pumping condition and higher pocket pressure	135
Table A-1 Codes for hydrostatic journal bearings.....	145
Table A-2 Codes for hydrostatic thrust bearings	147
Table B-1 The materials readily machinable by diamond turning (Gerchman, 1986)	149
Table B-2 The materials not readily machinable by diamond turning (Gerchman, 1986)	150
Table F-1 The specifications for NI 9217 RTD Analog input C series module	155
Table H-1 The specifications for LEMO FGG.00 temperature measuring connector.....	158

LIST OF EQUATIONS

Equation 1	10
Equation 2	10
Equation 3	10
Equation 4	10
Equation 5	10
Equation 6	10
Equation 7	10
Equation 8	10
Equation 9	10
Equation 10	10
Equation 11	10
Equation 12	11
Equation 13	11
Equation 14	11
Equation 15	11
Equation 16	11
Equation 17	11
Equation 18	11
Equation 19	11
Equation 20	11
Equation 21	22
Equation 22	22
Equation 23	22
Equation 24	22
Equation 25	22
Equation 26	22
Equation 27	22
Equation 28	22

Equation 29	39
Equation 30	75
Equation 31	81
Equation 32	93
Equation 33	106
Equation 34	118
Equation 35	118

LIST OF ABBREVIATIONS

Table 1 Abbreviations for journal bearings

For Journal Bearings

n	Number of pockets
d_B	Diameter of bearings
L_B	Length of bearings
C_a	Width of axial land
C_c	Width of circumferential land
$h_{L(av)}$	Radial Clearance
H_p	Depth of pocket
P_1	Supply pressure
N_d	Rotational speed
ξ	Resistance ratio
η	Viscosity of oil
ρ	Density of oil
C_m	Specific heat capacity of oil
Φ	The bearing shape factor ratio $L_B/(\pi d_B/n)$ for cylindrical journal bearing
E_a	The bearing shape factor L_{Pa}/L_B for cylindrical journal bearing
E_c	The bearing shape factor $L_{Pc}/(\pi d_B/n)$ cylindrical journal bearing
L_{Pa}	The denotation of $L_B - 2C_c$
L_{Pc}	The denotation of $\pi d_B/4 - C_a$
k	The denotation of $1 - 4h_{L(av)}/h_p$
R_{od}	Outflow resistance
R_i	Inflow resistance
W_u	Ultimate load capacity
S_l	Radial stiffness
Q	Rate of oil flow
P_p	Pumping power
P_f	Frictional power
Δt	Temperature rise

Table 2 Abbreviations for thrust bearingsFor Thrust Bearings

n	Number of pockets
D_B	Outer diameter of thrust pad
D_P	Outer diameter of annular pocket
d_P	Inner diameter of annular pocket
d_B	Inner diameter of thrust pad
T	Ratio A_{v2}/A_{v1} for a pair of opposed plane pads or rotary thrust bearings
Ξ	Ratio ξ_1/ξ_2 for a pair of opposed plane pads or rotary thrust bearings
h_d	Clearance at the lands of each thrust pad at no load
h_P	Clearance at the pocket
P_1	Supply pressure
N_d	Rotational speed
ξ	Resistance ratio
η	Viscosity of oil
ρ	Density of oil
C_m	Specific heat capacity of oil
A_v	The virtual area of the thrust pad
R_o	Outflow resistance
R_i	Inflow resistance
$T_{(net)}$	Ultimate thrust capacity
S_T	Stiffness
Q	Rate of oil flow
P_p	Pumping power
P_f	Frictional power
Δt	Temperature rise

1 INTRODUCTION

1.1 BACKGROUND

1.1.1 INTRODUCTION TO PLASTIC ELECTRONICS PRODUCTION SYSTEMS

A UK company called Plastic Logic¹ is developing truly flexible displays. It has demonstrated an array of end applications for robust, flexible displays, in everything from smartphone accessories to large-area digital signage.

The manufacture of the flexible displays needs a reel to reel manufacturing system of high accuracy to provide an effective production capability for film-based products and devices.² A critical machine technology for any reel to reel film processing system is associated with the primary rotary motion systems.

The traditional rolling bearing element is not able to provide the level of motion accuracy which enables the achievement of the functional demands specified for the R2R system, so high precision spindles with ultra-precision hydrostatic bearing systems are considered as one of the applicable solutions to the R2R platform.

Typical steel-made bearing systems have a relatively wide speed range than is needed for the plastic film processes. In addition, they have a much higher cost, which means they are over-qualified for the reel to reel manufacturing purpose.

So the aim of this research project is to perform a more economic fluid film bearing design and some validation testing of a newly proposed R2R spindle system development.

¹ <http://plasticlogic.com/>

² EPSRC annual report 2012/2013

1.1.2 THE CHARACTERISTICS OF THE HYDROSTATIC BEARINGS

Recently, ultra-precision manufacturing and micro manufacturing are both emerging as the key enabling production technologies for next generation high-value-added products. These manufacturing technologies enable improved quality and reliability for established products, and they also make possible entirely new products and processes (Cheng and Shore, 2010). The manufacturing processes of the hydrostatic bearing systems also benefit a lot from the ultra-precision and micro manufacturing production technologies. The purposes of the hydrostatic bearing systems are to provide rotor support and lift off capability at zero speed, and maintain separation between the rotor and shaft at all times when the hydrodynamic bearings were not operating (Martin, 2004b).

The hydrostatic bearing is defined as:

“A bearing permitting relative sliding movement of the members and in which the load exerted by one member on the other is supported by fluid pressure between bearing pads and the opposing surface and in which the pressure of the fluid is maintained by means of a pump”.(Stansfield, 1970)

The external pump system used in the hydrostatic bearing system provides a supply of pressurized fluid into the bearing, the advantages of the hydrostatic bearing system are listed in the following (Loxham and Hemp, 1964):

1. Extremely low friction and high stiffness³;
2. Extremely high load-carrying capacity at low speeds;
3. High positional accuracy in high-speed, light-load applications;
4. Excellent vibration and shock resistance for liquid bearing⁴;

³ Stiffness is defined as “the ratio of the change in the oil film thickness to the change in load” (Poli, 1975)

⁴ The vibration and shock resistance for gas bearing is relatively poorer than the liquid one.

5. Excellent performance of low friction and wear during the working conditions of start-up and very low rotational speeds (De Pellegrin and Hargreaves, 2012).

But there are also some disadvantages of the hydrostatic bearing system:

1. The dynamic friction within the system generates heat, which increases the viscous shear and the pumping power;
2. The lubrication support system is relatively complicated and its installation and maintenance cost is high;
3. The high-precision system is intolerant of dirt and other hazardous environment⁵;
4. High power consumption due to pumping losses.

With the development of a coating technology, the coatings on the components of the hydrostatic bearing system are able to protect them against wear, chemical attack, and the excessive heat, which greatly increase the mechanical properties as well as the tribological behaviour of the hydrostatic bearings (Manojkumar et al., 2014). The aluminium bearing system used in this project also has a layer of electroless nickel-based coating, which greatly strengthens the mechanical properties and tribological behaviour of the bearing system.

⁵ The hazardous environment includes high temperature, high moisture, etc..

1.1.3 THE APPLICATIONS OF THE HYDROSTATIC BEARINGS

Hydrostatic thrust bearing systems, especially multi-recess hydrostatic journal bearings (El-Sherbiny et al., 1984a), have been used in many industrial areas due to the following advantage: high load-carrying capacity, virtual independence of speed, almost zero friction of bearing surfaces, very low friction at low or zero speeds, large fluid film stiffness and damping, reduced vibrations and good positional accuracy.

Typical industrial applications of hydrostatic thrust bearings are in the machining equipment such as high-precision milling machines, high speed machining centres, internal grinding machines, telescope bearings, testing equipment, medical equipment, movable stage areas, auxiliary manufacturing machine such as saw machines (Safar, 1980), aerospace equipment such as gyroscopes, and even advanced cryogenic turbo pump⁶ (Sharma et al., 2002).

For some heavy hydrostatic bearings, their large bearing capacity, low friction coefficient and high working stability and reliability are all the essential qualities of the high precision heavy CNC equipment. The performance of the hydrostatic bearing systems directly influences the machining quality and the working efficiency (ZHANG et al., 2013).

⁶ The rotating parts of the advanced cryogenic turbo pump unit consist of an oxidizer pump, a fuel pump, and a driven turbine, whose shaft is supported by the non-contact hydrostatic bearings (Ha et al., 2002).

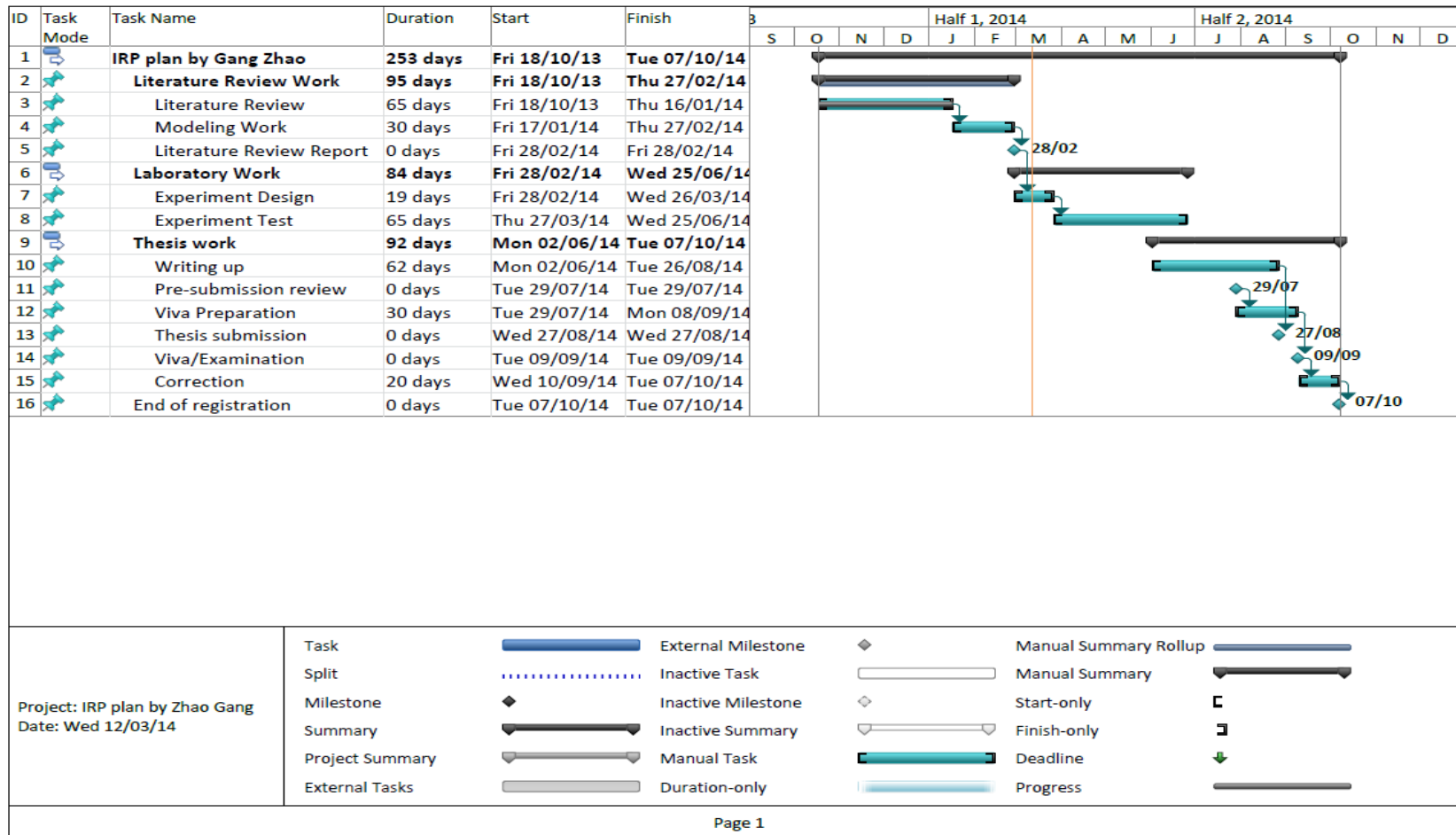
1.2 THE PROJECT PLAN

The project was decided as: “Advanced Bearing System for Ultra Precision Plastic Electronics Production Systems”. It is a development project leading to the creation of new rotational bearing systems. The created bearing units will form a cornerstone of a plastic electronics reel to reel research platform system.

As the *Figure 1 Gantt chart of the IRP plan by Gang Zhao* shows, the entire individual research project will last about 253 workdays from October 18, 2013 to October 07, 2014. The project is consisted of three parts: the literature review work, which involved the literature review work and the modelling work, from October 2013 to February 2014, the laboratory work from March 2014 to June 2014 and the thesis work from June 2014 to October 2014. Two milestones, the initial review and the pre-submission review, are included in the plan. The viva examination was scheduled for September 9, 2014, followed by a thesis correction time of 20 workdays. The registration ends on October 7, 2014.

1.3 GANTT CHART OF THE IRP PLAN

Figure 1 Gantt chart of the IRP plan by Gang Zhao



1.4 AIMS AND OBJECTIVES

The aim of this research project is to investigate the application of aluminium as the structural material for the main components of an ultra-precision spindle defined for use in R2R production systems. This was achieved by:

- Input parameters selection and output parameters calculation by using the function module of the Excel spreadsheet software.
- Cost analysis of the two materials: steel and aluminium.
- Finite element modelling analysis by ANSYS software.
- The assessment of the experiment of the aluminium hydrostatic bearings

2 LITERATURE REVIEW

2.1 ASSUMPTIONS

Calculations in this report are based on some basic parameters of the journal bearing and thrust bearing systems using the methodology of “fixed-constant method” which is introduced to analyse interrelationships within the parameters of the bearing system. Therefore, some assumptions shall be made as the limitations of using these basic equations and methodology. The hypotheses⁷ are listed here:

1. Bearings and shafts are perfectly circular in cross section and perfectly cylindrical as an ideal condition, because any small manufacturing errors will cause errors in rotational accuracy and vibration, which will finally influence the normal use of the hydrostatic bearing system as well as to the analytical predictions by all the equations quoted in this report;
2. The viscosity is constant throughout the bearing system during the whole operation process, which means the viscosity of the supply fluid will not be changed when the temperature of the supply fluid is changing, and also means the viscosity in the pocket and over the land is equal. Because the temperature difference between the fluid in a pocket and the fluid over the land is not considered in this report. So it also implies the temperature anywhere in the whole bearing system at one time is always the same as an ideal condition⁸. In operational condition, as the rise of the temperature of the oil, the thermal and oxidation

⁷All the assumptions listed above are proposed or abstracted from the book (Stansfield, 1970) to meet the requirements of all the equations and the “fixed-constant method” in this report.

⁸ The hydraulic power systems for hydraulic transmission, hydrodynamic lubrication, hydraulic sliding and the hydrostatic thrust bearing, almost all take the oil as their lubricant, so, the characteristics of the working medium have important effects on the performance and working reliability of the hydraulic systems. The oil viscosity is treated as a designed constant value, the influence of the temperature rise and the pressure on the lubricating oil viscosity is neglected, which will definitely cause some level of errors. Especially for a heavy hydrostatic thrust bearing with a high linear velocity, this assumption leads to a large error as compared with the actual cases (SHAO et al., 2011).

characteristics as well as the volatility of the oil will all change, which would cause the malfunction or even the collapse of the hydrostatic system (Moore, 1969);

3. The bearing fluid is Newtonian, which means the viscosity has a constant rate of change of shear strain (Lebeck, 1988);
4. The lubricating fluid is incompressible, i.e. the flow rate will not be influenced by the volume change of the fluid due to the temperature change;
5. The density of the fluid is assumed constant, which implies the pressure change will not change the density of the fluid as well as the heat capacity of the fluid;
6. The total flow from the bearing is equal to the sum of the flows through the compensator units, i.e. there is no flow loss or leakage within the whole hydrostatic bearing system;
7. The pressure distribution in a pocket is uniform. Although the depth of the pocket is about 10 times greater than the radial clearance between the shaft and the bearing, all the complex fluid motions, such as the inter-pocket circumferential flow and the turbulence within the pocket, at a high rotational speed are not being considered into this initial report as well as all the equations in this report, the presence of the pockets can have negative impact on performance when the system is at high oil viscosity and high bearing speed (De Pellegrin and Hargreaves, 2012);
8. All the heat energy is transported within the hydraulic circuit, which implies the parameter of “temperature rise, Δt ” is just the difference between the inflow temperature and the outflow temperature and there is no other way of temperature lose such as the heat conduction through the bearing materials, the power consumption of liquid friction is completely converted into heat and this heat could be completely absorbed by the lubricating oil, according to the energy balance principle and the temperature rise in the lubricating oil of the hydrostatic bearing mainly comes from the heat produced by the oil film shear driven by worktable’s rotation as well as the system itself (SHAO et al., 2011). The

heat loss in a rotating hydrostatic bearing results from two parts: one part is the consumption of the hydraulic power delivered by the pump in head loss through the restrictor and to drive the laminar Poiseuille flow in the bearing clearance, another is the frictional power in the Couette shear flow generated by the relative motion between the spindle and the bearing pads and spared by the spindle motor. (Chen et al., 2011). The heat dissipation of the bearing system usually includes two parts: one is the heat conduction by the bearing house and the shaft, another is the heat carried away by the oil (Kher and Cowley, 1970);

9. The flow within the system is laminar, not turbulent;
10. The direction of loading is towards the centre of the pocket, because the stiffness of the fluid changes with the direction of the loading and all the equations used for hydrostatic journal bearings in this report are based on the condition of the load direction towards the centre of the pockets. And if the direction of loading is towards the inter-pocket land, the stiffness would be lower.
11. The bearing house of the hydrostatic bearing systems is absolutely rigid⁹.

⁹ The effects of the flexibility of the bearing house on the bearing characteristics are significant and must be considered (Sinhasan et al., 1989).

2.2 REVIEW OF THE THEORETICAL DESIGN APPLIED TO ULTRA-PRECISION SPINDLE

The equations of the initial calculation work come from the book: Hydrostatic bearings for machine tools and similar applications (Stansfield, 1970). The equations help to solve the problems of some basic hydrostatic bearing systems such as journal bearing systems and thrust bearing systems.

An Excel spreadsheet was established based on the equations in the Stansfield's book to get the basic.

The equations (Stansfield, 1970, Page 123-163) used to calculate the parameters of the journal bearings are listed in the *Table 3 Formulas for journal bearings calculations (Stansfield, 1970, Page 123-163)* below.

The equations (Stansfield, 1970, Page 164-191) used to calculate the parameters of the thrust bearings are listed in the *Table 4 Formulas for thrust bearings calculations (Stansfield, 1970, Page 164-191)* below:

Table 3 Formulas for journal bearings calculations (Stansfield, 1970, Page 123-163)

For the journal bearings ¹⁰		
Bearing shape factor ratio	$\phi = \frac{L_B}{\frac{\pi d_B}{4}}$	Equation 1
Bearing shape factor Ea	$E_a = \frac{L_{Pa}}{L_B}$	Equation 2
Bearing shape factor Ec	$E_c = \frac{L_{Pc}}{\frac{\pi d_B}{4}}$	Equation 3
Outflow resistance Rod	$R_{od} = 0.75 \frac{n\eta\phi(1 - E_a)}{h_{L(av)}^3}$	Equation 4
Inflow resistance Ri	$R_i = \xi R_{od}$	Equation 5
Ultimate load capacity Wu	$W_u = \frac{1.47\xi\phi(1 - E_c)(1 + E_a)}{\xi(\xi + 0.4)\phi^2 E_a(1 - E_a) + 0.642(\xi + 0.207)(\xi + 1)} \times p_1 d_B^2$	Equation 6
Radial stiffness Sl	$S_l = \frac{1.5\xi\phi(1 + E_a)}{(1 + \xi)^2 \left[1 + \frac{0.5\xi\phi^2 E_a(1 - E_a)}{(1 + \xi)(1 - E_c)} \right]} \frac{p_1 d_B^2}{h_{L(av)}}$	Equation 7
Rate of flow Q	$Q = \frac{1.33}{(1 + \xi)\phi(1 - E_a)} \frac{p_1 h_{L(av)}^3}{\eta}$	Equation 8
Pumping power Pp	$P_p = \frac{1.33}{(1 + \xi)\phi(1 - E_a)} \frac{p_1^2 h_{L(av)}^3}{\eta}$	Equation 9
Frictional power Pf	$P_f = 0.00677\phi(1 - kE_c E_a) \left(1 + \frac{0.25kE_a(1 - E_c)(n - 4)}{1 - kE_c E_a} \right) \frac{\eta d_B^4 N_d^2}{h_{L(av)}}$	Equation 10
Temperature rise Δt	$\Delta t = \frac{p_1 + \frac{P_f}{Q}}{\rho c_m}$	Equation 11

¹⁰ All the abbreviations have been shown in the *Table 3 Formulas for journal bearings calculations* (Stansfield, 1970, Page 123-163)

Table 4 Formulas for thrust bearings calculations (Stansfield, 1970, Page 164-191)

For the thrust bearings¹¹

Virtual area of the thrust pad	$A_v = \frac{\pi D_B^2 - D_P^2}{8 \log_e \frac{D_B}{D_P}} - \frac{\pi d_P^2 - d_B^2}{8 \log_e \frac{d_P}{d_B}}$	Equation 12
--------------------------------	---	-------------

Outflow resistance Ro(net)	$\frac{1}{R_{o(net)}} = \frac{1}{\frac{6 \eta}{\pi h_d^3} \log_e \frac{D_B}{D_P}} + \frac{1}{\frac{6 \eta}{\pi h_d^3} \log_e \frac{d_P}{d_B}}$	Equation 13
-------------------------------	--	-------------

Inflow resistance Ri	$R_i = \xi R_{od}$	Equation 14
----------------------	--------------------	-------------

Ultimate thrust capacity T(net)	$T_{(net)} = p_1 A_{v(1)} \left(1 - \frac{Y}{1 + 8 \times \Xi Y}\right)$	Equation 15
---------------------------------	--	-------------

Stiffness ST	$S_T = \frac{dT_{(net)}}{dh} = -\frac{p_1 A_{v(1)}}{h_d} \left(\frac{3\xi_{(1)} \left(\frac{h_{(1)}}{h_d}\right)^2}{\left[1 + \xi_{(1)} \left(\frac{h_{(1)}}{h_d}\right)^3\right]^2} + \frac{3Y\Xi\xi_{(1)} \left(2 - \frac{h_{(1)}}{h_d}\right)^2}{\left[1 + \Xi\xi_{(1)} \left(2 - \frac{h_{(1)}}{h_d}\right)^3\right]^2} \right)$	Equation 16
--------------	---	-------------

Rate of flow Q	$Q = \frac{p_1}{(1 + \xi_{(1)}) R_{o(net)}}$	Equation 17
----------------	--	-------------

Pumping power Pp	$P_p = \frac{p_1^2}{(1 + \xi) R_{o(net)}}$	Equation 18
------------------	--	-------------

Frictional power Pf	$P_f = 1.078 \times 10^{-3} \left(\frac{\eta N^2 (D_B^4 - D_P^4)}{h_d} + \frac{\eta N^2 (D_P^4 - d_P^4)}{h_d} + \frac{\eta N^2 (d_P^4 - d_B^4)}{h_d} \right)$	Equation 19
---------------------	--	-------------

Temperature rise Δt	$\Delta t = \frac{p_1 + \frac{P_f}{Q}}{\rho c_m}$	Equation 20
---------------------	---	-------------

¹¹All the abbreviations have been shown in the *Table 4 Formulas for thrust bearings calculations* (Stansfield, 1970, Page 164-191)

Applying these equations into the Excel spreadsheet, some important operational parameters of the bearing system, such as the ultimate load capacity, the radial stiffness, the flow, the pumping power, the frictional power and the temperature rise, could be calculated automatically by inputting basic bearing parameters, such as the number of pockets, the diameter of bearing, the length of bearing, the width of axial land, the width of circumferential land, the radial clearance, the depth of pocket, the depth of pocket, the supply pressure, the rotational speed, the resistance ratio, the viscosity of oil, the density of oil and the specific heat capacity of oil.

The parameter input and output window of the calculation of hydrostatic journal bearings is shown in the *Figure 2 The parameter input and output window of the calculations of hydrostatic journal bearings in the Excel spreadsheet below.*

The upper part is designed for parameters input and the lower part which is highlighted by the blue filling colour is designed for the output of some important operational parameters. The output data will be generated automatically after inputting the parameters in the upper part.

Figure 2 The parameter input and output window of the calculations of hydrostatic journal bearings in the Excel spreadsheet

Hydrostatic journal bearings		
Number of pockets:n=	5.000000	
Diameter of bearing:d _B =	0.099800	m
Length of bearing:L _B =	0.072000	m
Width of axial land:c _a =	0.050000	m
Width of circumferential land:c _c =	0.012800	m
Radial clearance:h _{L(av)} =	0.000065	m
Depth of pocket:h _p =	0.001300	m
Supply Pressure:p ₁ =	278000.000000	Pa
Rotational speed:N _d =	500.000000	rev/min
Resistance ratio:ξ=	1.000000	
Viscosity of oil:η=	0.017000	Ns/m ²
Density of oil:ρ=	900.000000	kg/m ³
Specific Heat capacity of oil:C _m =	2000.000000	J/(kg*K)
Constant:k=	0.800000	
Bearing shape factor:Φ=	0.919036	
Bearing shape factor:E _a =	0.644444	
Bearing shape factor:E _c =	0.361781	
Outflow resistance:R _{od} =	758.542444	10 ⁸ Ns/m ⁵
Inflow resistance:R _i =	758.542444	10 ⁸ Ns/m ⁵
Ultimate load capacity:W _u =	1048.960292	N
Radial stiffness:S ₁ =	0.224409	10 ⁸ N/m
Flow:Q=	9.139403	10 ⁻⁶ M ³ /s
Pumping power:P _p =	2.540754	W
Friction power:P _f =	36.149414	W
Temperature rise:Δt≈	2.351854	° C

The next step is to choose the four parameters highlighted by the yellow filling colour above as the four most important input parameters and to analyse the relationships between these four parameters of the hydrostatic bearing systems.

The reasons why choosing these four parameters are listed in the the following table:

Table 5 Reasons for choosing the four specific parameters as the input parameters

Parameters	Reasons
Radial clearance	One of the most important parameters of a hydrostatic bearing. The value of radial clearance can be regarded as the ease of manufacturing, i.e. the smaller the value of the radial clearance is, the harder the bearing is to be manufactured, which also means a relatively higher cost. And the radial clearance also affects the rotational accuracy of the shaft, flow rate of the bearing system as well as the temperature change of the fluid greatly.
Supply pressure	One of the most important input values which can be controlled after the bearing system is manufactured. Different supply pressure means different ultimate load capacity and different power consumption, which are both very important to the operational cost of the bearing system.
Rotational speed	Rotational speed has a great impact on the temperature performance of the bearing system. For any specific bearing system, there is a range of the rotational speed. If the speed exceeds the range, the system will probably break down.
Viscosity of oil	One of the most important input values which decides the performance of the bearing system. For a specific bearing design, the different sorts of oil will lead to different performances. By changing different sorts of supply fluid, different flow rate and temperature change condition can be obtained.

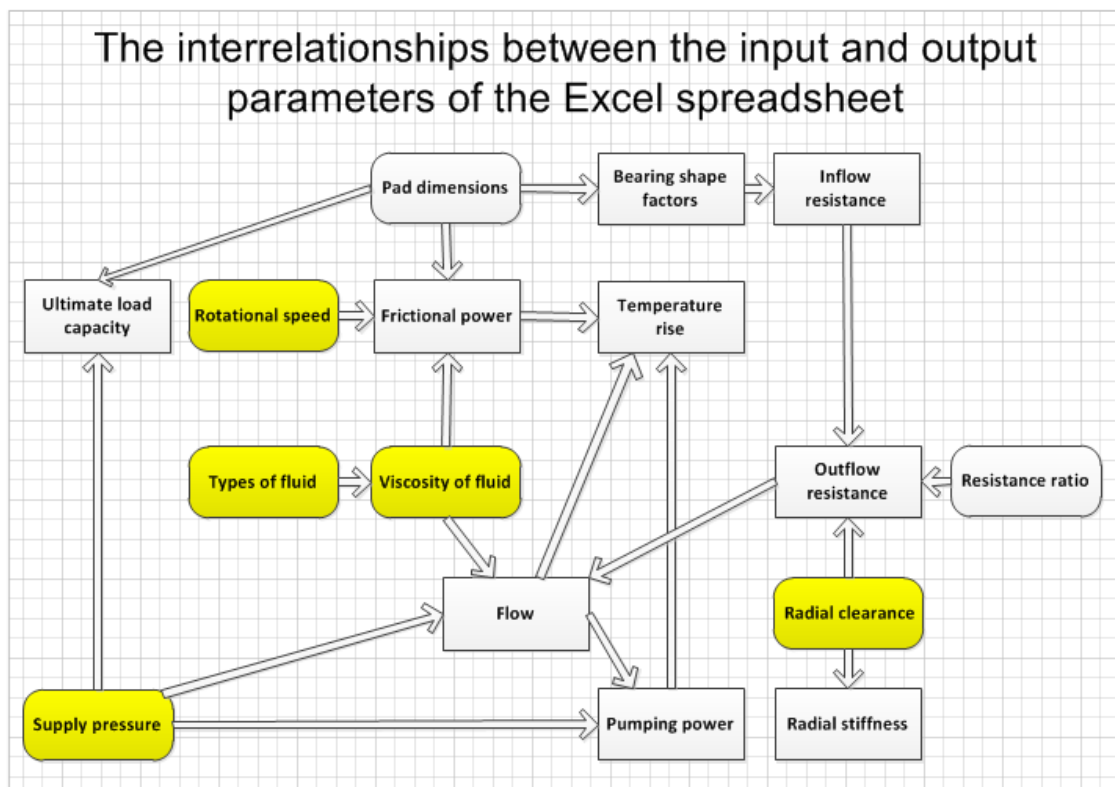
The interrelationships between the input and output parameters of the Excel spreadsheet are shown in the *Figure 3 The interrelationships between the input and output parameters of the Excel spreadsheet* below:

Since the viscosity of the fluid is determined by the type of the fluid, the five yellow boxes actually represent the four major input parameters of the hydrostatic bearing system. By the help of the equations (Stansfield, 1970), all the other output parameters are generated automatically by the Excel

spreadsheet program. The codes of the program are shown in the appendices in the end of this report.

According to the *Figure 3 The interrelationships between the input and output parameters of the Excel spreadsheet*, there are complex interrelationships within the parameters of the hydrostatic bearing system. A slight change of any one parameter leads to the change of some other parameters. These changes make it relatively difficult to analyse the interrelationship within these parameters. So the methodology of “fixed constant method” is introduced to solve this problem.

Figure 3 The interrelationships between the input and output parameters of the Excel spreadsheet



For example, the radial clearance is fixed at 30µm; the viscosity of the fluid is fixed at 0.017 Ns/m², the rotational speed is fixed at 1000 rev/min, and then the relationships between the supply pressure and the ultimate load capacity/temperature change/radial stiffness/flow are shown in *Table 6 The relationship between the supply pressure and some output parameters:*

Table 6 The relationship between the supply pressure and some output parameters

h=30 μ m η =0.017Ns/m ² n=1000rev/min					
P ₁ (10 ⁶ Pa)	L(N)	$\Delta t(^{\circ}C)$	S(10 ⁸ N/m)	Q(10 ⁻⁶ m ³ /s)	Q(L/min)
1.000000	3773.238462	54.405359	1.748988	3.232189	0.193931
2.000000	7546.476924	28.036013	3.497977	6.464378	0.387863
3.000000	11319.715386	19.616601	5.246965	9.696566	0.581794
4.000000	15092.953849	15.684673	6.995954	12.928755	0.775725
5.000000	18866.192311	13.547739	8.744942	16.160944	0.969657
6.000000	22639.430773	12.308301	10.493931	19.393133	1.163588

According to the table above, the diagrams of the relationships between the supply pressure and the temperature change/flow are plotted in the *Figure 4 The relationship between the supply pressure and the temperature change for a specific kind of hydrostatic bearing* and the *Figure 5 The relationship between the supply pressure and the flow for a specific kind of hydrostatic bearing* below:

Figure 4 The relationship between the supply pressure and the temperature change for a specific kind of hydrostatic bearing

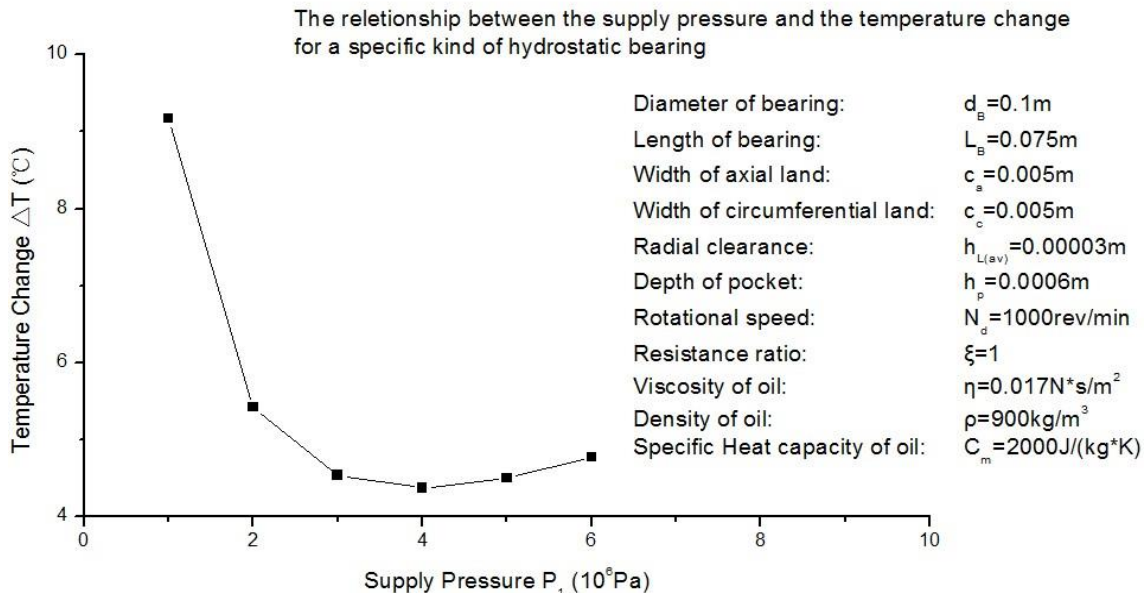
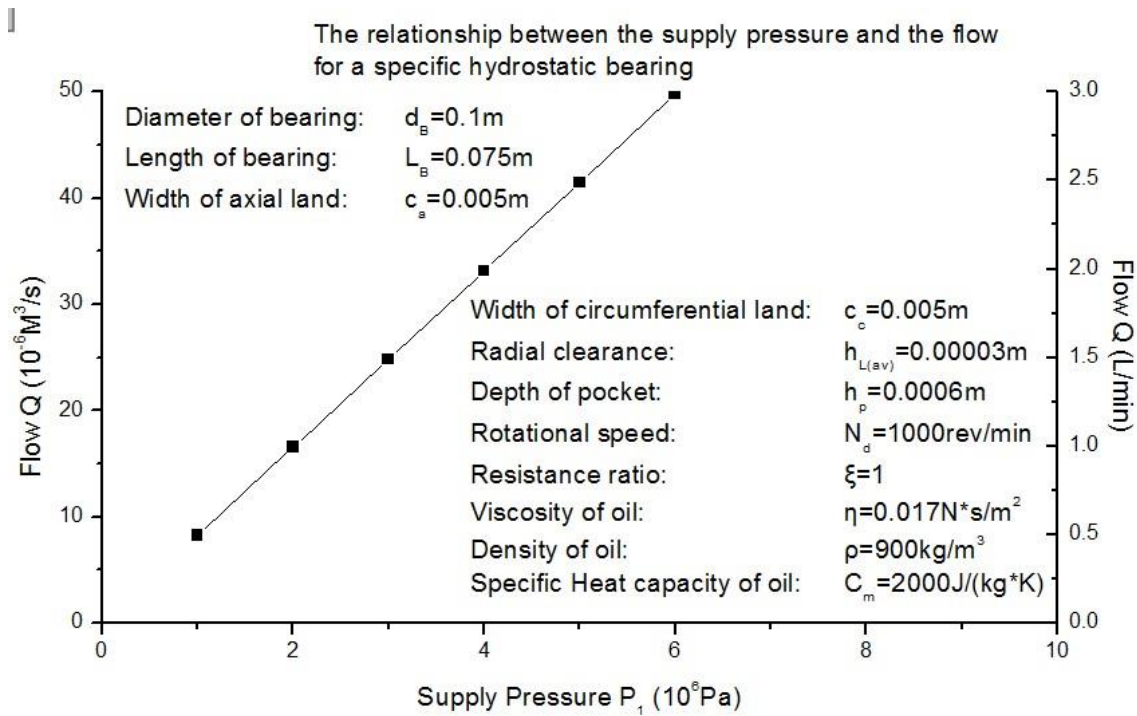


Figure 5 The relationship between the supply pressure and the flow for a specific kind of hydrostatic bearing



By using the same “fixed-constant method”, changing the parameters of the radial clearance, the viscosity of the fluid, and the rotational speed respectively, the other three tables and six figures are listed below:

Table 7 The relationship between the radial clearance and some output parameters

$P_1=20\text{bar}$ $\eta = 0.017\text{Ns}/\text{m}^2$ $n=1000\text{rev}/\text{min}$					
$h(10^{-6}\text{m})$	$L(\text{N})$	$\Delta t(^{\circ}\text{C})$	$S(10^8\text{N}/\text{m})$	$Q(10^{-6}\text{m}^3/\text{s})$	$Q(\text{L}/\text{min})$
20.000000	7546.476924	134.672504	5.246965	1.915371	0.114922
30.000000	7546.476924	27.614143	3.497977	6.464378	0.387863
40.000000	7546.476924	9.534974	2.623483	15.322969	0.919378
50.000000	7546.476924	4.577147	2.098786	29.927674	1.795660
60.000000	7546.476924	2.790151	1.748988	51.715021	3.102901
70.000000	7546.476924	2.021481	1.499133	82.121538	4.927292

Figure 6 The relationship between the radial clearance and the temperature change for a specific kind of hydrostatic bearing

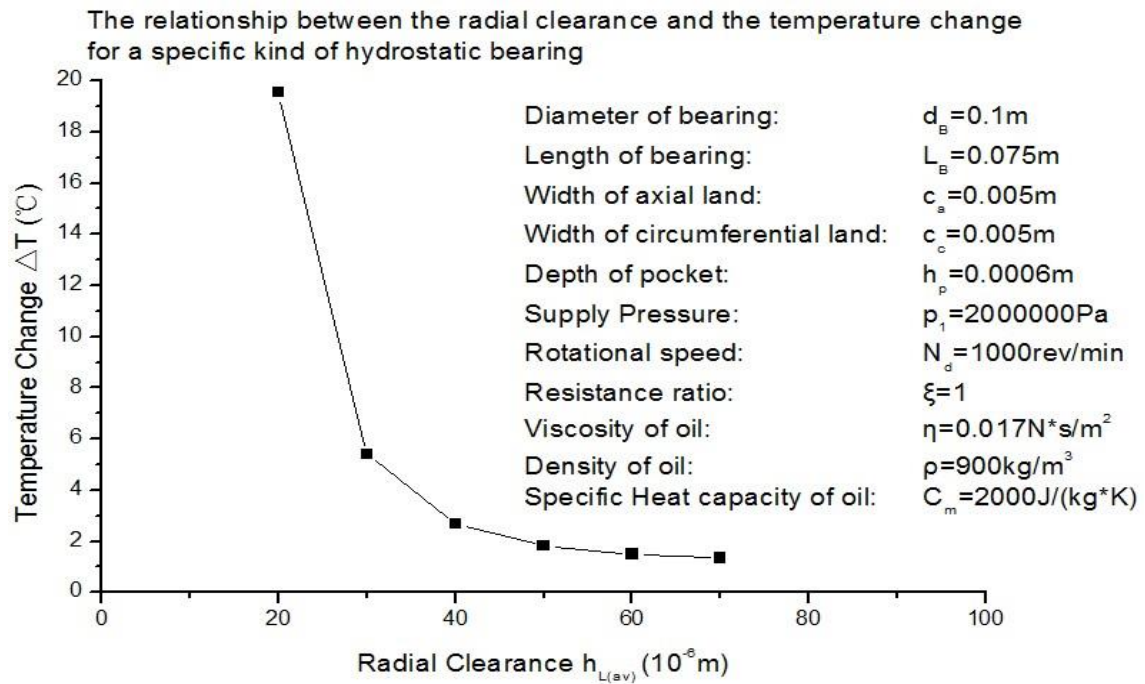


Figure 7 The relationship between the radial clearance and the radial stiffness for a specific kind of hydrostatic bearing

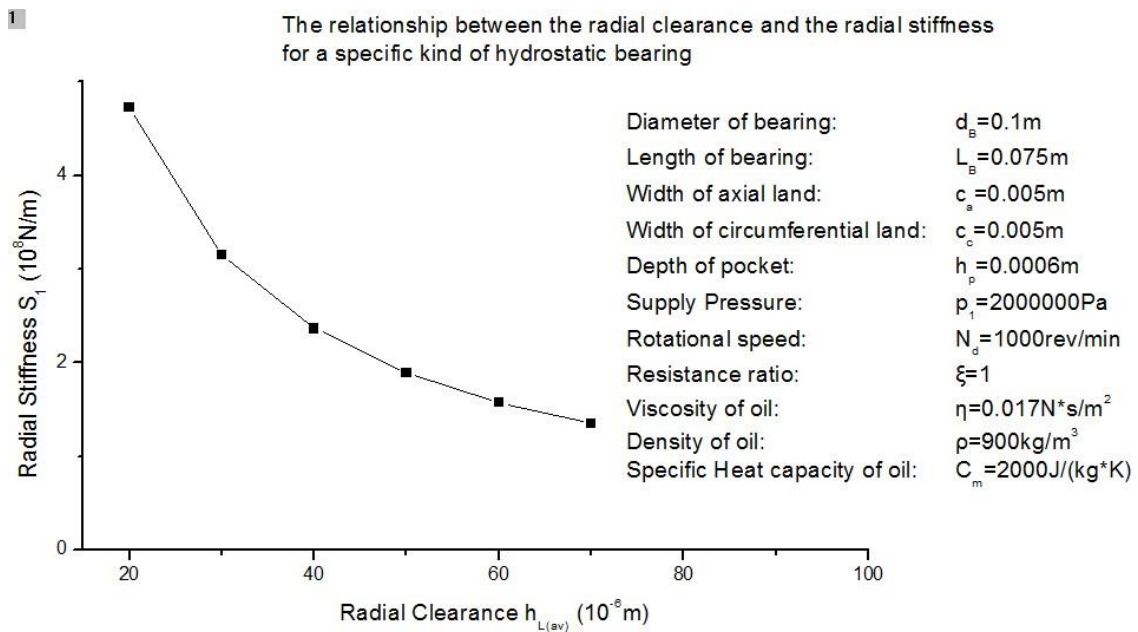


Figure 8 The relationship between the radial clearance and the flow for a specific kind of hydrostatic bearing

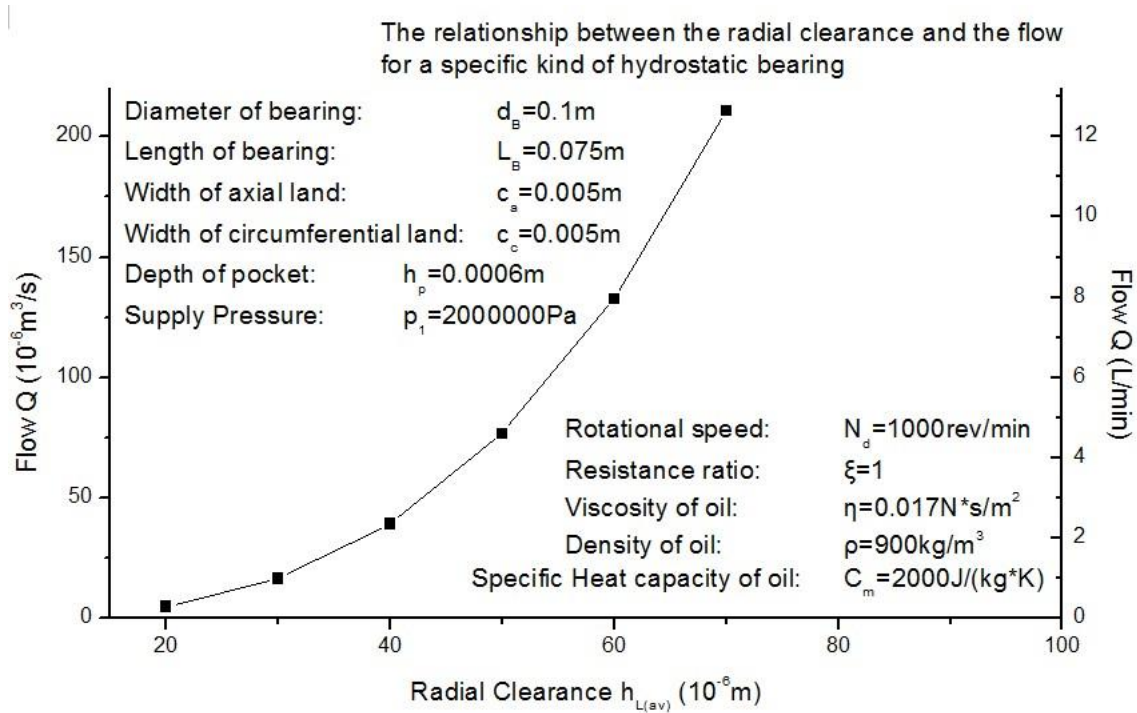
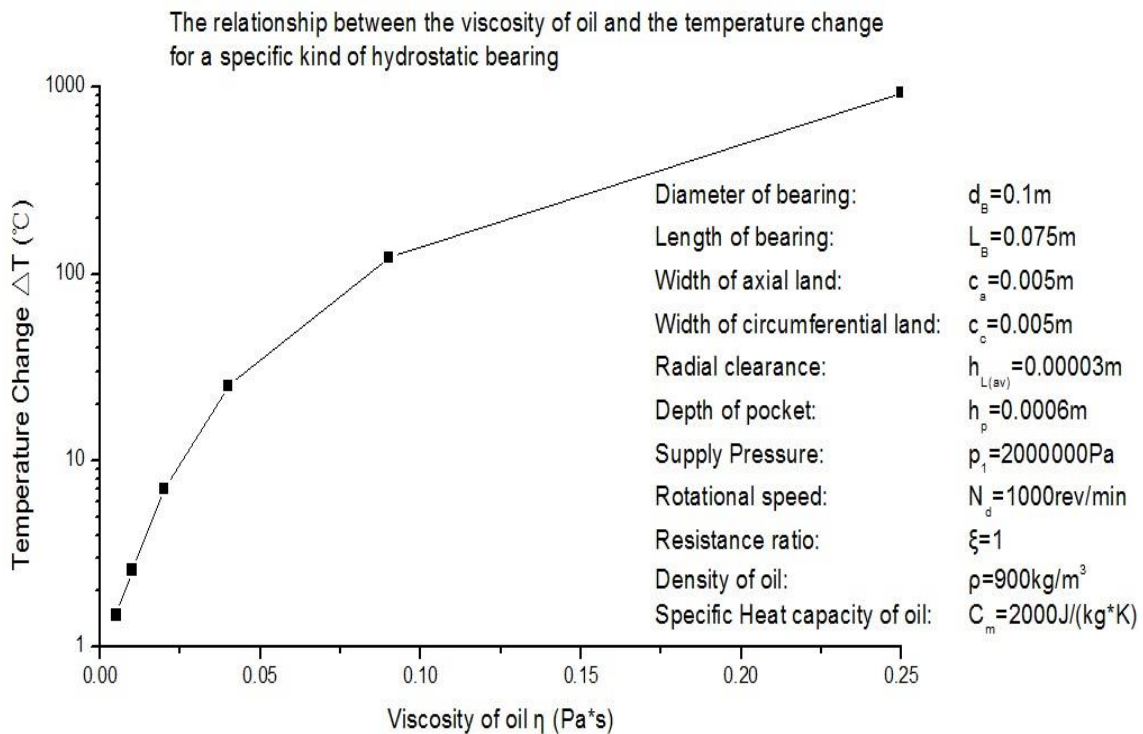


Table 8 The relationship between the viscosity of the fluid and some output parameters

$P_1=20\text{bar}$ $h=30\mu\text{m}$ $n=1000\text{rev}/\text{min}$					
η (Pa*s)	L(N)	Δt (° C)	S($10^8\text{N}/\text{m}$)	Q($10^{-6}\text{m}^3/\text{s}$)	Q(L/min)
0.005000	7546.476924	3.440255	3.497977	21.978884	1.318733
0.010000	7546.476924	10.427686	3.497977	10.989442	0.659367
0.020000	7546.476924	38.377411	3.497977	5.494721	0.329683
0.040000	7546.476924	150.176312	3.497977	2.747360	0.164842
0.090000	7546.476924	755.753692	3.497977	1.221049	0.073263
0.250000	7546.476924	5823.970532	3.497977	0.439578	0.026375

Figure 9 The relationship between the viscosity of the fluid and the temperature change for a specific kind of hydrostatic bearing



Due to the large oil flow rate, the oil carries away approximately half of the total heat in the actual operational condition dissipated by the bearing housing and the oil together. Since the temperature rise is higher under higher rotational speed condition, the larger reduction in oil viscosity due to the temperature rise causes even greater oil flow rate, which on the other side helps to keep the ratio of the heat dissipation by the two elements the same for various spindle speeds (Kher and Cowley, 1970). So the 1000°C in the figure above is just the unrealistic result by the program calculation under the assumption 2¹².

¹² Assumption 2: The viscosity is constant throughout the bearing system during the whole operation process, which means the viscosity of the supply fluid will not be changed when the temperature of the supply fluid is changing, and also means the viscosity in the pocket and over the land is equal. Because the temperature difference between the fluid in a pocket and the fluid over the land is not considered in this report. So it also implies the temperature anywhere in the whole bearing system at one time is always the same as an ideal condition¹². In operational condition, as the rise of the temperature of the oil, the thermal and oxidation characteristics as well as the volatility of the oil will all change, which would cause the malfunction or even the collapse of the hydrostatic system (Moore, 1969)

Figure 10 The relationship between the viscosity of the fluid and the flow for a specific kind of hydrostatic bearing

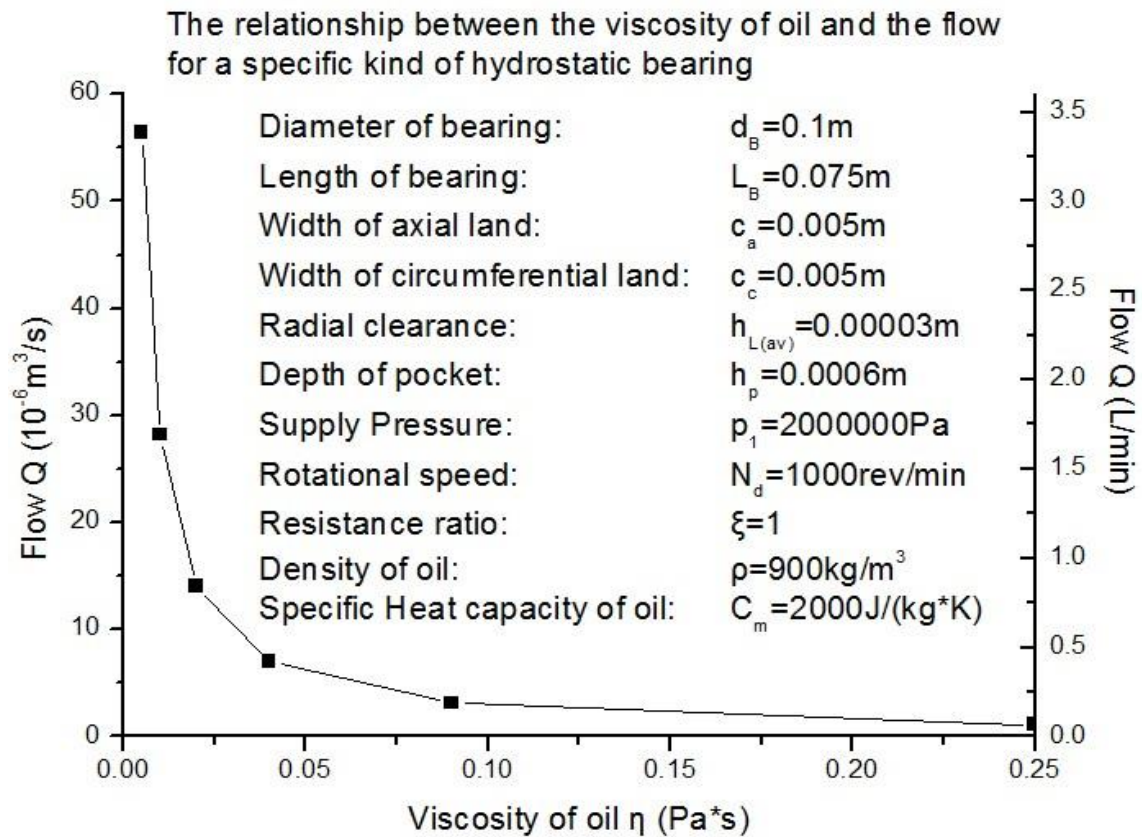
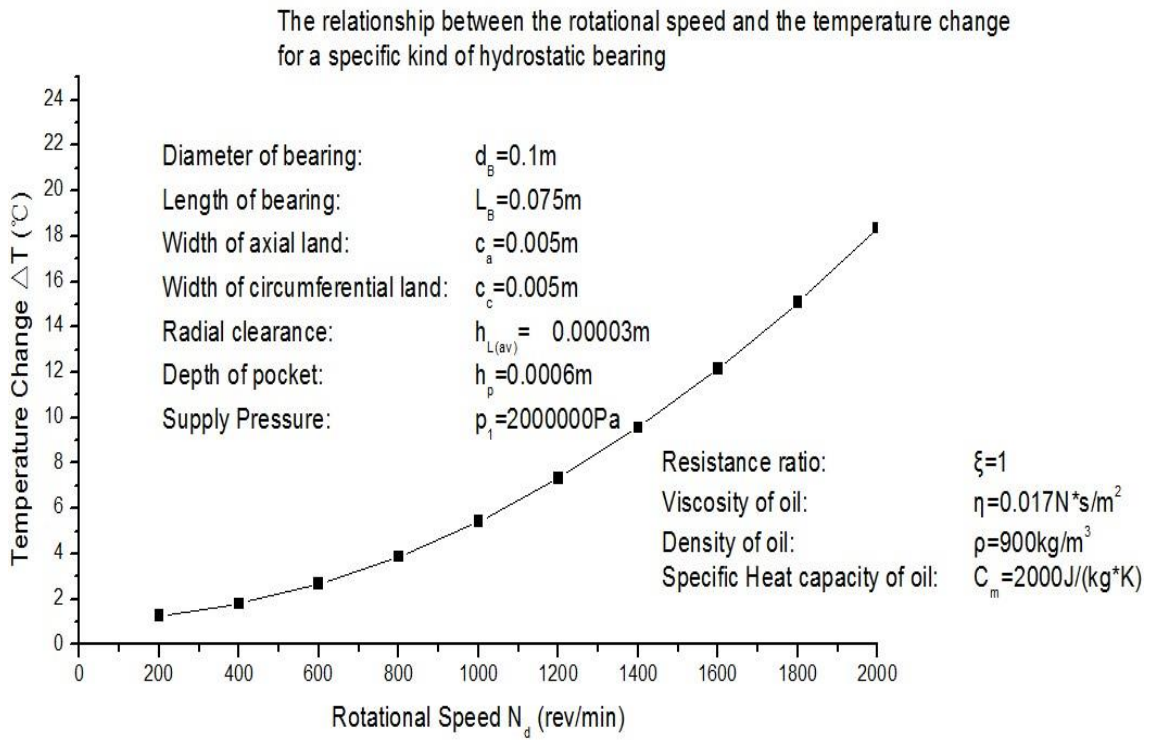


Table 9 The relationship between the rotational speed and some output parameters

$P_1=20\text{bar}$ $h=0.00003\text{m}$ $\eta =0.017\text{Ns/m}^2$					
N(rev/min)	L(N)	$\Delta t(^{\circ}\text{C})$	S(10^8N/m)	Q($10^{-6}\text{m}^3/\text{s}$)	Q(L/min)
200.000000	7546.476924	2.188107	3.497977	6.464378	0.387863
400.000000	7546.476924	5.419095	3.497977	6.464378	0.387863
600.000000	7546.476924	10.804076	3.497977	6.464378	0.387863
800.000000	7546.476924	18.343048	3.497977	6.464378	0.387863
1000.000000	7546.476924	28.036013	3.497977	6.464378	0.387863
1200.000000	7546.476924	39.882970	3.497977	6.464378	0.387863
1400.000000	7546.476924	53.883919	3.497977	6.464378	0.387863
1600.000000	7546.476924	70.038860	3.497977	6.464378	0.387863
1800.000000	7546.476924	88.347793	3.497977	6.464378	0.387863
2000.000000	7546.476924	108.810719	3.497977	6.464378	0.387863

Figure 11 The relationship between the rotational speed and the temperature change for a specific kind of hydrostatic bearing



From all the figures above, the initial conclusion of the relationships within these parameters can be illustrated in the following equations:

Table 10 The relationship within the parameters of the hydrostatic bearings

$Q \propto C_1 \times P_1$	Equation 21
$Q \propto C_1 \times h_{L(av)}^3$	Equation 22
$Q \propto C_1 / \eta$	Equation 23
$S \propto C_1 / h_{L(av)}$	Equation 24
$\Delta t \propto C_1 \times P_1 + C_2 / P_1$	Equation 25
$\Delta t \propto C_1 + C_2 / h_{L(av)}^3$	Equation 26
$\Delta t \propto C_1 + C_2 \times \eta^2$	Equation 27
$\Delta t \propto C_1 + C_2 \times N_d^2$	Equation 28

Since the flow rate is closely related to the energy consumption of the system, i.e. the more flow rate the system has, the more external pumping power the system needs. And for the definite working condition, the smaller the flow rate is, the better the energy saving goal will be achieved.

According to the *Equation 21, Equation 22, and Equation 23*, the flow rate is proportional to the cube of the radial clearance $h_{L(av)}$ and inversely proportional to the viscosity of the fluid. So if a smaller flow rate is needed, the radial clearance shall be smaller and the viscosity of the fluid shall be larger.

And for Equation 24, the stiffness of the fluid is inversely proportional to the value of the radial clearance $h_{L(av)}$. High stiffness leads to high load capacity of the bearing system. So the smaller radial clearance is needed to achieve a higher load capacity.

From *Equation 25, Equation 26, Equation 27, and Equation 28*, it is initially concluded that the temperature is proportional to the square of the viscosity, the square of the rotational speed, inversely proportional to the cube of the radial clearance $h_{L(av)}$ and has a complex relationship with the supply pressure which is proportional to the sum of both the supply pressure and the reciprocal of the supply pressure.

Since the temperature rise will not only increase the energy consumption of the whole bearing system, but also influence the normal operational behaviour of the bearing system, such as the accuracy of the bearing system, the vibration of the shaft as well as the features of the fluid, the lowest temperature rise is required to protect the optimal or normal operation of the hydrostatic bearing system.

To minimise the temperature rise, the best way is to reduce the friction, because the friction is not just a source of mechanical inefficiency but also a source of heat that, if dissipated ineffectively, has the potential to degrade both the lubricating oil and the bearing surfaces (De Pellegrin and Hargreaves, 2012).

Then the dilemma comes out that the purpose of having lower flow rate requires the smaller radial clearance and larger viscosity of the fluid, and at the same time, the purpose of having lower temperature rise requires the larger radial clearance and the smaller viscosity of the fluid. Both the flow rate and the temperature rise are very important operational parameters of the hydrostatic bearing systems, so some optimization works must be done to achieve the optimal balance between these two parameters to solve the dilemma.

To obtain a larger stiffness, which means greater load capacity, the smaller radial clearance is recommended, but the smaller radial clearance also leads to the higher manufacturing cost.

As a result, carefully choosing the suitable value of the radial clearance as well as the appropriate type of the fluid is partly the solution to improve the performance of the bearing system and the essence of the optimization work of designing a hydrostatic bearing system of some specific manufacturing objectives. And the optimization work shall be proved to be pragmatic by the experimental works.

3 DESIGN OF SPINDLE SYSTEM

3.1 THE INITIAL DESIGN OF THE SYSTEM

The design of a hydrostatic bearing system is usually the strategy of the selections of the bearing type and configuration, the fluid feeding device and the bearing material (Cheng and Rowe, 1995).

For most of the design work, three most influential factors of hydrostatic bearing design are cost, packaging, and manufacturing constraints (Martin, 2004a), which will be taken into consideration in the improvement process. The optimum design includes maximizing load carrying capacity, minimum temperature rise and maximum stiffness (El-Sherbiny et al., 1984a).

The bearings with large clearances and a pressure ratio¹³ of about 0.5 under high supply pressure are optimal for getting high load capacity (El-Sherbiny et al., 1984a). And for minimum power losses for the hydrostatic bearing system design, the clearance should be economically small, the high supply pressure should be avoided, the pressure ratio is near 0.5, the area ratio¹⁴ is 0.5, and the oils with lower viscosity are recommend¹⁵ (El-Sherbiny et al., 1984b). But for some particular usage, the favourable design might be using the minimum cost to finish the objective in every specification.

For the hydrostatic bearing used in a machine tool, it is generally considered that the spindle system is one of the most important parts since the properties of the spindle system are closely related to the machining precision. The dimensions, the location, and the stiffness of the bearings as well as the working load, all of which cause the deformation of the spindle, which also cause the change of the pressure and thickness of the lubrication film affecting the bearing stiffness (Chen et al., 2012). The thermal error is also one of the

¹³ Pressure ratio=Recess Pressure/Supply Pressure

¹⁴ Area ratio=Total recess area/Total bearing area

¹⁵ Viscous oils can be tolerated only for larger bearing clearances (El-Sherbiny et al., 1984b).

most influential error sources in high precision structures (Chen et al., 2011). The minimum power loss, minimum size (or maximum load-carrying capacity) and maximum moment stiffness, as well as maximum stiffness, are adopted as the optimum conditions for the improvement of the design of the hydrostatic bearings (Kazama and Yamaguchi, 1993).

The maximum stiffness is needed in some cases because the main purpose of the hydrostatic bearings is to support the sliding or rotating parts with a high stiffness and the minimum power loss is required for avoiding the excessive flow rate as well as the temperature rise to achieve less energy consumption, which finally saves the cost of both manufacturing and operation processes (Rowe and Stout, 1972). The production requires the hydrostatic bearing systems with high dimensional and geometrical accuracy, which is especially important for standardized mass production (Dumbrava, 1985).

For high speed bearing systems, the frictional power is the dominant factor which causes the temperature rise of the oil. And for a traditional journal bearing at low speed, three most important parameters are flow rate, stiffness and the safe maximum load (Anonymous1969).

The hydrostatic bearing system specially designed for the plastic electronics reel to reel production system has two opposite thrust bearings and one journal bearing. The hydrostatic oil is pressurized to the bearing with a hydraulic pump, and a thin film is formed between the spindle shaft and the bearing.

The traditional hydrostatic thrust pad bearing systems for the plastic electronics reel to reel production system are mostly made of the material of steel, which means a high Young modulus property and high manufacturing cost. Generally, hydrostatic thrust pad bearing systems are designed to operate with parallel surfaces. For hydrostatic thrust pad bearings operating under load, the elastic deformation of the bearing pad alters the fluid film profile and hence the performance characteristics. The Young modulus of the material of the bearing pad affects the performance characteristics (Sharma et al., 2002).

The force exerted on the thrust bearings of the hydrostatic bearing systems is made up of two parts: the force formed by the internal fluid and the external work load of the production system. Since the force causes the deformation of the thrust plate of the bearing system, and the non-parallelism of the bearing and the runner surfaces causes a reduction in the load, stiffness and damping, and an increase in the lubricant flow rate (Osman et al., 1991), the substitution of the material of steel should have at least the equivalent property of the Young modulus compared with the steel bearing system to guarantee the normal operation of the whole production system.

In this project, the material of aluminium alloy is considered to be the substitution of the steel. Whether it is a qualified material will be analysed and proved by the following analysis and experimental works.

3.2 THE COMPARISON ANALYSIS BETWEEN THE MATERIALS OF STEEL AND ALUMINIUM

Steel is generally used as the material of bearing shafts for the following advantages¹⁶:

- Resistance to corrosion in moisture and other corrosive environments;
- Highly versatile, sealed versions available with different grease fillings;
- High pressure and working load tolerated (high hardness and Young's Modulus);
- High temperature tolerated (up to 300°C dependent on lubricant).

The aim of this individual research project is to investigate the application of aluminium for the main components of an ultra-precision spindle defined for the use in R2R production systems. The primary target is reducing the total cost of the hydrostatic bearing systems. Aluminium alloy, as the substitution, has the following advantages:

- Relatively inexpensive material cost (Cheng et al., 2013);
- Excellent workability (HINO et al., 2009);
- Good electric and thermal conductivity (Rudnik and Jucha, 2013);
- High specific strength and stiffness at low density (Saxena et al., 2006);

There are some diamond-turning machines in the Cranfield Ultra-precision Manufacturing Centre. If the bearing manufacturing process can be finished by the means of diamond turning, the cost of manufacturing the bearing system would be greatly reduced.

Normally, the steel, as a typical ferrous material, is not readily machinable by diamond tools due to the reason that the carbon element within the diamond tools will chemically react with the substrate which generates excessive wear causing the tool damage and dulling after short cut lengths (Moriwaki and Shamoto, 1991). The temperature in ultra-precision diamond cutting of copper

¹⁶ Sources: <http://www.acorn-ind.co.uk/product/special-bearings/stainless-steel-bearings>

can reach up to 150°C (Moriwaki et al., 1990). So if the material is stainless steel, which has higher values of hardness and Young's modulus than the copper, the temperature rise will be even larger, influencing the machining accuracy of the ultra-precision manufacturing process.

3.2.1 THE MATERIAL PROPERTIES COMPARISON

The material property analysis is listed in the *Table 11 The material property analysis of steel and aluminium*:

Table 11 The material property analysis of steel and aluminium

	Stainless Steel	Aluminium alloy
Density (kg/m ³)	7750	2770
CTE ¹⁷ (1/°C)	1.7*10 ⁻⁵	2.3*10 ⁻⁵
Young's Modulus ¹⁸ (Pa)	1.93*10 ¹¹	7.1*10 ¹⁰
Hardness ¹⁹ (HV)	223 ²⁰	107 ²¹
Poisson's Ratio ²²	0.31	0.33
Specific heat capacity ²³ (J/(kg-°C))	480	875
Thermal Conductivity ²⁴ (W/m-K)	16	167

The ultra-precision machining community has generally accepted the premise that only some certain materials are “diamond turnable”²⁵ (Evans and Bryan,

¹⁷ CTE stands for Coefficient of Thermal Expansion

¹⁸ Young's modulus is the ratio of stress (which has units of pressure) to strain (which is dimensionless), and so Young's modulus has units of pressure.

¹⁹ Vickers Pyramid Number is then determined by the ratio F/A , where F is the force applied to the diamond in kilograms-force and A is the surface area of the resulting indentation in square millimetres.

²⁰ The hardness value for 347L stainless steel, Data from:
<http://asm.matweb.com/search/SpecificMaterial.asp?bassnum=MQ347AQ>

²¹ The hardness value for Aluminium 6061-T6, Data from:
<http://asm.matweb.com/search/SpecificMaterial.asp?bassnum=MA6061t6>.

²² Poisson's ratio, named after Siméon Poisson, is the negative ratio of transverse to axial strain.

²³ Specific Heat Capacity is the measurable physical quantity of heat energy required to change the temperature of an object per unit mass of a material.

²⁴ In physics, thermal conductivity (often denoted k , λ , or κ) is the property of a material to conduct heat.

1991). The generally accepted diamond turnable and unturnable materials are listed in the Appendices *Table B-1 The materials readily machinable by diamond turning (Gerchman, 1986)* and *Table B-2 The materials not readily machinable by diamond turning (Gerchman, 1986)*. It is well known that ferrous metals are not readily “diamond turnable” for the reason that carbon in the diamond tool chemically reacts with the substrate, leading to tool damage and dulling after short cut lengths.

Since the hardness of the stainless steel is much higher than that of the aluminium alloy, the temperature rise of the diamond tools when turning the steel components is relatively higher than those of the aluminium ones, which increases the machining error due to the thermal expansion on the condition that the difference of CTE values of both materials is not vary large.

The thermal conductivity of aluminium alloy is much higher than that of the stainless steel, which means it has better heat dissipation performance during the turning process. The wear of the diamond tools as well as the machining error due to the thermal expansion is greatly reduced when the aluminium alloy is being machined. Although the coolant, such as mineral oils and synthetic coolants²⁶, can be used to reduce the temperature rise, the basic properties, such as hardness and thermal conductivity, of two different materials still have the dominant effects on the thermal performance during the manufacturing process.

However, aluminium alloy has some poor apparent properties such as low hardness, low wear resistance and low corrosion resistance (Gu et al., 2011). So the protective layers, i.e. coatings, are used to enhance the limiting properties of the aluminium alloys. Nickel composites coatings are used in this project for the reason that aluminium can easily be coated with electroless

²⁵ Diamond turnable materials are those where the tool wear rate is low enough that reasonable areas of specular surface can economically be produced (Evans and Bryan, 1991).

²⁶ Source: http://en.wikipedia.org/wiki/Cutting_fluid#Types

nickel and, at elevated temperatures, aluminium is prone to diffuse and create a more integral bond (Forman et al., 2000). Electroless nickel coating is one of the most widely accepted coatings in engineering application due to its unique characteristics, including excellent corrosion, wear and abrasion resistance, ductility, lubrication, soldering, and electrical properties. These coatings are more uniform in thickness than electroplated nickel coatings (Sudagar et al., 2013).

3.2.2 THE COST ANALYSIS

A manufacturing cost analysis of the two materials is listed in the *Table 12 The cost analysis of materials of steel and aluminium*:

Table 12 The cost analysis of materials of steel and aluminium

	Stainless Steel	Aluminium alloy
Material price (£/tonne)	1400 ²⁷	1119 ²⁸
Each shaft material cost (£/10kg)	14.00	11.19
Manufacturing cost (£)	600	200
Coating cost (£)	/	300 ²⁹
Total cost (£)	614.00	511.19

From the table above, it is obviously concluded that the material price difference is not very noticeable due to the fact that the shaft of a hydrostatic system is not a heavy component. The average weight of the bearing shaft is about 5-10 kilograms, which means the material weight cost is just a small part of the whole manufacturing cost.

Traditionally, the machining of steel components has been the domain of grinding operation (Benga and Abrao, 2003). However precision hard turning has emerged as a viable alternative to grinding for finish machining of hardened steels (Sood et al., 2000). Since the early 1980s, hard turning has been applied in many cases in making bearings, gears, cams, shafts, axels, and other mechanical components. Compared with grinding technology, the greatest

²⁷ The price is the world hot rolled coil stainless steel price in Nov. 2013, Data from: <http://www.meps.co.uk/Stainless%20Prices.htm>

²⁸ The price is the LME official price in Dec. 2013, Data from: <http://www.lme.com/en-gb/metals/non-ferrous/aluminium/>

²⁹ The rough cost estimation of electroless nickel composite coating on a single aluminium alloy bearing shaft and a thrust plate (Anonymous1997). Electroless nickel is not pure metal but includes other element(s) also derived from the reducing agent, such as phosphorus or boron, or elements such as thallium, lead or cadmium derived from other bath additives (Sudagar et al., 2013).

difference between grinding and hard turning is that hard turning may induce a relatively deep surface compressive residual stress while achieving an equivalent or better surface finish, form, and size accuracy (Guo and Yen, 2004). Polycrystalline cubic boron nitride (PCBN) cutting tools³⁰ as well as some new ceramic tools supported by cutting fluid are now the most influential ways of machining a hard steel component. And even today, the processes of finishing the surfaces of the steel components are still a high-energy and cost-intensive grinding or turning one (König et al., 1993).

As mentioned before, there are some diamond turning machines in the laboratory of Cranfield University making ultra-precision machining operations feasible and at low cost. So Cranfield University is also researching coating techniques to apply to aluminium bearing components.

Since steel has a good performance in hardness and anti-corrosion properties, the shaft made of steel does not need to have a coating. Only the aluminium alloy bearing needs the electroless nickel composite coating. The estimation of the cost of the nickel-based coating is about £300 for each aluminium bearing shaft. The estimation is based on a relative project of coating on a 3m aluminium reel conducted by another PhD researcher, Mr P. Xia, in Cranfield University. In his project, the market price of coating a 25cm diameter by 300cm long aluminium reel is about £3000. The bearing spindle shaft and the thrust plate in the hydrostatic bearing systems of the R2R production system is about the same diameter and one tenth of the length as the aluminium reel in the Xia's project. The coating cost on the market mostly depends on the size of the components being coated. So the cost of the electroless nickel composite coating on a single aluminium alloy bearing shaft and a thrust plate is about £300.

³⁰ PCBN cutting tools provide longer tool life than ceramics, when turning 100Cr6 bearing steel, for a cutting speed range between 100 and 180 m/min and a feed rate range between 0.06 and 0.22 mm/rev (Benga and Abrao, 2003).

After the cost analysis of two materials, an initial conclusion has been made that the aluminium alloy has some advantages in production properties to reduce the manufacturing cost, but whether it can be used as a substitute of the steel shaft depends on the mechanical properties and the operational parameters during the actual working process of the hydrostatic bearing systems. The finite element modelling analysis and the experimental works in the next stage would show the feasibility of substituting the shaft material on the condition that no compromise of reducing the normal working specifications is allowed.

4 THEORETICAL CALCULATION OF HYDROSTATIC BEARINGS

4.1 CALCULATION FOR THE JOURNAL BEARING

Based on the equations listed in the chapter of *REVIEW OF THE THEORETICAL DESIGN APPLIED TO ULTRA-PRECISION SPINDLE*, the basic operational parameters of the bearing system were worked using the tools of the MS Excel spreadsheet software package.

For the journal bearing, its required radial working load is 1500N. Assuming the radial clearance is 20 μ m, the viscosity of the oil is 0.009Ns/m²(10.00cSt)³¹, to find the proper supply pressure (guarantee the value of the “Ultimate load capacity” being greater than 1500N), the supply pressure is at least 0.5MPa. For the safety consideration, the minimum supply pressure should be multiplied by a factor of safety of 3, so the supply pressure is 1.5MPa. The calculation process is illustrated in the following table:

Table 13 The initial theoretical calculation of the journal bearing of the R2R hydrostatic bearing system ($h_{L(av)}=20\mu\text{m}$, $p=1.5\text{MPa}$, $N=0\text{rpm}$, $\eta=10.00\text{cSt}$)

Number of pockets: $n=$	5
Diameter of bearing: $d_B=$	0.099800 m
Length of bearing: $L_B=$	0.059000 m
Width of axial land: $c_a=$	0.065000 m
Width of circumferential land: $c_c=$	0.013000 m
Radial clearance: $h_{L(av)}=$	0.000020 m
Depth of pocket: $h_p=$	0.000200 m
Supply Pressure: $p_1=$	1500000 Pa
Rotational speed: $N_d=$	0 rev/min
Resistance ratio: $\xi=$	1

³¹ Ns/m² is the unit of dynamic viscosity, the density of the oil is 0.9g/cm³, 1cP=0.001Ns/m², m²/s is the unit of kinematic viscosity, 1cSt=10⁻⁶m²/s, 1cSt=1cP/(g/cm³), 0.009Ns/m²=9cP/(0.9g/cm³)=10.00cSt

Viscosity of oil: η =	0.009	Ns/m ²
Density of oil: ρ =	900	kg/m ³
Specific Heat capacity of oil: C_m =	2000	J/(kg*K)
Constant: k =	0.6	
Bearing shape factor: Φ =	0.753099	
Bearing shape factor: E_a =	0.559322	
Bearing shape factor: E_c =	0.170315	
Outflow resistance: R_{od} =	14000.931800	10 ⁸ Ns/m ⁵
Inflow resistance: R_i =	14000.931800	10 ⁸ Ns/m ⁵
Ultimate load capacity: W_u =	4544.042007	N
Radial stiffness: S_l =	3.156621	10 ⁸ N/m
Flow: Q =	2.671697	10 ⁻⁶ M ³ /s
Pumping power: P_p =	4.007546	W
Frictional power: P_f =	0.00	W
Temperature rise: $\Delta t \approx$	0.833	°C

The working range of the rotational speed of the R2R hydrostatic bearing system is 0~300 rpm. By the Excel spreadsheet, the relationship between the rotational speed and the temperature rise for the journal bearing is showed in the follow table:

Table 14 The theoretical relationship between the rotational speed and the temperature rise for the journal bearing of the R2R hydrostatic bearing system ($h_{L(av)}=20\mu\text{m}$, $p=1.5\text{MPa}$, $\eta=10.00\text{cSt}$)

The rotational speed (rpm)	Temperature rise (°C)
0	0.833
50	0.953
100	1.313
150	1.911
200	2.750
250	3.828
300	5.146

Under the upper limit of the rotational speed, 300rpm, the temperature rise of the oil within the journal bearing will be 5.146°C. From the *Table 11 The material property analysis of steel and aluminium*, since the coefficient of thermal expansion of aluminium alloy is $2.3 \times 10^{-5}/^{\circ}\text{C}$, the thermal expansion can be calculated in *Equation 29*:

$$\text{Thermal expansion} \quad L = \alpha \times L_1(T_2 - T_1) \quad \text{Equation 29}$$

Where

L=Linear Expansion

L_1 =Initial Length

α =Coefficient of Linear expansion of the Material

T_1 =Initial Temperature

T_2 =Final Temperature

For $T_2 - T_1 = 5.146^{\circ}\text{C}$ and the initial length is 0.0499m, the linear expansion of the aluminium alloy is 5.906 μm , which is about 30% of the radial clearance.

However, the thermal expansion happens not only in the bearing shaft components, but also in the bearing house. Both of the rotor and housing expand as the temperature rises.

As illustrated in the *Table 10 The relationship within the parameters of the hydrostatic bearings*, the temperature rise is determined by the *Equation 25, Equation 26, Equation 27, Equation 28*. To lower the temperature rise, the ways of increasing the supply pressure, increasing the radial clearance, decreasing the viscosity of the oil are all the appropriate choice.

The following table shows several appropriate combinations of the parameters at the rotational speed of 300rev/min and the temperature rise being less than 3°C.

Table 15 The appropriate combinations of the parameters to meet the demand of the journal bearing system ($h_{L(av)}=20\mu\text{m}$, $N=300\text{rpm}$, temperature rise $<3^\circ\text{C}$)

$h_{L(av)}=20\mu\text{m}$, $N=300\text{rpm}$	Set 1	Set 2	Set 3	Set 4	Set 5
Supply pressure (MPa)	0.4	0.5	1	1.5	3
Viscosity of oil (Ns/m^2)	0.0037	0.0041	0.0055	0.0063	0.0070
Viscosity of oil (cSt)	4.11	4.56	6.11	7.00	7.78
Temperature rise ($^\circ\text{C}$)	2.955	2.963	2.971	2.946	2.971
Ultimate load capacity (N)	1211.7	1514.7	3029.4	4544.0	9088.1

The relationship between the temperature rise and the rotational speed under the $30\mu\text{m}$ clearance is showed in the following table:

Table 16 The theoretical relationship between the rotational speed and the temperature rise for the journal bearing of the R2R hydrostatic bearing system ($h_{L(av)}=30\mu\text{m}$, $p=1.5\text{MPa}$, $\eta=10.00\text{cSt}$)

The rotational speed (rpm)	Temperature rise ($^\circ\text{C}$)
0	0.833
50	0.857
100	0.928
150	1.045
200	1.210
250	1.422
300	1.682

Obviously, when the shaft reaches 300rpm , the temperature rise is 1.682°C , which is almost half of the limit temperature rise. So, the combination of the viscosity of 10.00cSt and the supply pressure of 1.5MPa meets the demand quite well. The following table shows several appropriate combinations of the parameters of the supply pressure and the viscosity at 300rev/min and the temperature rise being less than 3°C .

Table 17 The appropriate combinations of the parameters to meet the demand of the journal bearing system ($h_{L(av)}=30\mu\text{m}$, $N=300\text{rpm}$, temperature rise $<3^\circ\text{C}$)

$h_{L(av)}=30\mu\text{m}$, $N=300\text{rpm}$	Set 1	Set 2	Set 3	Set 4	Set 5
---	-------	-------	-------	-------	-------

Supply pressure (MPa)	0.4	0.5	1	1.5	3
Viscosity of oil (Ns/m ²)	0.0084	0.0093	0.0124	0.0143	0.0159
Viscosity of oil (cSt)	9.33	10.33	13.78	15.89	17.67
Temperature rise (°C)	2.994	2.995	2.971	2.975	2.991
Ultimate load capacity (N)	1211.7	1514.7	3029.4	4544.0	9088.1

To have the theoretically minimum energy consumption, the ultimate load capacity shall be greater than 1500N, so the most energy-saving and efficient combination is “Set 2” for both $h_{L(av)}=20\mu\text{m}$ and $h_{L(av)}=30\mu\text{m}$ on the condition that the viscosity of oil is 4.56cSt and 10.33cSt respectively and the supply pressure is 0.5MPa.

But in real operational condition, the supply pressure shall be set much higher due to the safety consideration. Timing a factor of safety of 3 to guarantee that there is no extra contact or friction under any extreme condition is a good way to protect the system. 1.5MPa has already been proved feasible in the *Table 16 The theoretical relationship between the rotational speed and the temperature rise for the journal bearing of the R2R hydrostatic bearing system ($h_{L(av)}=30\mu\text{m}$, $p=1.5\text{MPa}$, $h=10.00\text{cSt}$).*

4.2 CALCULATION FOR THE THRUST BEARING

For the thrust bearing, its required axial working load is 500N. Assuming the clearance at the lands of each thrust pad at no load is 20 μ m, the viscosity of the oil is 0.009Ns/m² (10.00cSt), the rotational speed is 0 for the initial condition, the proper supply pressure (guarantee the value of the “Ultimate load capacity” being greater than 500N) shall be at least 0.3MPa, taking the factor of safety 3 into consideration. The calculation is showed in the following table:

Table 18 The initial theoretical calculation of the thrust bearings of the R2R hydrostatic bearing system ($h_{L(av)}=20\mu\text{m}$, $p=0.3\text{MPa}$, $N=0\text{rpm}$, $\eta=10.00\text{cSt}$)

Outer diameter of thrust pad: $D_B=$	0.163725	m
Outer diameter of annular pocket: $D_P=$	0.145000	m
Inner diameter of annular pocket: $d_P=$	0.135000	m
Inner diameter of thrust pad: $d_B=$	0.120000	m
Clearance at the lands of each thrust pad at no load: $h_d=$	0.000020	m
Clearance at the pocket: $h_P=$	0.000200	m
Supply pressure: $p_1=$	100000	Pa
Speed of rotation: $n=$	0	rev/min
Resistance ratio: $\xi=$	1	
Viscosity of the fluid: $\eta=$	0.009	Ns/m ²
Density of oil: $\rho=$	900	kg/m ³
Specific Heat capacity of oil: $C_m=$	2000	J/(kg*K)
Ratio ξ_2/ξ_1 for a pair of opposed plane pads or rotary thrust bearings: $\Xi=$	1	
Ratio A_{v2}/A_{v1} for a pair of opposed plane pads or rotary thrust bearings: $T=$	1	
Virtual area of the thrust pad: $A_{v2}=A_{v1}=$	0.005935	M ²
$R_{o(1)}=$	26.108838	10 ¹⁰ Ns/m ⁵
$R_{o(2)}=$	25.319602	10 ¹⁰ Ns/m ⁵
Outflow resistance: $R_{o(net)}=$	12.854082	10 ¹⁰ Ns/m ⁵
Inflow resistance: $R_i=$	12.854082	10 ¹⁰ Ns/m ⁵
Ultimate thrust capacity: $T_{(net)}=$	1582.780055	N

Stiffness: $S_T =$ when $h_{(1)}=h_d$	1.335471	10^8N/m
Flow: $Q =$	1.166944	$10^{-6} \text{M}^3/\text{s}$
Total Pumping power: $P_p =$	0.700167	W
Total Frictional power: $P_f =$	0.000000	W
Temperature rise: $\Delta t \approx$	0.167	K

The working range of the rotational speed of the R2R hydrostatic bearing system is 0~300 rpm. The relationship between the rotational speed and temperature rise for the thrust bearing is shown in the following table:

Table 19 The theoretical relationship between the rotational speed and the temperature rise for the thrust bearings of the R2R hydrostatic bearing system ($h_d=20\mu\text{m}$, $p=0.3\text{MPa}$, $\eta=10.00\text{cSt}$)

The rotational speed (rpm)	Temperature rise ($^{\circ}\text{C}$)
0	0.167
50	0.643
100	2.071
150	4.451
200	7.784
250	12.069
300	17.305

The temperature rise of the oil within the thrust bearing at 300rpm is 17.305°C . From the *Table 11 The material property analysis of steel and aluminium*, the coefficient of thermal expansion of aluminium alloy is $2.3 \times 10^{-5}/^{\circ}\text{C}$, the thermal expansion can be calculated by *Equation 29*.

At $T_2 - T_1 = 17.305^{\circ}\text{C}$ and the initial length of 0.0537m , the linear expansion of the aluminium alloy is $21.37\mu\text{m}$, which is larger than the radial clearance. So this temperature rise is not allowed for it will cause the collapse of the hydrostatic bearing system at 300rpm. As a result, this specific combination of the parameters for the journal bearing is not recommended.

As explained in the previous texts, increasing the supply pressure, increasing the radial clearance, or decreasing the viscosity of the oil are the ways to improve the hydrostatic bearing system's heat condition. The maximum

temperature rise should be controlled at 3°C. The following table shows several appropriate combinations of the parameters of the supply pressure and the viscosity at 300rev/min, 20 μ m and the temperature rise being less than 3°C.

Table 20 The appropriate combinations of the parameters to meet the demand of the thrust bearing system ($h_d=20\mu\text{m}$, $N=300\text{rpm}$, temperature rise $<3^\circ\text{C}$)

$h_d=20\mu\text{m}$, $N=300\text{rpm}$	Set 1	Set 2	Set 3	Set 4	Set 5
Supply pressure (MPa)	0.1	0.2	0.5	1	2
Viscosity of oil (Ns/m ²)	0.0021	0.0030	0.0046	0.0062	0.0077
Viscosity of oil (cSt)	2.33	3.33	5.11	6.89	8.56
Temperature rise (°C)	2.855	2.968	2.964	2.996	2.993
Ultimate thrust capacity (N)	527.6	1055.2	2638.0	5275.9	10551.9

If the initial clearance is 30 μ m, the relationship between the temperature rise and the rotational speed is showed in the following table:

Table 21 The theoretical relationship between the rotational speed and the temperature rise for the thrust bearings of the R2R hydrostatic bearing system ($h_d=30\mu\text{m}$, $p=0.3\text{MPa}$, $\eta=10.00\text{cSt}$)

The rotational speed (rpm)	Temperature rise (°C)
0	0.167
50	0.262
100	0.548
150	1.024
200	1.691
250	2.549
300	3.597

The temperature rise slightly exceeds 3°C. Whether this combination of supply pressure (0.3MPa) and viscosity (10.00cSt) is suitable or not should be analysed by further experimental works.

The following table shows several appropriate combinations of the parameters of the supply pressure and the viscosity at 300rev/min, and the temperature rise being less than 3°C.

Table 22 The appropriate combinations of the parameters to meet the demand of the thrust bearing system ($h_d=30\mu\text{m}$, $N=300\text{rpm}$, temperature rise $<3^\circ\text{C}$)

$h_d=30\mu\text{m}$, $N=300\text{rpm}$	Set 1	Set 2	Set 3	Set 4	Set 5
Supply pressure (MPa)	0.1	0.2	0.5	1	2
Viscosity of oil (Ns/m^2)	0.0048	0.0067	0.0103	0.0138	0.0172
Viscosity of oil (cSt)	5.33	7.44	11.44	15.33	19.11
Temperature rise ($^\circ\text{C}$)	2.983	2.963	2.974	2.975	2.991
Ultimate thrust capacity (N)	527.6	1055.2	2638.0	5275.9	10551.9

To meet the load capacity demand, the ultimate thrust capacity should be greater than 500N. Theoretically, most energy-saving and efficient combination is Set 1 for both $h_d=20\mu\text{m}$ and $h_d=30\mu\text{m}$ at 2.33cSt, 5.33cSt respectively and 0.1MPa.

But in real operational condition, the supply pressure needs to be set much larger, setting a factor of safety of 3, to guarantee not any extra contact or friction under some extreme condition. However, the 0.3MPa is still considered to be low for the normal supply pressure of the hydrostatic bearing system, which is about 1~3MPa and it is not suitable in the condition of $20\mu\text{m}\sim 30\mu\text{m}$ and 10cSt. So the feasibility of larger supply pressure of the thrust bearings as well as the viscosity, such as 15cSt, needs to be analysed by further experimental works.

5 FEA OF BEARING COMPONENTS

FEA (finite element analysis) is a traditional analysis method to analyse the dynamic behaviour of the fluid within the hydrostatic thrust bearing about three decades ago (Prabhu and Ganesan, 1984). Finite Element Modelling and Analysis is considered as a good tool for predicting the system's behaviour related to the required performance in the high-precision field (Mekid, 2000). It has a good approximation to the real experimental results to predict the real condition of the forced components (Silva Mamede et al., 2013).

Finite element analysis is helpful to better understand and predict various variables in the hydrostatic bearing systems (Kagnaya et al., 2014). For example, static deformation has been achieved by FEA method to determine the deformation of the mechanical parts.

FEA software available on the market includes Abaqus³², ANSYS³³, LUSAS³⁴, Nastran³⁵ et al. The reason why this individual research project chooses ANSYS as the analysis software is because it is easier to use for the beginner and it doesn't require users to have high-level understanding of either mechanics or finite elements necessarily.

For a level of application engineering analysis, the ANSYS provides complete material data information, does well with minimal user input, easily handles the complex geometries and creates very little mesh generation hassles, etc. Solutions can be done in short orders and the parameters of the mesh quality can be adjusted simply. So the ANSYS is the very suitable software to solve this closely industrial-related research project of simulating the deformation condition of the hydrostatic bearing systems.

³² Abaqus is an advanced Franco-USA software from SIMULIA, owned by Dassault Systemes.

³³ ANSYS is a USA software.

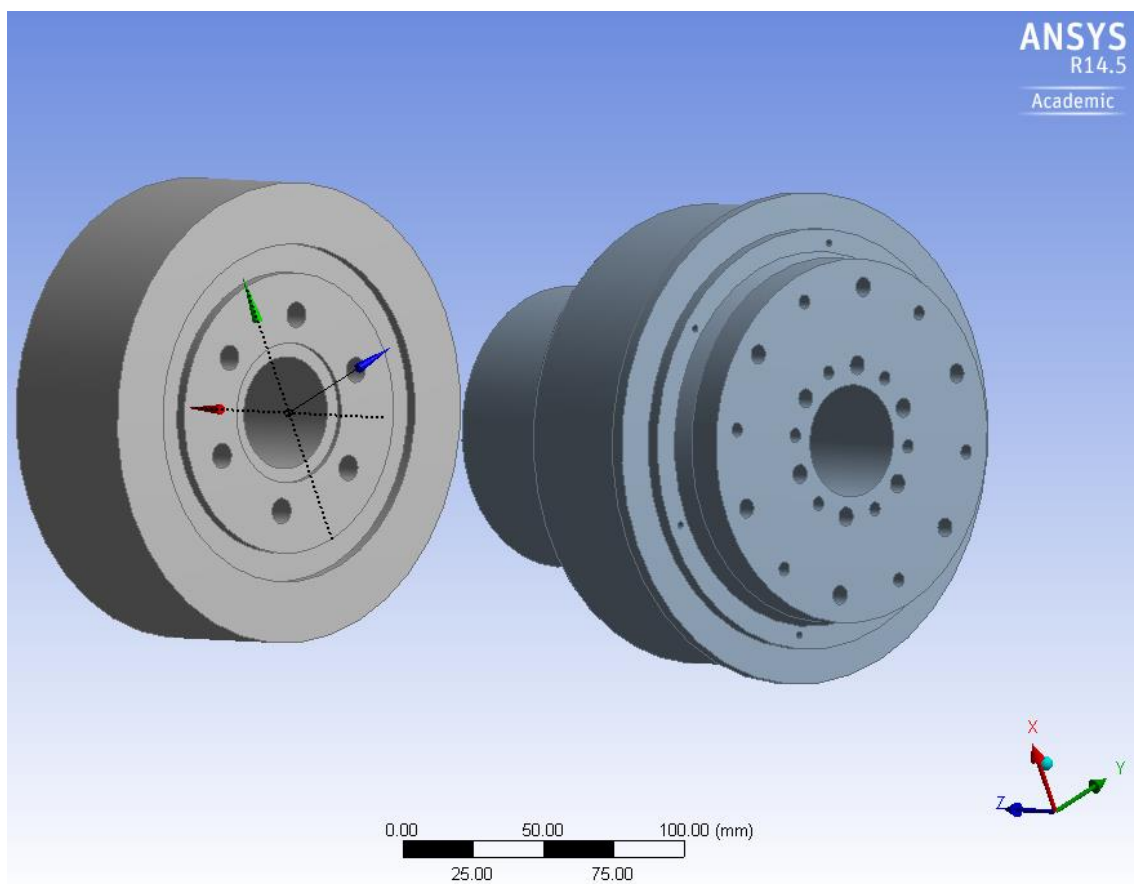
³⁴ LUSAS is a UK software.

³⁵ Nastran is a USA software, from MSC Software.

5.1 MODELLING OF THE BEARING SHAFT AND THRUST PLATES

The following two pictures are the ANSYS FEA modelling of the shaft and the thrust plate of the hydrostatic bearing system for the plastic electronics reel to reel production system. All the dimensions come from the original drafts of the bearing system³⁶ designed by Cranfield University.

Figure 12 The initial design of the shaft of the hydrostatic bearing system for the ultra-precision plastic electronics production systems (Separated)

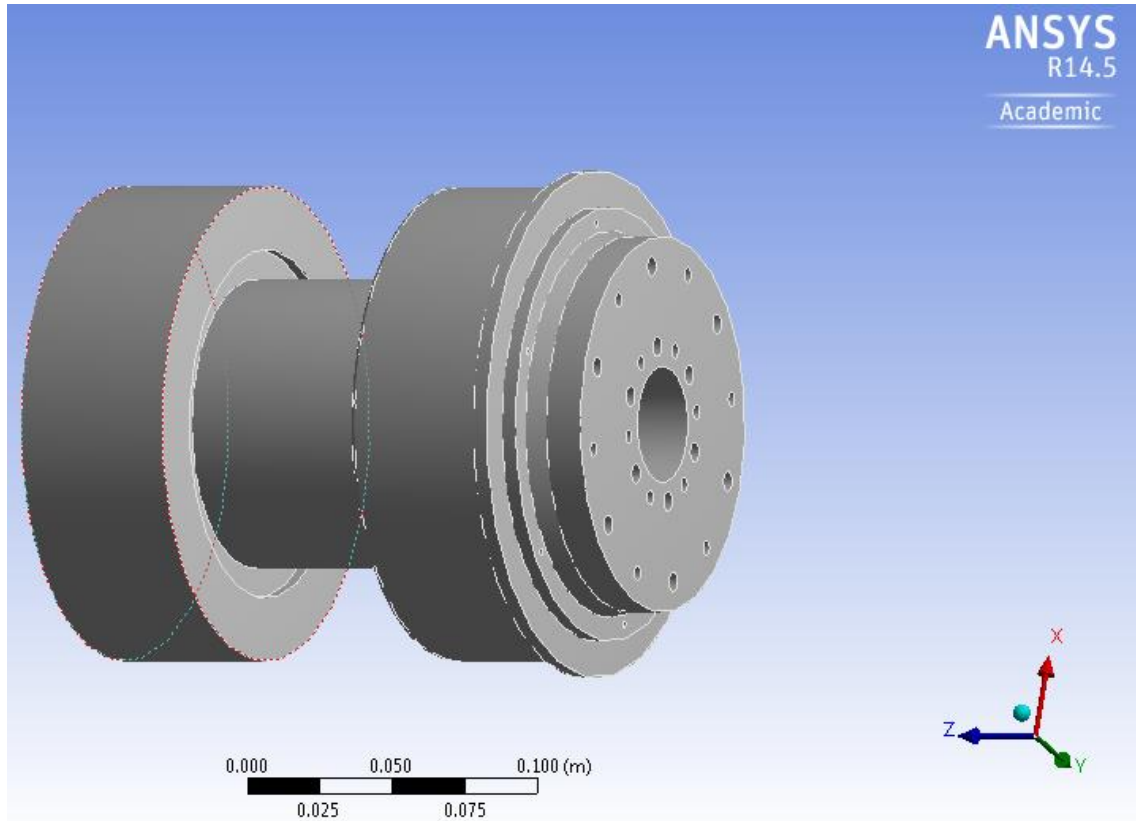


The two parts are bolted together to be a hydrostatic bearing with a journal bearing in the middle and two identical thrust bearings opposite to each other, which was showed in the *Figure 13 The initial design of the shaft of the*

³⁶ The copyright of the drafts belongs to the Precision Engineering Institute of Cranfield University.

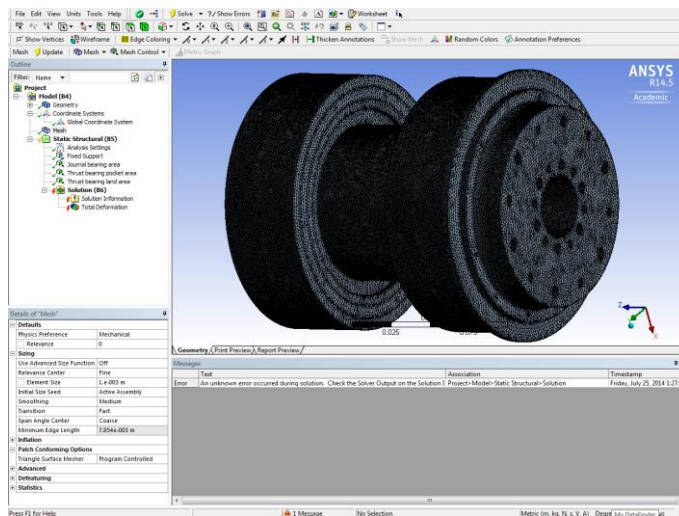
hydrostatic bearing system for the ultra-precision plastic electronics production systems (Bolted together).

Figure 13 The initial design of the shaft of the hydrostatic bearing system for the ultra-precision plastic electronics production systems (Bolted together)



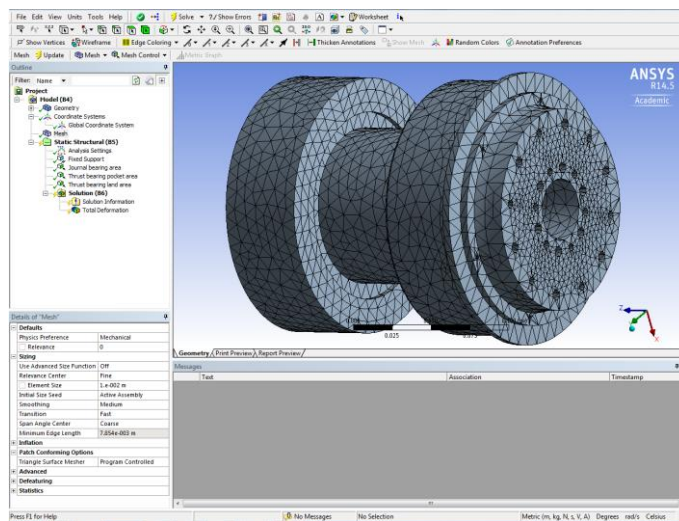
For the meshing part, the different element-size meshing conditions are showed in the following figures.

Figure 14 0.001m element size meshing



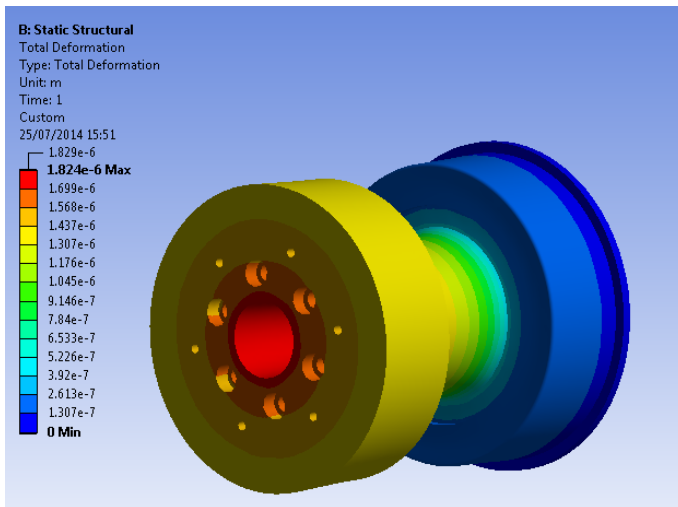
For this very small element size, the solution process of the ANSYS software will take quite a long time. And sometimes there is some error with the final calculation results. So this mesh element size is not recommended.

Figure 15 0.01m element size meshing



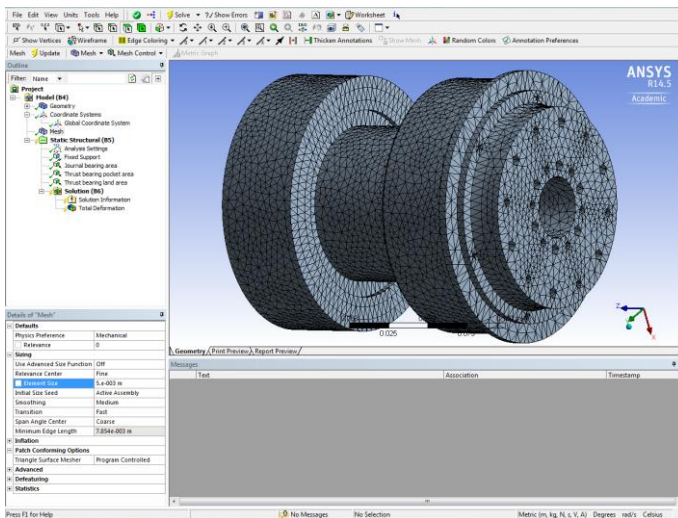
From the figure above, the meshing element size is relatively coarse. The FEA modelling results based on this element size are showed in the following figure.

Figure 16 The FEA results with element size of 0.01m



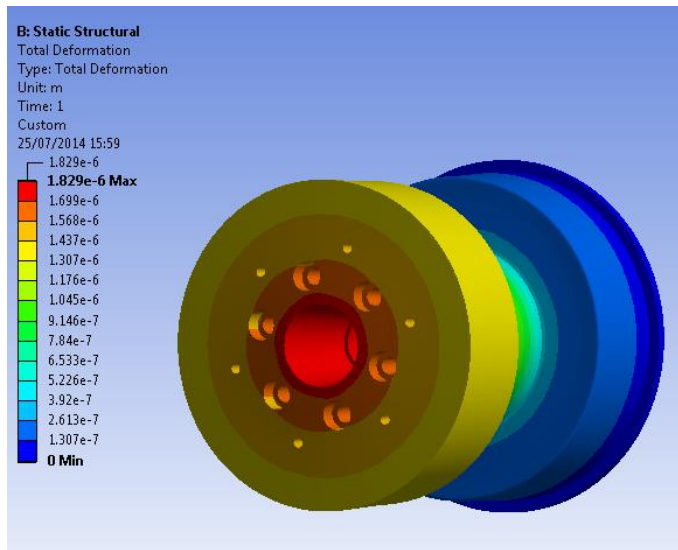
The following figure shows the meshing condition of element size of 0.005m, which is the mid value of 0.01m and 0.001m.

Figure 17 0.005m element size meshing



The FEA modelling results under the same pressure condition of the previous simulation are showed in the following figure.

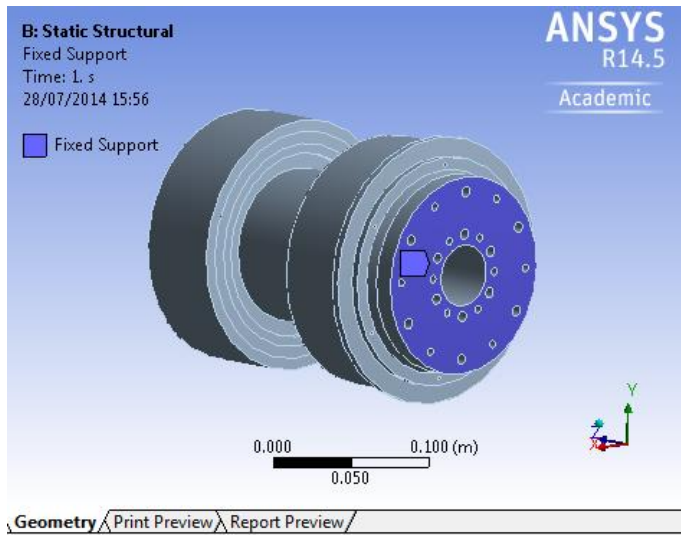
Figure 18 The FEA results with element size of 0.005m



From the figures above, the simulated deformation conditions of both the 0.005m element size and 0.001m element are almost the same and the 0.005m element size simulation costs less time and less computer work. So the meshing size of 0.005m is chosen as the final simulation value.

The fixed (constrained) surface is chosen as the blue highlighted surface of the bearing spindle in *Figure 19 The fixed support face of the bearing spindle*. Onto the spindle is bolted a motor at the opposite side to the indicated blue shaft surface. The blue surface is the mounting surface and it is considered as a non-deformation surface. For this reason, this surface is chosen as the fixed (constrained) surface. The fixed support surface is the boundary condition of the FEA modelling and will make the simulation results convergent values.

Figure 19 The fixed support face of the bearing spindle



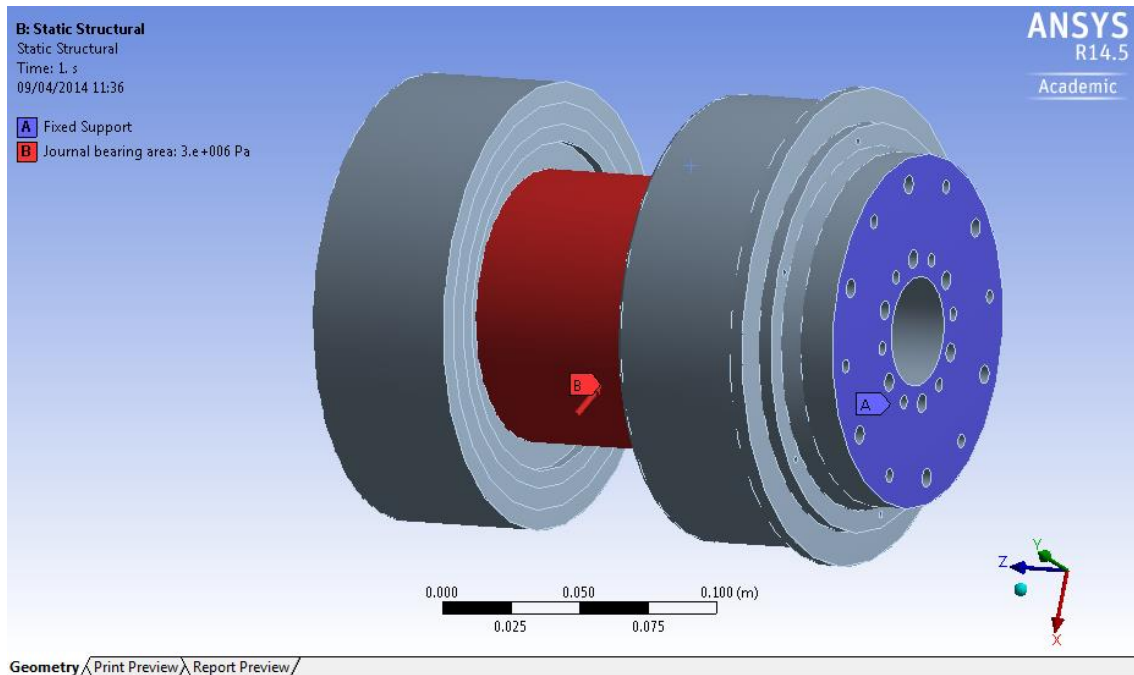
5.2 THE FEA DEFORMATION ANALYSIS FOR THE HYDROSTATIC BEARING SYSTEM

The Static Structural module is used in this FEA process. Although the pocket pressure will change in working condition, the maximum supply pressure is used to analyse the maximum deformation of the components. Under max-pressure condition, the Static Structural module of ANSYS software is the most suitable module for solving the problem. Because it not only reflects the max-pressure condition, but also greatly reduces the calculation time of solution process.

5.2.1.1 THE FEA DEFORMATION ANALYSIS FOR THE JOURNAL BEARING

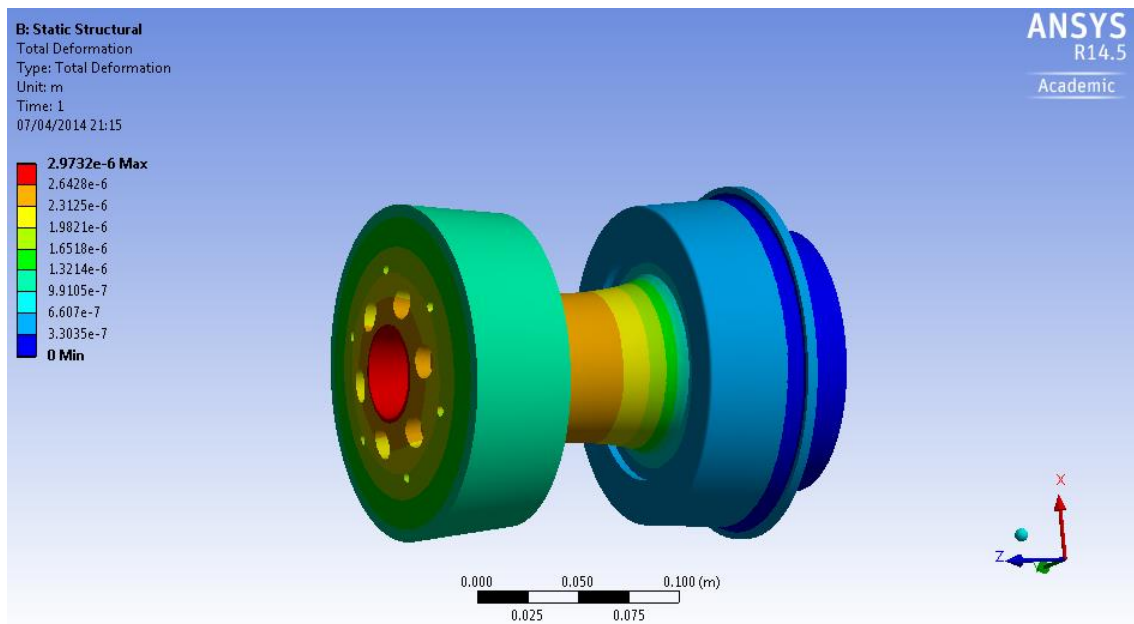
The red area in *Figure 20* The journal bearing area is the journal bearing area to be analysed.

Figure 20 The journal bearing area under the pressure of 3MPa



As shown in *Table 15* The appropriate combinations of the parameters to meet the demand of the journal bearing system ($hL(av)=20\mu\text{m}$, $N=300\text{rpm}$, temperature rise $<3^\circ\text{C}$), the supply pressure is chosen as the largest one, 3MPa, and the material of the bearing is selected as aluminium alloy, the total deformation of the component is showed in the *Figure 21* The total deformation of the journal bearing under the pressure of 3MPa below.

Figure 21 The total deformation of the journal bearing under the pressure of 3MPa



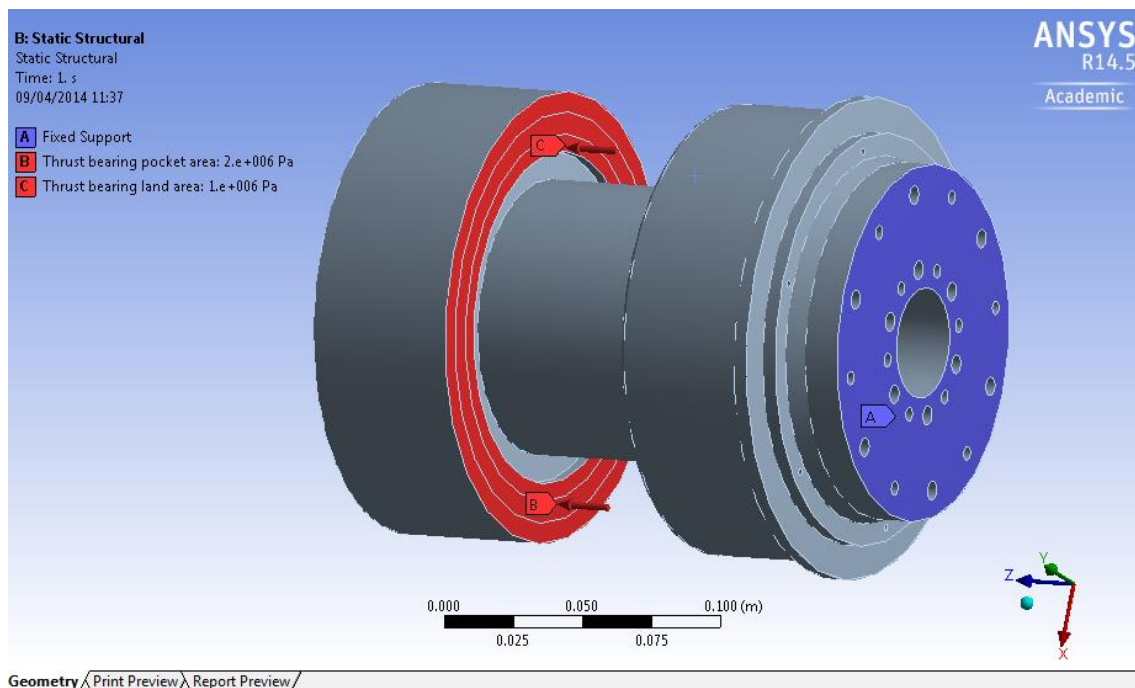
From the figure above, the maximum deformation, i.e. the red part, happens in the middle of the bearing thrust plate, whose value is about $2.973\mu\text{m}$. Since it is an inward deformation, it will not cause extra wear or friction to the inner surface of the pocket house. In the area of green or yellow colour, the deformation is even smaller, about $2\mu\text{m}$ and also inward direction.

So from the FEA modelling analysis, the aluminium bearing shaft is capable of the supply pressure of 3MPa and its deformation will not influence the normal working of the hydrostatic bearing system. But the deformation will slightly increase the flow rate at some level due to the small increase of the radial clearance.

5.2.1.2 THE FEA DEFORMATION ANALYSIS FOR THE THRUST BEARING

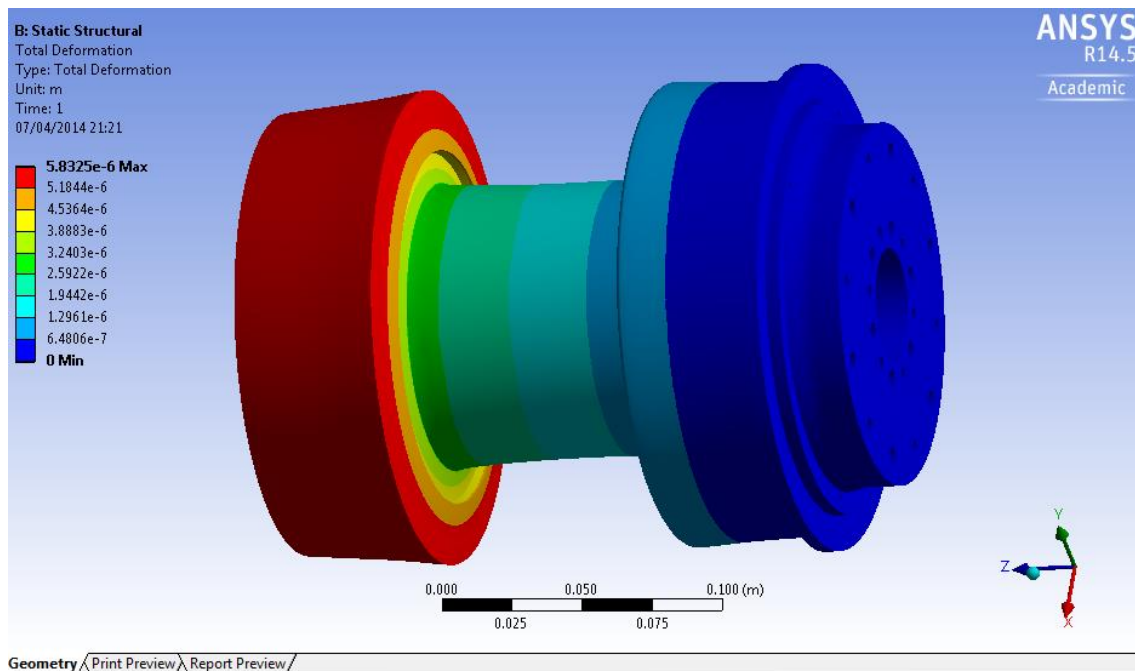
The middle circular ring of the red area in the following figure is the thrust bearing pocket area, and the inner and outer rings of the red area is the land area of the thrust bearing plate. The pocket area and the land area will be applied different pressure to analyse the deformation condition due to the decrease of the pocket pressure.

Figure 22 The thrust bearing area under the pocket area pressure of 2MPa and the average land area pressure of 1MPa



As recommended in the *Table 20* The appropriate combinations of the parameters to meet the demand of the thrust bearing system ($hd=20\mu\text{m}$, $N=300\text{rpm}$, temperature rise $<3^\circ\text{C}$), the supply pressure in the pocket area is 2MPa, the average pressure in the land area is 1MPa, and the material of the bearing is selected as aluminium alloy, the total deformation of the component is shown in the *Figure 23* The total deformation of the thrust bearing under the pocket area pressure of 2MPa and the average land area pressure of 1MPa below.

Figure 23 The total deformation of the thrust bearing under the pocket area pressure of 2MPa and the average land area pressure of 1MPa

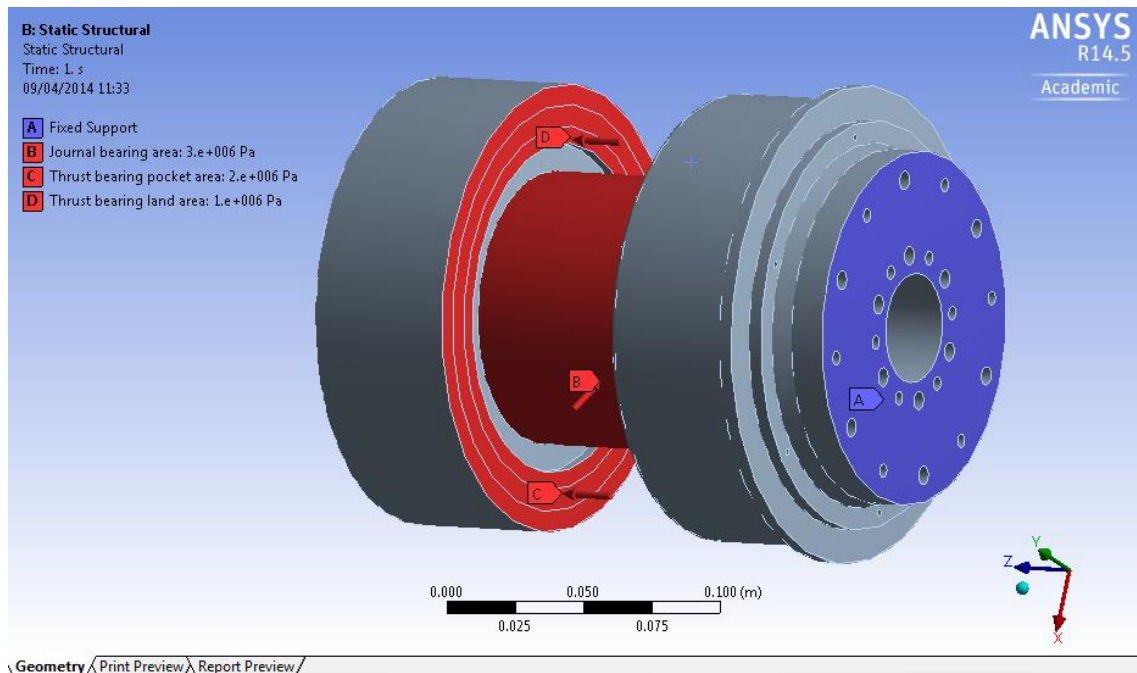


From the figure above, the maximum deformation, i.e. the red part, happens in the edge of the thrust plate, $5.833\mu\text{m}$, which is about one-fourth of the clearance of $20\mu\text{m}$. According to the FEA modelling analysis, the aluminium bearing thrust plate is capable of the pocket area pressure of 2MPa and the land area pressure of 1MPa. Its total deformation will not influence the normal working of the hydrostatic bearing system, but will increase the flow rate at some level due to the increase of the clearance between the land area and the inner surface of the bearing house.

5.2.1.3 THE FEA DEFORMATION ANALYSIS FOR BOTH THE THRUST BEARINGS AND THE JOURNAL BEARING

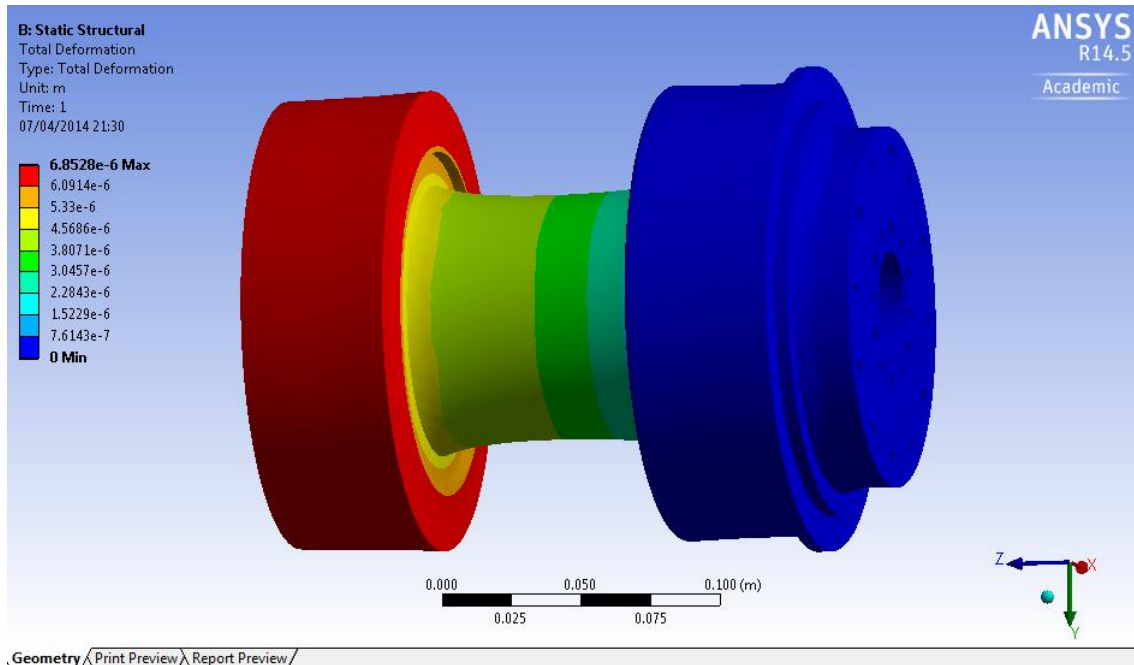
Combining two pressure conditions together, 3MPa on the journal bearing area, 2MPa on the thrust plate pocket area, and 1MPa on the thrust plate land area, the pressure condition is shown in *Figure 24* The overall pressure condition for the combination of journal bearing pressure 3MPa, thrust plate pocket area pressure 2MPa, and the thrust plate land area pressure 1MPa.

Figure 24 The overall pressure condition for the combination of journal bearing pressure 3MPa, thrust plate pocket area pressure 2MPa, and the thrust plate land area pressure 1MPa



The total deformation analysis solution of the bearing system is showed in the following figure.

Figure 25 The total deformation for the combination of journal bearing pressure 3MPa, thrust plate pocket area pressure 2MPa, and the thrust plate land area pressure 1MPa



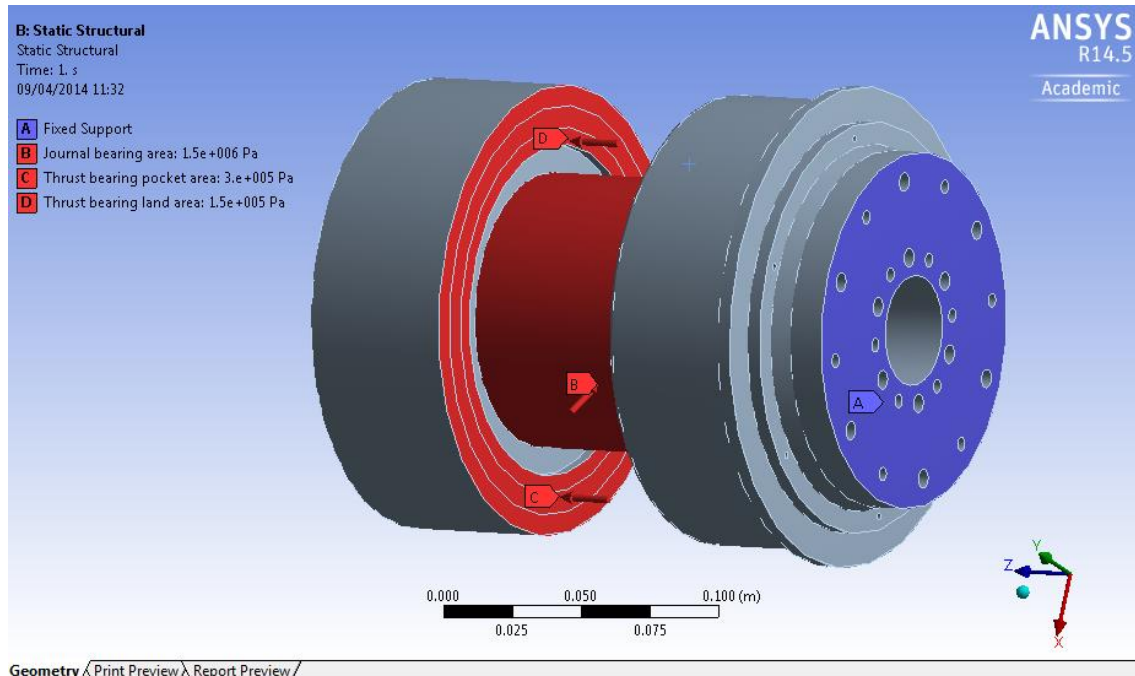
The maximum deformation happens in the edge of the thrust plate, which is about 6.853 μ m.

Under 20 μ m and less than 3 $^{\circ}$ C, the 6.853 μ m is about 34.3% of the clearance. As a result, whether the pressure and the oil viscosity are appropriate or not needs to be analysed in further experimental works.

For the clearance of 30 μ m and the temperature rise smaller than 3 $^{\circ}$ C, the 6.853 μ m is about 22.8% of the clearance. Similarly, whether the combination is feasible or not needs to be analysed in further experimental works.

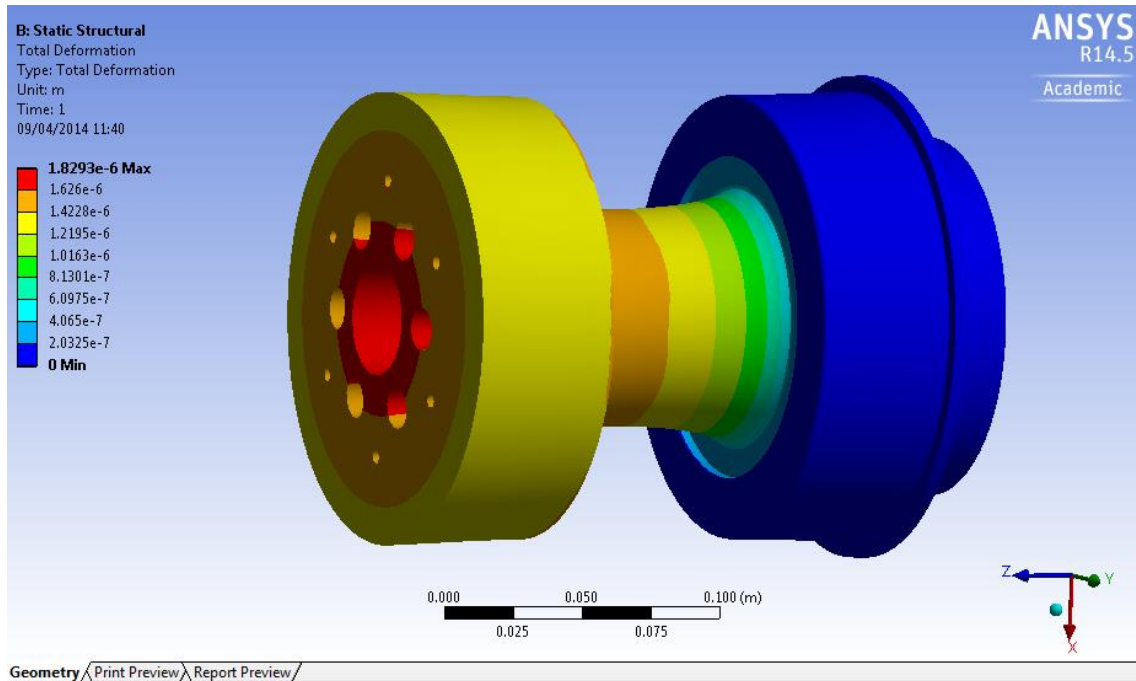
Considering the 3 times factor of safety, the pressure on the journal area is 1.5MPa, the pressure on the thrust pocket area is 0.3MPa and the pressure on the thrust land area is 0.15MPa, the overall pressure condition is shown in *Figure 26 The overall pressure condition for the combination of journal bearing pressure 1.5MPa, thrust plate pocket area pressure 0.3MPa, and the thrust plate land area pressure 0.15MPa.*

Figure 26 The overall pressure condition for the combination of journal bearing pressure 1.5MPa, thrust plate pocket area pressure 0.3MPa, and the thrust plate land area pressure 0.15MPa



The total deformation analysis solution of the bearing system is shown in *Figure 27*. The total deformation for the combination of journal bearing pressure 1.5MPa, thrust plate pocket area pressure 0.3MPa, and the thrust plate land area pressure 0.15MPa. Due to the neutralization of the displacement generated separately by the pressure on journal bearing and the thrust bearing, the maximum deformation, about 1.829 μ m, does not happen on the edge of the thrust plate but in the middle of it, which will cause less effect on the normal working process and will probably not cause the extra friction or contact inside the bearing house. So, the combination of relatively larger journal bearing pressure and smaller thrust bearing pressure will tend to neutralize the deformation conditions and partly strengthen the performance of the hydrostatic bearing system.

Figure 27 The total deformation for the combination of journal bearing pressure 1.5MPa, thrust plate pocket area pressure 0.3MPa, and the thrust plate land area pressure 0.15MPa

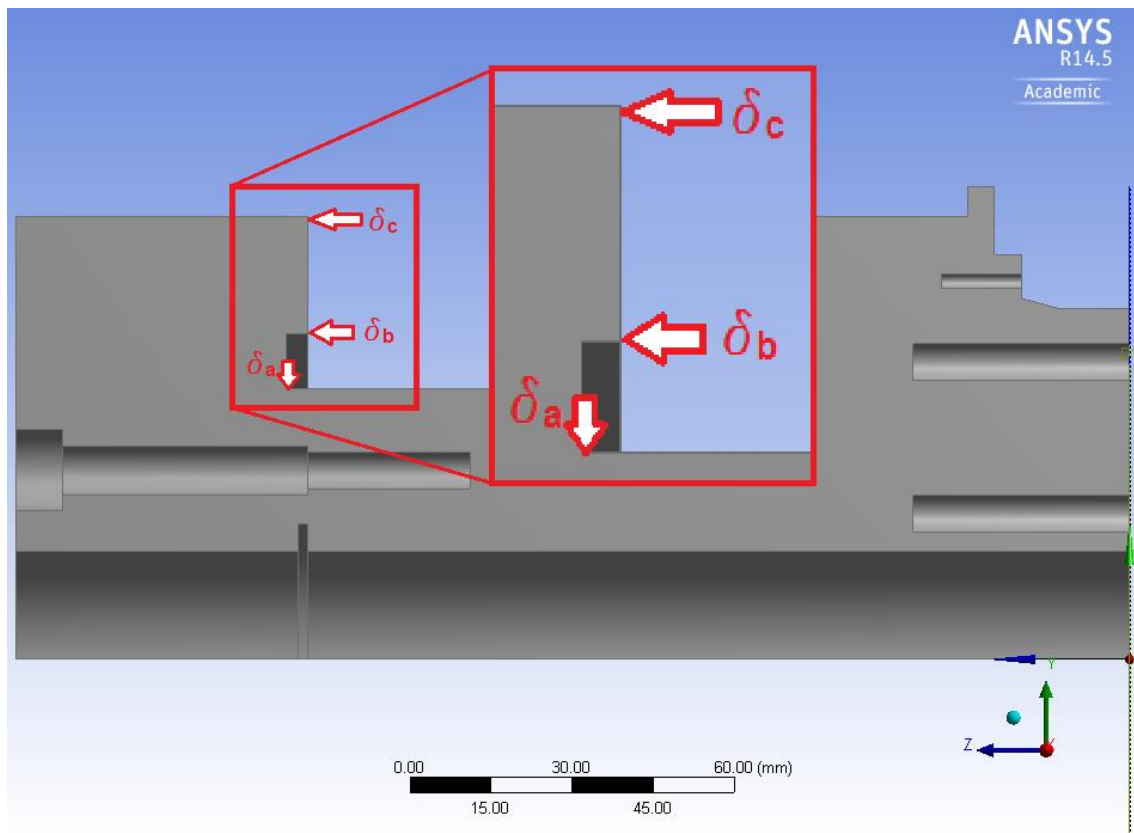


5.2.1.4 THE FEA ANALYSIS RESULTS OF THE TABLES OF SOME SETS OF THE COMBINATIONS OF SUPPLY PRESSURE AND OIL VISCOSITY

After the optimization works done in the previous sections, the viscosity of oil is selected as two values, 5cSt and 10cSt. For each of these two viscosities, set the journal supply pressure as 1.5MPa, 3MPa and 5MPa, the thrust bearing pocket pressure as 0.3MPa, 0.5MPa and 1MPa.

Set δ_a , δ_b , and δ_c as three observation points to analyse the deformation condition of the hydrostatic bearing, which is showed in the following figure. δ_a is the radial clearance of the journal bearing, δ_b is the minimum deformation place of the thrust plate and δ_c is the maximum deformation place of the thrust plate.

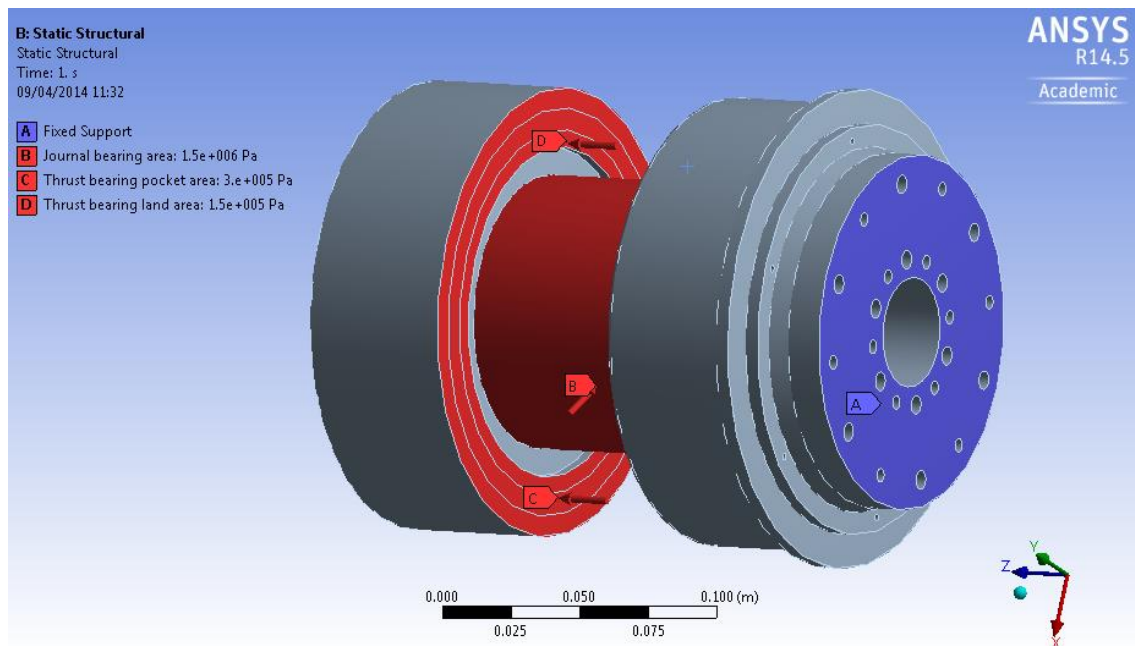
Figure 28 Three deformation analysis points



According to Equation 8 and Equation 17, the value of the flow rate is proportional to the cube of the bearing clearance. So after the deformation, the actual clearances both in journal bearing and thrust bearing will be larger than the nominal clearance, which means the actual flow rate will be larger than the nominal flow rate as well as the temperature rise is smaller than the nominal value. So the values of the nominal clearance, actual clearance, nominal flow rate, actual flow rate, nominal temperature rise, and actual temperature rise for both journal bearing and thrust bearing are also showed in the FEA results tables.

For the Set 1 analysis ($h_c=20\mu\text{m}$, $\eta=5\text{cSt}$ $P_{\text{journal}}=1.5\text{MPa}$, $P_{\text{thrust pocket}}=0.3\text{MPa}$, $P_{\text{thrust land}}=0.15\text{MPa}$, $N=300\text{rpm}$), as showed in the follow figures, the deformation of $\delta_a=1.307\mu\text{m}$, $\delta_b=1.437\mu\text{m}$, and $\delta_c=1.307\mu\text{m}$.

Figure 29 The pressure condition for Set 1 analysis



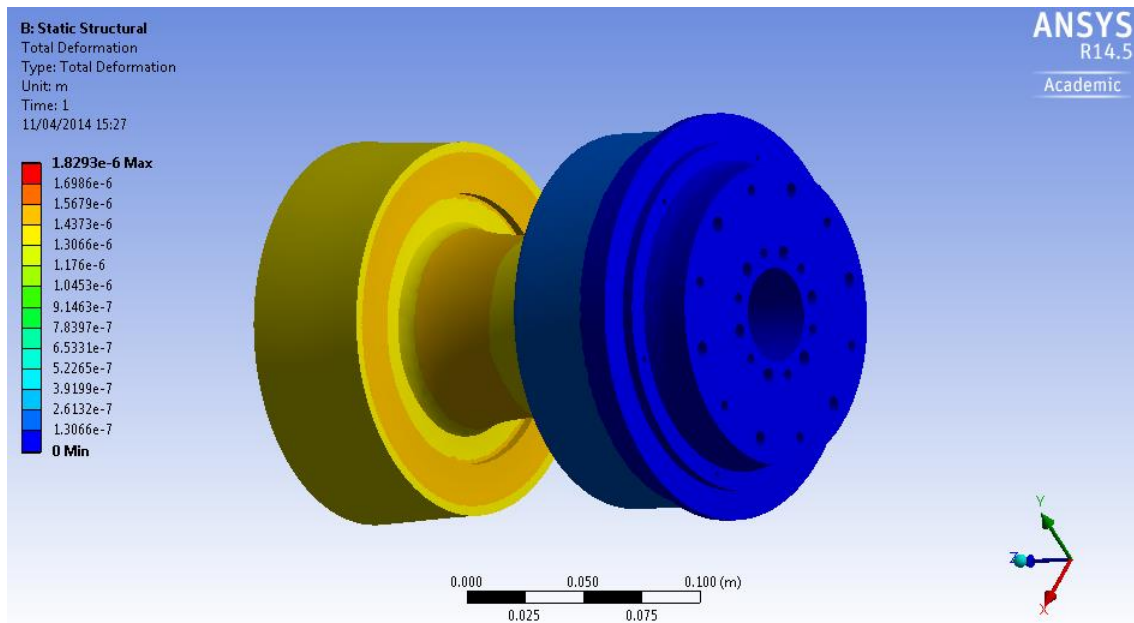
The flow rate is show in the following table.

Table 23 The FEA results table for set 1 analysis

$\eta=5\text{cSt}, N=300\text{rpm}$ $P_{\text{journal}}=1.5\text{MPa}, P_{\text{thrust}}=0.3\text{MPa}$	Clearance (μm)	Flow rate (L/min)	Temperature rise ($^{\circ}\text{C}$)
--	--------------------------------	----------------------	--

Journal bearing	Nominal value	20	0.321	1.911
	Actual value	21.307 ³⁷	0.388	1.670
Thrust bearing	Nominal value	20	0.140	4.451
	Actual value	21.372 ³⁸	0.171	3.459

Figure 30 The deformation solution for Set 1 analysis



From the *Table 23 The FEA results table for set 1 analysis*, it is concluded that the actual flow rate is larger and the actual temperature rise is smaller than the nominal ones due to the deformation of the bearing component. So at this level, the appropriate deformation is somehow beneficial to the hydrostatic bearing systems.

The following table shows all sets of the FEA analysis results. The clearances are 20 μ m and 30 μ m, the viscosities are 5cSt and 10cSt, the rotational speed is 300rpm, and the supply pressure combinations are $P_{\text{journal}}=1.5\text{MPa}$ & $P_{\text{thrust pocket}}=0.3\text{MPa}$, $P_{\text{journal}}=3\text{MPa}$ & $P_{\text{thrust pocket}}=1\text{MPa}$, and $P_{\text{journal}}=5\text{MPa}$ & $P_{\text{thrust pocket}}=2\text{MPa}$.

³⁷ Actual journal bearing clearance=nominal journal bearing clearance + δ_a

³⁸ Actual thrust bearing clearance=nominal thrust bearing clearance + $0.5*(\delta_b + \delta_c)$

Table 24 The FEA analysis results

Rotational speed N=300rpm	Bearing clearance (μm)	20						30							
	Viscosity (cSt)	5			10			5			10				
Journal bearing	Nominal value	Pressure (MPa)	1.5	3	5	1.5	3	5	1.5	3	5	1.5	3	5	
		Clearance (μm)	20	20	20	20	20	20	30	30	30	30	30	30	
		Flow rate (L/min)	0.321	0.641	1.069	0.160	0.321	0.534	1.082	2.164	3.607	0.541	1.082	1.803	
		Temperature rise ($^{\circ}\text{C}$)	1.911	2.206	3.101	5.146	3.823	4.072	1.045	1.773	2.841	1.682	2.091	3.032	
		Actual value	δ_a (μm)	1.307	2.952	5.958	1.307	2.952	5.958	1.307	2.952	5.958	1.307	2.952	5.958
			Clearance (μm)	21.307	22.952	25.958	21.307	22.952	25.958	31.307	32.952	35.958	31.307	32.952	35.958
			Flow rate (L/min)	0.388	0.969	2.337	0.194	0.485	1.168	1.230	2.868	6.211	0.615	1.434	3.105
			Temperature rise ($^{\circ}\text{C}$)	1.670	1.977	2.891	4.179	2.908	3.233	1.012	1.739	2.809	1.548	1.958	2.901
	Thrust bearing	Nominal value	Pressure (MPa)	0.3	1	2	0.3	1	2	0.3	1	2	0.3	1	2
			Clearance (μm)	20	20	20	20	20	20	30	30	30	30	30	30
		Flow rate (L/min)	0.140	0.467	0.934	0.070	0.233	0.467	0.473	1.575	3.151	0.236	0.788	1.575	
		Temperature rise ($^{\circ}\text{C}$)	4.451	1.841	1.754	17.305	5.697	3.682	1.024	0.813	1.240	3.597	1.585	1.626	
		Actual value	δ_b (μm)	1.437	3.543	6.499	1.437	3.543	6.499	1.437	3.543	6.499	1.437	3.543	6.499
			δ_c (μm)	1.307	3.838	7.041	1.307	3.838	7.041	1.307	3.838	7.041	1.307	3.838	7.041
			Clearance (μm)	21.372	23.691	26.770	21.372	23.691	26.770	31.372	33.691	36.770	31.372	33.691	36.770
			Flow rate (L/min)	0.171	0.776	2.239	0.085	0.388	1.119	0.540	2.231	5.801	0.270	1.116	2.901
			Temperature rise ($^{\circ}\text{C}$)	3.459	1.212	1.313	13.334	3.180	1.919	0.885	0.718	1.169	3.041	1.206	1.341

From the table above, the deformation of the bearing components due to the large pressure exerted on their surfaces will affect the actual performance of the hydrostatic bearing systems. The actual flow rate is larger than the nominal flow rate and the actual temperature rise is smaller than the nominal one due to the increasing flow rate of the oil.

However the increasing bearing clearance has a limited influence on the temperature rise of the bearing systems. When the original bearing clearance is large, the influence on the temperature rise by increasing the bearing clearance is relatively small compared with the situation that the original bearing clearance is relatively small as illustrated in the following table:

Table 25 The comparison between the influences on the temperature rise by increasing bearing clearance at different initial bearing clearance

Journal bearing	Viscosity (cSt)	10	10
	Bearing pressure (MPa)	5	5
	Nominal bearing clearance (μm)	20	30
	Actual bearing clearance (μm)	25.958	35.958
	Nominal flow rate (L/min)	0.534	1.803
	Actual flow rate (L/min)	1.168	3.105
	Nominal temperature rise ($^{\circ}\text{C}$)	4.072	3.032
	Actual temperature rise ($^{\circ}\text{C}$)	3.233	2.901
Thrust bearing	Viscosity (cSt)	10	10
	Bearing pressure (MPa)	2	2
	Nominal bearing clearance (μm)	20	30
	Actual bearing clearance (μm)	26.770	36.770
	Nominal flow rate (L/min)	0.467	1.575
	Actual flow rate (L/min)	1.119	2.901
	Nominal temperature rise ($^{\circ}\text{C}$)	3.682	1.626
	Actual temperature rise ($^{\circ}\text{C}$)	1.919	1.341

From the table above, the actual temperature rise drops more at the initial bearing clearance of $20\mu\text{m}$ than that of $30\mu\text{m}$.

For the journal bearing, the actual temperature rise drops about 20.6% at the initial clearance of 20 μm and only 4.3% at the initial clearance of 30 μm .

For the thrust bearing, the actual temperature rise drops about 47.9% at the initial clearance of 20 μm and only 17.5% at the initial clearance of 30 μm .

By the definition of the equation of the temperature rise, Equation 11 and Equation 20, the two main source of the temperature rise is pumping power and the frictional power.

Under the larger initial clearance condition, the larger initial flow rate due to the larger initial bearing clearance almost brings all the frictional power generated by the frictional force due to the friction between the bearing surfaces and the oil even before the deformation happens, so the main energy source of the temperature rise is just the pumping power. The larger the pumping power is, the higher the supply pressure will be, and the higher the temperature rise will be regardless of the subsequent increasing bearing clearance due to the deformation of the bearing components.

For the smaller initial clearance cases, the frictional power is partially carried away by the relatively small flow rate, so the rest of the frictional power as well as the pumping power are both the main sources of the temperature rise. When the bearing clearance increases, the flow rate also increases and then carries away more frictional power. So in this condition, the deformation of the bearing part is beneficial to lower the temperature rise without at the cost of losing the accuracy by increasing the initial bearing clearance.

As a conclusion, the influence to reduce the temperature rise by increasing the bearing clearance is limited. Within a specific range of initial bearing clearance, the deformation of the bearing part at the supply pressure has a relatively large influence on reducing the temperature rise of the bearing system. But when the initial bearing clearance exceeds a specific value, which is about 30 μm in this case, the influence on reducing the temperature rise under the deformation condition is greatly diminished for there is no more extra frictional power to be carried away at an unchanged rotational speed.

For the following table, when the initial clearance is 20 μm , the viscosity of oil is 10cSt, the journal supply pressure is 1.5MPa, and the thrust bearing supply pressure is 0.3MPa, the temperature rise performance is not very satisfied, being 4.179°C and 13.334°C respectively, which does not meet the requirement of the temperature rise being less than 3 °C. So in a real experimental, this combination of the input parameters shall be avoided.

Table 26 The flow rate and temperature rise conditions at low supply pressure and high oil viscosity

Journal bearing	Viscosity (cSt)	10
	Bearing pressure (MPa)	1.5
	Nominal bearing clearance (μm)	20
	Actual bearing clearance (μm)	21.307
	Nominal flow rate (L/min)	0.160
	Actual flow rate (L/min)	0.194
	Nominal temperature rise (°C)	5.146
	Actual temperature rise (°C)	4.179
Thrust bearing	Viscosity (cSt)	10
	Bearing pressure (MPa)	0.3
	Nominal bearing clearance (μm)	20
	Actual bearing clearance (μm)	21.372
	Nominal flow rate (L/min)	0.070
	Actual flow rate (L/min)	0.085
	Nominal temperature rise (°C)	17.305
	Actual temperature rise (°C)	13.334

From the *Table 24 The FEA analysis results*, most of the actual temperature rise is less than 3°C. The experimental input parameters can be chosen not only according to the ANSYS analysis results but also to the availability of the actual experimental equipment of different parameters, because for most of the combinations in the result analysis, the temperature rise lies within the requirement range less than 3°C.

6 EXPERIMENTAL PROCEDURES

6.1 THE EXPERIMENTAL INPUT PARAMETERS SELECTIONS BASED ON THE THEORETICAL CALCULATIONS AND FINITE ELEMENT ANALYSIS

After the theoretical calculations and FEA work, the experimental input parameters could be decided preliminarily.

6.1.1 THE OIL TYPE

From the *Table 24 The FEA analysis results*, except the extreme condition illustrated in the *Table 26 The flow rate and temperature rise conditions at low supply pressure and high oil viscosity*, whose temperature rise greatly exceeds 3°C, most of the results are suitable for the normal operational conditions of the system.

The lower viscosity is recommended to be used in the hydrostatic bearing system such as 10cSt or 15cSt.

6.1.2 THE SUPPLY PRESSURE

For the lower pressure supply, journal bearing pressure 3MPa and thrust bearing pressure 1.5MPa, the temperature rise is always larger than 3°C, so this combination can be removed.

For the journal bearing pressure 2MPa and thrust bearing pressure 1MPa or the journal bearing pressure 5MPa and thrust bearing pressure 2MPa, the temperature rise is appropriate. The higher supply pressure means the higher energy consumption and pumping power generation. And the temperature rise of higher supply pressure is higher than that of lower supply pressure under some conditions. So the 5MPa and 2MPa combination can also be ignored.

As a result, the combination of journal bearing pocket pressure 3MPa and thrust bearing pocket pressure 1MPa is chosen as the experimental supply pressure. Considering the resistance ratio of journal resistor is 1 and thrust resistor is 5, the supply can be set at about 6MPa (60Bar) to get the pocket pressure of 3MPa and 1MPa respectively.

6.1.3 THE BEARING CLEARANCE

The bearing clearance is closely related to the radial stiffness and the manufacturing cost. The larger the bearing clearance is, the lower the radial stiffness and the manufacturing cost will be. Apparently, the lower cost is good for the project, but the low stiffness is not beneficial to the system.

For the journal bearing, the relationship within radial clearance, radial stiffness and temperature rise is showed in the following table.

Table 27 The relationship between the radial clearance, radial stiffness and temperature rise of the journal bearing ($p=3\text{MPa}$, $\eta=10.00\text{cSt}$, $N=300\text{rpm}$)

Radial clearance(μm)	Radial stiffness (10^8N/m)	Temperature rise ($^{\circ}\text{C}$)
10	12.626	36.308
20	6.313	3.823
25	5.051	2.548
30	4.209	2.091
40	3.157	1.800
50	2.525	1.721
60	2.104	1.693

For the journal loading condition of 1500N, the displacement of the bearing shaft under the radial stiffness of $4.209 \times 10^8\text{N/m}$ is $3.563\mu\text{m}$, which is an acceptable value compared with original radial clearance of $30\mu\text{m}$. And the temperature rise for $30\mu\text{m}$ clearance is 2.091°C , which is also an acceptable value. The suitable radial clearance for journal bearing is $30\mu\text{m}$.

For the thrust bearing, the relationship within radial clearance, radial stiffness and temperature rise is showed in the following table.

Table 28 The relationship between the thrust bearing clearance, stiffness and temperature rise of the thrust bearing ($p=1\text{MPa}$, $\eta=10.00\text{cSt}$, $N=300\text{rpm}$)

Clearance (μm)	Stiffness (10^8N/m)	Temperature rise ($^{\circ}\text{C}$)
10	8.903	87.725
20	4.452	5.697

25	3.561	2.676
30	2.968	1.585
40	2.226	0.885
50	1.781	0.692
60	1.484	0.622

For the thrust loading condition of 500N, the displacement of the thrust plate under the stiffness of $2.968 \times 10^8 \text{N/m}$ is $1.685 \mu\text{m}$, which is an acceptable value compared with the original clearance of $30 \mu\text{m}$. And the temperature rise for $30 \mu\text{m}$ is 1.585°C , which is also an acceptable value. The suitable clearance for thrust bearing is also $30 \mu\text{m}$.

There is still another choice that the bearing clearance could be chosen as the mid value of $20 \mu\text{m}$ and $30 \mu\text{m}$, which is $25 \mu\text{m}$. The theoretical calculation table is showed in the following table.

Table 29 The theoretical calculation table when the clearance is $25 \mu\text{m}$

Rotational speed N=300rpm	Bearing clearance (μm)	25						
		5			10			
Journal bearing	Nominal value	Pressure (MPa)	1.5	3	5	1.5	3	5
	Actual value	Clearance (μm)	25	25	25	25	25	25
		Flow rate (L/min)	0.626	1.252	2.087	0.313	0.730	1.044
		Temperature rise ($^\circ\text{C}$)	1.274	1.887	2.910	2.596	2.385	3.307
		δ_a (μm)	1.307	2.952	5.958	1.307	2.952	5.958
	Actual value	Clearance (μm)	26.307	27.952	30.958	26.307	27.952	30.958
		Flow rate (L/min)	0.730	1.750	3.963	0.365	0.875	1.982
		Temperature rise ($^\circ\text{C}$)	1.193	1.807	2.834	2.270	2.230	3.002
		Pressure (MPa)	0.3	1	2	0.3	1	2
	Thrust bearing	Nominal value	Clearance (μm)	25	25	25	25	25
Actual value		Flow rate (L/min)	0.274	0.912	1.823	0.137	0.456	0.912
		Temperature rise ($^\circ\text{C}$)	1.933	1.086	1.376	7.233	2.676	2.171
		δ_b (μm)	1.437	3.543	6.499	1.437	3.543	6.499
		δ_c (μm)	1.307	3.838	7.041	1.307	3.838	7.041

Clearance (μm)	26.372	28.691	31.770	26.372	28.691	31.770
Flow rate (L/min)	0.321	1.378	3.742	0.161	0.689	1.871
Temperature rise ($^{\circ}\text{C}$)	1.596	0.863	1.214	5.884	1.784	1.521

From the data above, although the clearance is selected as the mid value of 20 μm and 30 μm , the most suitable combination is still 10cSt, journal bearing pressure 3MPa and thrust bearing pressure 1MPa. And according to the *Table 27 The relationship between the radial clearance, radial stiffness and temperature rise of the journal bearing ($p=3\text{MPa}$, $\eta=10.00\text{cSt}$, $N=300\text{rpm}$)* and *Table 28 The relationship between the thrust bearing clearance, stiffness and temperature rise of the thrust bearing ($p=1\text{MPa}$, $\eta=10.00\text{cSt}$, $N=300\text{rpm}$)*, the clearance of 25 μm can always meet all the requirement of journal radial stiffness, thrust axial stiffness and the temperature rise. So if the experimental budget is sufficient, the hydrostatic bearing systems of the bearing clearance of 25 μm are also strongly recommended to be manufactured to analyse and test the systems in the further experimental works.

6.1.4 THE EXPERIMENTAL INPUT PARAMETERS COMBINATION

As a general conclusion based on the initial calculation, ANSYS modelling simulation and the initial data analysis, one of the theoretically suitable input parameters is listed in the following table:

Table 30 One of the suitable experimental input parameters combinations

Experimental input parameters selections		
Oil viscosity	10	cSt
Journal bearing supply pressure	3	MPa
Thrust bearing supply pressure	1	MPa
Bearing clearance	25 or 30	μm
Rotational speed	300	rpm

If the budget is sufficient, the hydrostatic bearing systems of both 25 μm clearance and 30 μm clearance or the oil viscosity of both 10cSt and 15cSt shall be tested to prove their working performance.

6.1.5 THE POWER CONSUMPTION CONDITION UNDER THE RECOMMENDED COMBINATION

Under 25 μ m, 300rpm, 10cSt, journal bearing pressure 3MPa and thrust bearing pressure 1MPa, the power consumption condition is showed in the following table.

Table 31 The power consumption condition under the recommended combination (h=25 μ m, N=300rpm, η =10cSt, $P_{journal}$ =3MPa, P_{thrust} =1MPa)

	Pumping power	Frictional power	Total power
Journal bearing	31.31W	16.56W	47.87W
Thrust bearing	15.19W	28.99W	44.18W

Under 30 μ m, 300rpm, 10cSt, journal bearing pressure 3MPa and thrust bearing pressure 1MPa, the power consumption condition is showed in the following table.

Table 32 The power consumption condition under the recommended combination (h=30 μ m, N=300rpm, η =10cSt, $P_{journal}$ =3MPa, P_{thrust} =1MPa)

	Pumping power	Frictional power	Total power
Journal bearing	54.10W	13.77W	67.87W
Thrust bearing	26.26W	24.32W	50.58W

If the deformation is taken into consideration, after the ANSYS modelling, the new tables are showed below.

Table 33 The power consumption condition under the recommended combination after ANSYS modelling (h=25 μ m, $h'_{journal}$ =27.952 μ m, h'_{thrust} =28.691 μ m, N=300rpm, η =10cSt, $P_{journal}$ =3MPa, P_{thrust} =1MPa)

	Pumping power	Frictional power	Total power
Journal bearing	43.76W	14.79W	58.55W
Thrust bearing	22.97W	25.39W	48.36W

Table 34 The power consumption condition under the recommended combination after ANSYS modelling ($h=30\mu\text{m}$, $h'_{\text{journal}}=32.952\mu\text{m}$, $h'_{\text{thrust}}=33.691\mu\text{m}$, $N=300\text{rpm}$, $\eta=10\text{cSt}$, $P_{\text{journal}}=3\text{MPa}$, $P_{\text{thrust}}=1\text{MPa}$)

	Pumping power	Frictional power	Total power
Journal bearing	71.70W	12.52W	84.22W
Thrust bearing	37.19W	21.76W	58.95W

From the tables above, the results can be listed as the following points:

- The total power consumption of journal bearing is larger than that of the thrust bearing;
- The pumping power increases after the deformation due to the extra energy to maintain the same supply pressure as well as the extra flow rate;
- The frictional power decreases after the deformation due to the increased clearance;
- The total power consumption of both initial clearance and both bearing types increases after the deformation.

6.1.6 THE REYNOLDS NUMBER CONDITION UNDER THE RECOMMENDED INPUT COMBINATION

The equations for frictional power, Equation 9, Equation 10, Equation 18 and Equation 19, are all based on the assumption that the fluid flow in the pocket is laminar flow³⁹. However, the flow will become turbulent above a particular speed of the journal or the thrust bearings. The turbulence in the pocket will cause the “fluid friction” over the area of the pocket rise more rapidly with speed (Stansfield, 1970).

The value of Reynolds Number (Re) indicates whether the turbulence is likely to occur. The equation for Re is listed below:

³⁹ Laminar flow (or streamline flow) occurs when a fluid flows in parallel layers, with no disruption between the layers.

Reynolds Number $Re = \frac{2\rho h_p v}{\eta}$ Equation 30

Under 25µm, 300rpm, 10cSt, journal bearing pressure 3MPa and thrust bearing pressure 1MPa, the Reynolds numbers are listed below:

Table 35 The Reynolds number condition under the recommended combination before and after ANSYS modelling (h=25µm, h'_{journal}=27.952µm, h'_{thrust}=28.691µm, N=300rpm, η=10cSt, P_{journal}=3MPa, P_{thrust}=1MPa)

	Journal bearing	Thrust bearing
Re (before deformation)	7.83	11.38
Re (after deformation)	8.76	13.06

Under 30µm, 300rpm, 10cSt, journal bearing pressure 3MPa and thrust bearing pressure 1MPa, the Reynolds numbers are listed below:

Table 36 The Reynolds numbers under the recommended combination before and after ANSYS modelling (h=30µm, h'_{journal}=32.952µm, h'_{thrust}=33.691µm, N=300rpm, η=10cSt, P_{journal}=3MPa, P_{thrust}=1MPa)

	Journal bearing	Thrust bearing
Re (before deformation)	9.40	13.66
Re (after deformation)	10.33	15.34

The Reynolds numbers under all the conditions are less than 2000, which is the critical point between laminar flow and turbulence, so the fluid within the hydrostatic bearings is always regarded as the laminar, just verifying the assumptions before.

Another conclusion is that the Reynolds numbers are slightly larger after the deformation. At lower rotational speed, the clearance change is not obvious enough to affect the Reynolds number. But at high rotational speed and low viscosity, the deformation is likely to increase the Reynolds number a lot and will influence the normal performance of the hydrostatic bearing systems.

6.2 THE MEASUREMENT AND MACHINING PROCESS OF THE HYDROSTATIC BEARINGS

6.2.1 THE MEASUREMENT OF THE BEARING COMPONENTS

To achieve the ideal bearing gap of about 25-30 μm , some ultra-precision measurement equipment is necessary to define the dimensions of the bearing parts.

Each component, including bearing shafts, thrust plates and bearing housing, shall be measured at least three times:

The 1st time: after the aluminium parts being machined by the diamond turning and before the parts being coated, to get the original dimension of the hydrostatic bearing system;

The 2nd time: after the bearing parts being coated and before the second diamond turning process, probably the most important measurement process not only to know the thickness of the coating and but also to decide the amount of the coating to be removed to achieve the target bearing clearance;

The 3rd time: after the second diamond turning, to check the final dimension of the bearing system to see whether it meets the design requirement.

The figures below are the components after being coated and before the second diamond turning process:

Figure 31 The bearing shaft after being coated and before the second diamond turning process



Figure 32 The thrust plate after being coated and before the second diamond turning process

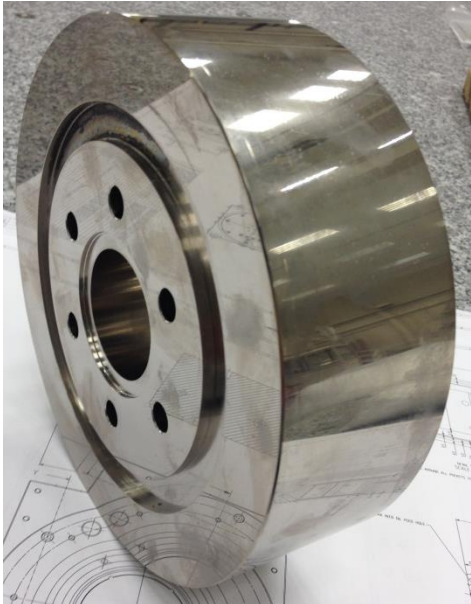
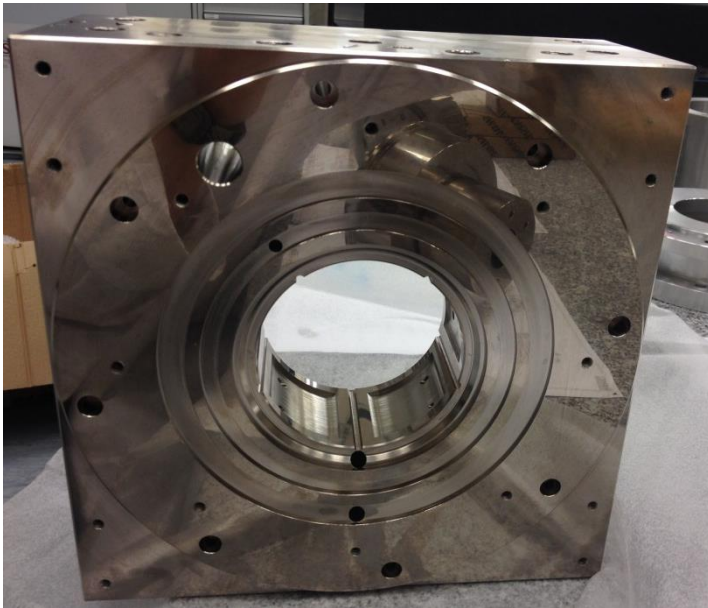


Figure 33 The bearing house after being coated and before the second diamond turning process



The following tools are some hand measuring tools in the laboratory:

The TESA IMICRO with analogue indication 90-100⁴⁰ is used to measure the inner diameter of the bearing house. Its measuring span is 90-100mm, its scale interval is 0.002mm and its maximum permissible error is 0.005 μ m.

Figure 34 TESA IMICRO with analogue indication 90-100

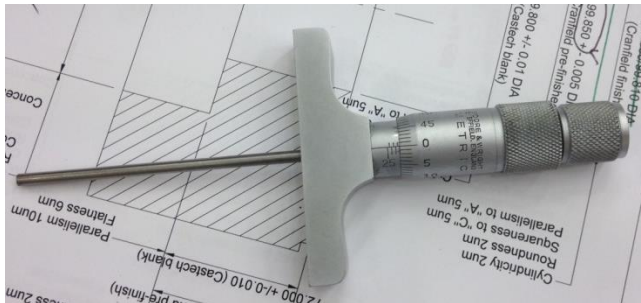


The Moore & Wright traditional depth gauge micrometer⁴¹ is used to measure the length of the journal and the depth of the bearing house. Its measuring span

⁴⁰ Data from: <http://www.tesagroup.co.uk/en-us/products/tesa-imicro-with-analogue-indication-metric-p152.htm?redirect=1&c=gb#.U3d6YqNwbcs>

is 0-75mm, its scale interval is 0.01mm and its maximum permissible error is 0.01mm.

Figure 35 The Moore & Wright depth gauge micrometer



The Moore & Wright outside micrometer⁴² is used to measure the thickness of the thrust bearing. Its measuring span is 50-75mm, its scale interval is 0.002mm and its maximum permissible error is 0.01mm.

Figure 36 The Moore & Wright outside micrometer



The Mitutoyo caliper digital absolute IP67⁴³ is used to measure both the inside and outside distances between two parallel surfaces. Its measuring span is 0-150mm, its scale interval is 0.01mm and its maximum permissible error is 0.01mm.

⁴¹ Data from: <http://www.moore-and-wright.com/products/show/13904?lang=English>

⁴² Data from: <http://www.moore-and-wright.com/products/show/4682?lang=English>

⁴³ Data from: <http://uk.farnell.com/mitutoyo/500-706-11/caliper-digital-absolute-ip67-150mm/dp/1698141>

Figure 37 The Mitutoyo caliper digital absolute IP67



The minimum error of all these hand measuring tools is $5\mu\text{m}$, which is relatively a large number compared with the target clearance of $25\text{-}30\mu\text{m}$. So the machining process based on these hand measuring tools is not reliable and will not actually reflect the results from the previous theoretical.

So the ultra-precision coordinate measuring machine, Leitz PMM-F 1000⁴⁴, is introduced to measure the dimension of the bearing house and shaft.

Figure 38 Leitz PMM-F 1000 CMM



⁴⁴ Data from:

http://www.hexagonmetrology.com.cn/uploadfiles/File/%E6%A0%B7%E6%9C%AC/Product_Overview_ErrorCharts.pdf

Its measuring span is 3000*2000*1000mm, its volumetric length measuring error E is defined in the following equation:

$$\text{Volumetric length measuring error } E^{45} \quad E = 1.7 + L/400 \quad \text{Equation 31}$$

For the bearing components less than 300mm, the error of the CMM machine on this specific component is less than 2.45 μm , which is smaller than the value of about 10% of the target clearance.

So the dimensions measured by the PMM-F 1000 can be used to machine the bearing components to get the required bearing clearance. The measuring process is showed in the following figure:

Figure 39 The bearing house is being measured by the Leitz CMM



⁴⁵ Data from:

http://www.hexagonmetrology.com.cn/uploadfiles/File/%E6%A0%B7%E6%9C%AC/Product_Overview_ErrorCharts.pdf

6.2.2 THE DIMENSIONS OF THE EXPERIMENTAL COMPONENTS

After the measurement by CMM, the dimensions of the components are listed below:

Table 37 The dimensions of the experimental components

Bearing housing		
Small inside diameter	99.805	Mm
Large inside diameter	163.765	Mm
Working thickness over lands	71.995	Mm

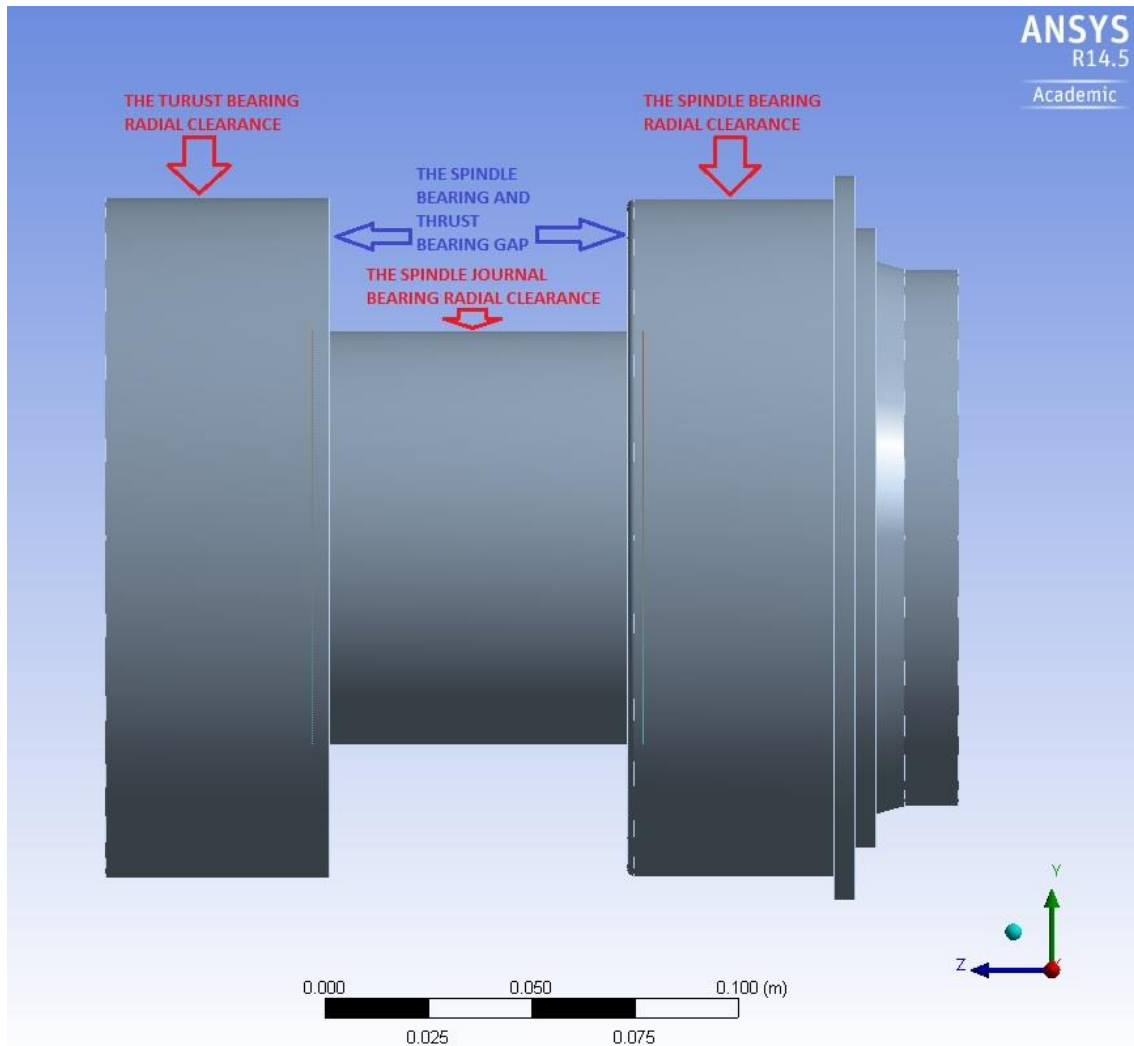
Spindle bearing		
Small diameter	99.748	Mm
Large diameter	163.718	Mm
Working thickness over lands	72.053	Mm

Thrust bearing		
Outside diameter	163.775	Mm
Thickness	53.700	Mm

Rear housing		
Large diameter	164.035	Mm

From the table above, the crucial dimensions showed in the following figure can be calculated.

Figure 40 The important dimensions of the experimental components



The spindle journal bearing radial clearance:

$$h = \frac{99.805 - 99.748}{2} = 28.5\mu m$$

The spindle bearing and thrust bearing gap:

$$h = \frac{72.053 - 71.995}{2} = 29\mu m$$

The spindle bearing radial clearance:

$$h = \frac{163.765 - 163.718}{2} = 23.5\mu m$$

The thrust bearing radial clearance:

$$h = \frac{164.035 - 163.775}{2} = 130\mu m$$

The spindle journal bearing radial clearance and the spindle bearing gap are the hydrostatic bearing parameters, which are both very important to the experiment. And their values are machined at about 30 μ m.

The spindle bearing radial clearance is 23.5 μ m, which is relatively small compared with the bearing clearance of about 30 μ m. However, it still conforms to the blueprint drawings. The other thrust bearing radial clearance, whose value is 130 μ m, is large enough to lay in the safety areas to prevent any extra wear circumstances.

6.2.3 THE MACHINING PROCESS OF THE BEARING COMPONENTS

The EPSRC Centre for innovative manufacturing in ultra-precision at Cranfield University uses the CUPE Nanocentre to machine the hydrostatic bearing components. It uses diamond tool to machine the aluminium alloy materials. And its error is about 100nm, which greatly meets the demand of the design of the hydrostatic bearing system of 25-30 μ m.

Figure 41 The CUPE nanocentre in the EPSRC Centre at Cranfield University



The following picture is the bearing house which is machined after the coating process.

Figure 42 The re-machined bearing house after the coating process



6.3 THE PARAMETERS MEASUREMENT AND THE TEST EQUIPMENT

The aim of the experimental works is to measure some important parameters of the system to find out whether the new aluminium hydrostatic bearing systems can be qualified and economical substitutions to the expensive steel ones.

6.3.1 THE INPUT PARAMETERS AND THE EQUIPMENT

6.3.1.1 THE SUPPLY PRESSURE

The supply pressure, one of the most important input parameters, could be set by the hydraulic supply system by adjusting the rotational speed of the pump motor. The higher the speed is, the higher the supply pressure will be. For any group of experiment result, the supply pressure is always one of the most fundamental precondition parameters. The supply pressure is relevant to most of the parameters of the hydrostatic bearing system, such as the ultimate load capacity, the flow rate, the power consumption, the bearing deformation (the x displacement), the stiffness, and even the temperature rise.

Figure 43 The experimental inverter



The inverter⁴⁶ is HITACHI SJ100 Series Inverter⁴⁷, which is showed in the figure above. Its main features are listed below and its specifications are showed in the 8Appendix C THE SPECIFICATIONS FOR SJ100 INVERTER.

Figure 44 HITACHI SJ100 Series Inverter



Figure 45 The ABB M2AA 090 L-4 motor



⁴⁶ The term inverter and variable-frequency drive are related and somewhat interchangeable. An electronic motor drive for an AC motor can control the motor's speed by varying the frequency of the power sent to the motor. An inverter, in general, is a device that converts DC power to AC power. The drive first converts incoming AC power to DC through a rectifier bridge, creating an internal DC bus voltage. Then the inverter circuit converts the DC back to AC again to power the motor. The special inverter can vary its output Frequency and voltage according to the desired motor speed.

⁴⁷ Data from: <https://www.automationdirect.com/static/manuals/sj100/sj100.pdf>

The motor is ABB M2AA 090 L-4⁴⁸ series motor, which is showed in the *Figure 45 The ABB M2AA 090 L-4 motor* above. It is a general-purpose aluminium motor. The three phase motors are ideal for a wide variety of applications including pumps, fans and process machinery drives. Motors in frame sizes 63-100 may be connected in either STAR (Y) for supply voltages of 380-420//440-480V 50/60Hz or DELTA for 220-240//250-280 50/60Hz. Motors in frame sizes 112-132 are suitable DELTA connected 380-420//440-480V 50/60Hz and are also suitable for STAR/DELTA starting. Its specifications are showed in *8Appendix D THE SPECIFICATIONS FOR ABB M2AA 090 L-4 MOTOR* and the following are its main characteristics:

- Top mounted terminal box with metric/Pg type knockouts;
- Energy efficient low noise design;
- Corrosion resistant, low copper aluminium alloy;
- Suitable for DOL starting or inverter drive use.

The supply pressure could be measured by 63mm pressure gauges⁴⁹, which is illustrated in the following picture.

Figure 46 The pressure gauge for pressure from 10MPa to 69MPa



⁴⁸ Data from: <http://il.rsdelivers.com/product/abb/m2aa-90l/3phase-2p-flange-induction-motor-22kw/3290874.aspx>

⁴⁹ Data from: <http://www.hydrotechnik.co.uk/catalog/measurement-equipment-sensors/gauges-switches-displays/analogue-pressure-gauges/63mm-bottom->

6.3.1.2 THE POCKET PRESSURE

The pocket pressure of each bearing pocket can be measured by the pressure gauges as the figure below. There are seven pockets on the bearing system: five journal bearing pockets and two thrust bearing pockets. Each of these pockets has a hole to the surface of the bearing housing. These holes can be inserted a pressure gauge to monitor the pocket pressure.

Figure 47 Pressure gauge to measure the pocket pressure



Figure 48 Hole on the bearing housing to insert the pressure gauge



6.3.1.3 THE FLUID VISCOSITY

For any oil lubrication system, oil viscosity⁵⁰ is always considered as one of the most important parameters. The fluid viscosity, also one of the most important input parameters relevant to the flow rate and the temperature change during the operational process, could be decided by the pre-selection of the oil type. However the viscosity of the oil is not constant, it will decrease as the temperature increases. So in this report, a basic assumption is made, as showed in the *Assumption 2* that the viscosity change due to the temperature change during the operational process of the hydrostatic bearing system is ignored. The only value considered is the viscosity of oils of the various types. The viscosity can usually be measured by means of the viscosity comparator a.k.a. viscostick, the viscotube, or the viscometer⁵¹. The dial reading viscometer is showed in the following figure.

Figure 49 Dial Reading Viscometer



⁵⁰ Viscosity can be defined as measurement of fluid internal resistance to flow at a specified temperature. There are two ways to measure a fluid's viscosity, namely Dynamic (Absolute) Viscosity and Kinematic Viscosity. Both dynamic and kinematic viscosity are interchangeable by using the formula below:

$$\text{Dynamic Viscosity (cP)} = \text{Kinematic Viscosity (cSt)} \times \text{Fluid Density (g/cm}^3\text{)}$$

⁵¹ Data from: http://www.kittiwake.com/sites/default/files/2%20-%20Viscosity%20Dec12_0.pdf

For the ultra-precision hydrostatic bearing system, whose components surfaces are separated by an oil film of about 20 microns or less and the supply pressure is relatively high, the viscosity monitoring is very important to maintain the viscosity of the oil staying within the suitable range of the correct oil viscosity values. Any sudden significant change of the oil viscosity, either reduction or increment, may affect the stability and the effectiveness of the lubrication film, which is showed in the following table:

Table 38 Effect of the change of the viscosity of the oil⁵²

Reduction in Viscosity	Increase in Viscosity
<ul style="list-style-type: none"> • Loss of oil film resulting in excessive wear • Increased mechanical friction causing excessive energy consumption and heat generation • Increased sensitivity to particle contamination due to reduced oil film thickness • Oil film failure at high temperatures, high loads during start-ups or coast-downs 	<ul style="list-style-type: none"> • Excessive heat generation resulting in oil oxidation, sludge and varnish build-up • Gaseous cavitation due to inadequate oil flow to pumps and bearings • Lubrication starvation due to inadequate oil flow • Oil whip in journal bearings • Excess energy consumption to overcome fluid friction • Poor air detrainment or demulsibility • Poor cold start pumpability.

The effects above will finally result in the shorter oil lifespan, shorter components lifecycle, increased oil consumption, high power consumption and reduced machine reliability. So it is very important to choose a suitable type of lubricant oil to optimize the performance of the hydrostatic bearing system.

The following table shows different oil products of the company of Millers Oils Ltd⁵³ with different viscosity.

⁵² Data from: http://www.kittiwake.com/sites/default/files/2%20-%20Viscosity%20Dec12_0.pdf

⁵³ Millers Oils Ltd, Brighouse, West Yorkshire HD6 3DP England, Company No. 00137671, England

Table 39 The products table of different mineral oil products from Millers Oils Ltd.⁵⁴

Mineral oil product type	SG ⁵⁵ (at 15°C)	Kinematic Viscosity (at 100°C, cSt)	Kinematic Viscosity (at 40°C, cSt)	Pour Point (°C)	Flash Point (°C)
Millube 5	0.821	1.46	4.5	-25	130
Millube 22	0.862	3.9	19.8	-20	200
Millube 32	0.873	5.2	30	-15	200
Millube 46	0.893	6.7	44.2	-15	200
Millube 68	0.881	8.9	68	-15	200
Millube 100	0.885	11.5	102	-15	200
Millube 155	0.887	14.1	141.2	-15	200

The lubricant oil some of the hydrostatic bearing systems use in the laboratory is Kristol M10⁵⁶. Its physical and chemical properties are listed in the following table.

Figure 50 The physical and chemical properties of Kristol M10

Oil name	Kristol M10
Appearance	Liquid
Colour	Colourless
Odour	No characteristics odour
Solubility	Insoluble in water
Initial boiling point and boiling range	270-430 under 760 mm Hg
Melting point	<-21°C
Specific Gravity	0.83-0.86515

⁵⁴ Website: <http://www.millersoils.co.uk/industrial/tds-industrial.asp?prodsegmentID=554§or=Machine%20Oil%20&%20Lubricants>

⁵⁵ Specific gravity is the ratio of the density of a substance to the density (mass of the same unit volume) of a reference substance. Apparent specific gravity is the ratio of the weight of a volume of the substance to the weight of an equal volume of the reference substance. The reference substance is nearly always water for liquids or air for gases.

⁵⁶ The oil data is obtained from the data files in the laboratory.

Viscosity	10 cSt at 40°C
Flash point	150 °C

6.3.1.4 THE ROTATIONAL SPEED

The rotational speed is the one of the most critical specifications of any hydrostatic bearing system. It must be guaranteed that the upper limit of the normal rotational speed is within the speed range of the bearing system itself. And the rotational speed is the main reason to cause the temperature rise during normal working processes.

The rotational speed, the supply pressure and the viscosity of the oil are the three fundamental preconditions. The value of the rotational speed of the bearing shaft is the value of the rotational speed of the motor, and can be got by the settings of the control system.

6.3.2 THE OUTPUT RESPONSES

6.3.2.1 THE TEMPERATURE RISE

Measuring the temperature of the oil is helpful to monitor the viscosity of the oil as well as the hydrostatic bearing system during the working period. The exponential mode of the relationship between viscosity and temperature is showed in *Equation 32*:

$$\text{Shear viscosity}^{57} \quad \mu = \mu_0 e^{-bT} \quad \text{Equation 32}$$

T is the temperature of the fluid, μ_0 and b are coefficients.

From this empirical model, the higher the temperature is, the lower the viscosity will be, which, on the contrary, will help to lower the temperature of the oil inversely⁵⁸.

⁵⁷ An exponential model for the temperature-dependence of shear viscosity (μ) was first proposed by Reynolds in 1886. This is an empirical model that usually works for a limited range of temperatures.

⁵⁸ The viscosity of a lubricant will decrease as the temperature increases.

The coefficient of the thermal expansion, i.e. CTE⁵⁹, of the aluminium is relatively not small, which means a high temperature rise will cause the expansion of the aluminium, causing some extra wear.

Measuring the temperature rise of the oil is also a convenient way to roughly estimate the total power consumption of the hydrostatic bearing system. The energy causing the temperature rise comes from both the pumping power by the supply pump and the shear frictional power driven by the shaft motor. The temperature rise is just an indicator of the efficiency of the total bearing system to judge whether the system is energy-saving or not.

To measure the temperature rise, the temperature needs to be measured initially before the rotational work and be measured after 60 minutes' normal work. And the temperature can also be real-timely monitored to make sure the hydrostatic bearing system is always under normal working conditions.

The temperature rise is measured by the NI 9217 RTD Analog input C Series module and LEMO FGG.00 temperature measuring connector and sensor. Equipment is showed in the following figures and their specifications are listed in the appendix.

Figure 51 NI 9217 RTD Analog input C Series module



⁵⁹ CTE is calculated by the *Equation 29*.

Figure 52 LEMO FGG.00 temperature measuring connector and sensor



To measure the inlet and outlet temperatures, two sensors were put on the inlet pipes and two sensors were put on the outlet pipes:

Figure 53 The positions of the four temperature sensors

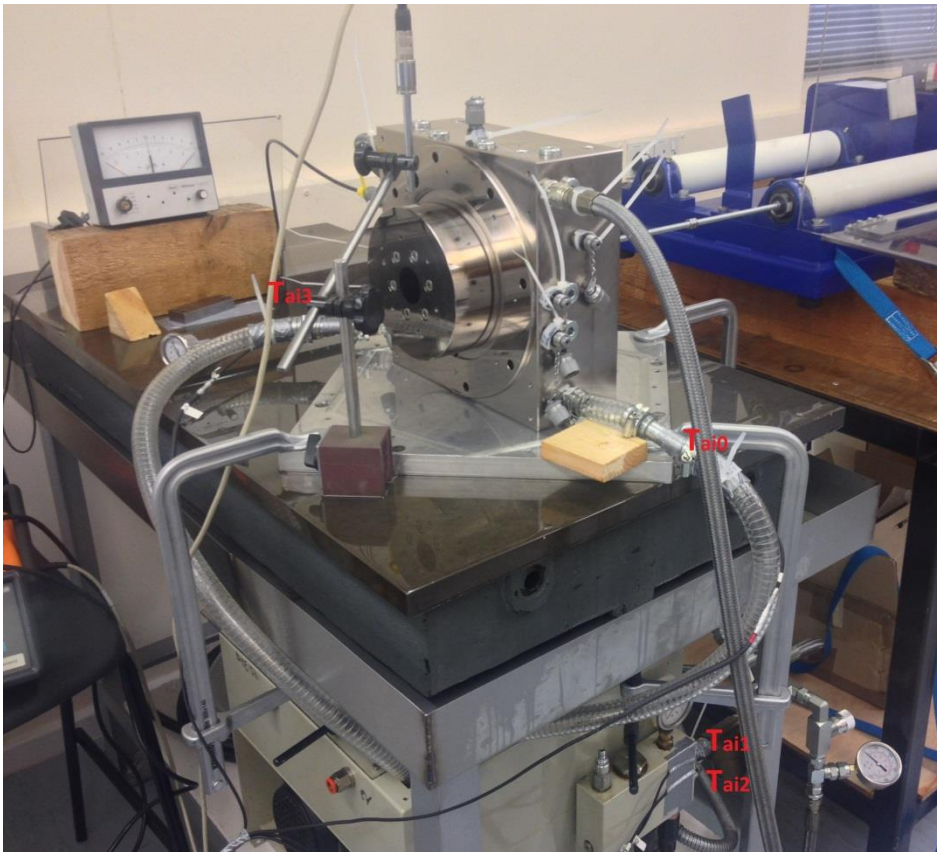


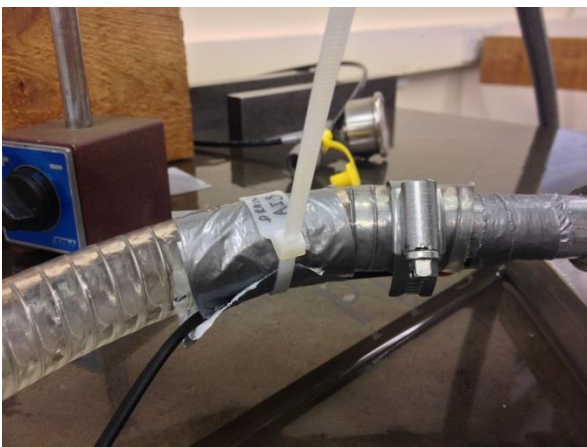
Figure 54 Temperature sensor Tai0 to measure one oil outflow pipe



Figure 55 Temperature sensor Tai1 and Tai2 to measure the oil flowing out from the pump



Figure 56 Temperature Tai3 to measure one oil outflow pipe



According to the results of the temperature rise tests in later chapter, the chilling system is needed to cool down the hydraulic system. HAAKE Phoenix II systems⁶⁰ are chosen as the external temperature control system for this hydrostatic bearing system. And its specifications are showed in the appendices.

Figure 57 HAAKE Phoenix II systems

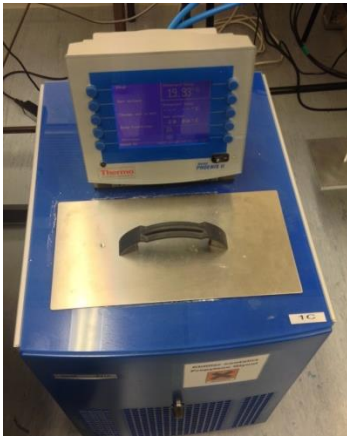
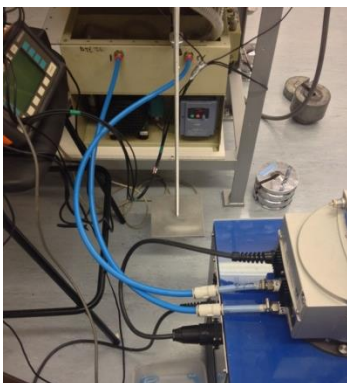


Figure 58 The connection of the HAAKE Phoenix II systems



⁶⁰ HAAKE Phoenix II systems for external temperature control are manufactured for applications that direct product contact is not allowed. Used in combination with a Pt sensor, HAAKE Phoenix II circulators ensure high temperature accuracy of 0.01 degree C for external applications within a temperature range of -90 to +280 degrees C.

6.3.2.2 THE FLOW RATE

As discussed in the chapter of *REVIEW OF THE THEORETICAL DESIGN APPLIED TO ULTRA-PRECISION SPINDLE*, the flow rate of the oil is determined by the supply pressure, the restrictors, the clearance and the viscosity of the oil. Since the supply pressure and the viscosity of the oil are already determined before the experiment, the real-time measurement of the flow rate is a good indicator of the deformation of the surface of the bearing shaft and the thrust plates.

The hydrostatic bearing is placed on a workbench showed in the *Figure 59 The workbench for the R2R hydrostatic bearing system*. There is an oil sink under the workbench, collecting all the oil outflowed from the system and sending it back to the hydraulic tank. The flow rate can be measured by the volume of all the oil collected within one minute (L/min).

Figure 59 The workbench for the R2R hydrostatic bearing system



6.3.2.3 THE BEARING STIFFNESS

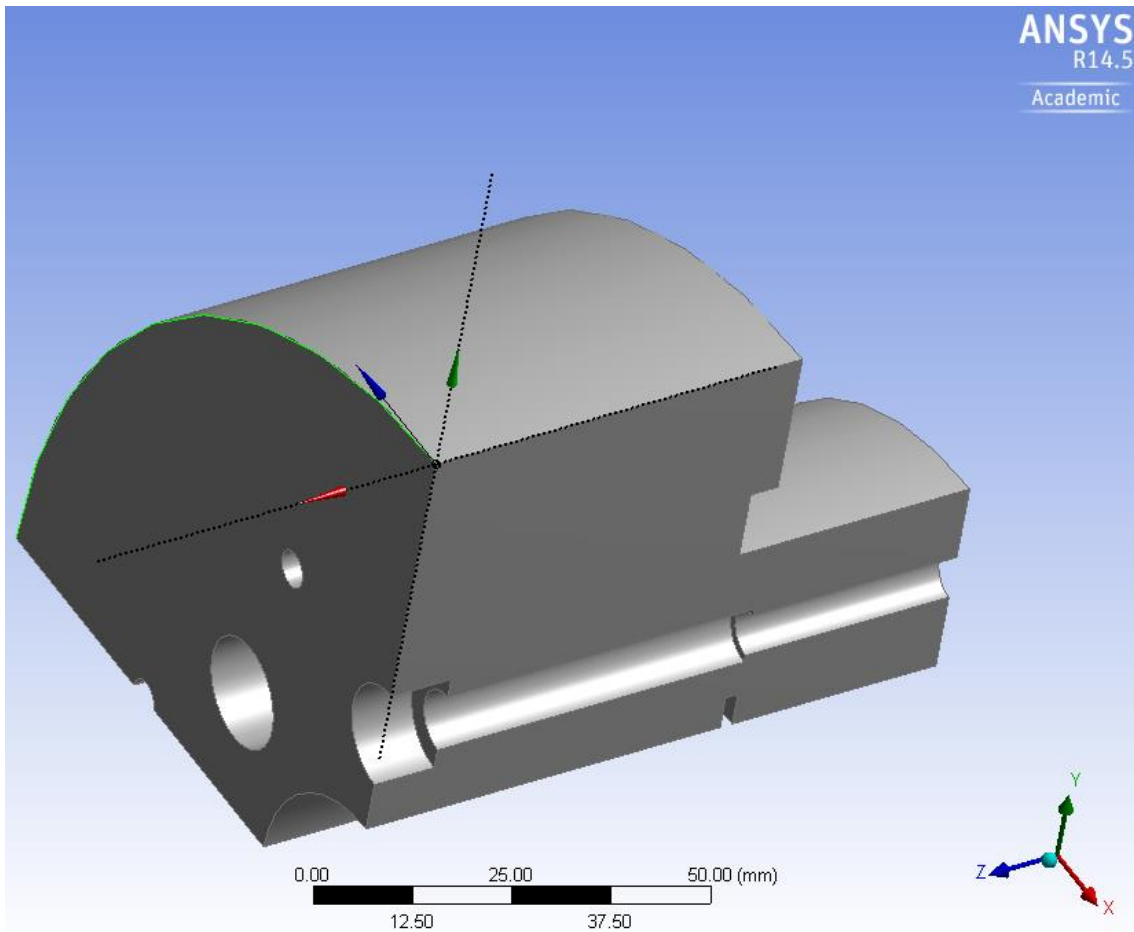
The bearing stiffness is the rate of change of T with respect to h : It is not constant but may be regarded as constant for practical purposes as the ratio of the change ΔT to the corresponding very small change Δh (Stansfield, 1970).

The ΔT can be simply obtained by adding known loads on the shaft, e.g. by applying known loads to the rotor by standard weights or non-contacting electromagnets (Martin, 2004b) as a more complex and alternative method. Δh can be measured by adding the displacement transducers to measure the y-axis displacement. Then the bearing stiffness can be calculated by the ratio of dT/dh .

6.3.2.4 THE INITIAL X DISPLACEMENT

The x displacement of the edge of the thrust plate, showed in the *Figure 60 The edge of measuring the x displacement*, is the deformation value in the x-axis direction of the thrust plate. The initial x displacement records the initial deformation of the thrust plate in the x-axis direction just at the supply pressure with slightly temperature rise compared with the 30-minute x displacement measurement. It should be recorded initially before the working process of the hydrostatic bearing system.

Figure 60 The edge of measuring the x displacement



The x displacement is measured by Millimar 1200 IC compact amplifier, which is showed in the following figures:

Figure 61 Mahr Millimar 1200 IC Compact Amplifier



Figure 62 The probe of the Millimar 1200 IC Amplifier



Its specifications are showed in the *8Appendix E THE SPECIFICATIONS FOR MILLIMAR 1200 IC COMPACT AMPLIFIER* and its characteristics are listed below:

- Compact housing;
- Battery powered for portable usage in the workshop;
- Large analog display with 2 tolerance markers;
- Quick and reliable display of the measured value;
- Switchable measuring direction;
- One inductive probe can be connected;
- Fine adjustment due to the large range zero setter;
- Battery operation with the commercial available round R14 batteries;
- Testing button for batteries;
- Mains adapter included.

The measuring range is listed below:

- $\pm 3 \mu\text{m} / 0.1 \mu\text{m}$
- $\pm 10 \mu\text{m} / 0.2 \mu\text{m}$
- $\pm 30 \mu\text{m} / 1 \mu\text{m}$
- $\pm 100 \mu\text{m} / 2 \mu\text{m}$
- $\pm 300 \mu\text{m} / 10 \mu\text{m}$

The x displacement can be measured effectively under the smaller range, such as $\pm 3 \mu\text{m}$ and $\pm 10 \mu\text{m}$.

6.3.2.5 THE 30-MINUTE X DISPLACEMENT

After the hydrostatic bearing system has been working for 30 minutes, the temperature of the bearing system will stay on a constant level due to the thermal equilibrium between the bearing system temperature and the ambient temperature. And due to the constant supply pressure on the plate of the thrust bearing, the thrust plate also achieved equilibrium between the internal stress and the external pressure, which results in a deformation of the whole plate. The maximum deformation happens in the edge of the plate as showed in the *Figure 60 The edge of measuring the x displacement*, so measuring the x displacement of the edge in the x-axis direction shall indicate the actual deformation condition during the working process of the hydrostatic bearing system.

6.4 ALUMINIUM HYDROSTATIC BEARING PERFORMANCE

6.4.1 THE ASSEMBLING AND DISASSEMBLING PROCESS

Due to the very small bearing clearance, the assembling process demands a high level of carefulness to the technicians. Before assembling the bearing shaft, the oil system was tested after the restrictors being put on. The holes of the restrictors should all been inspected by microscope. The figures below show the clean restrictors and the restrictors with some burs on the top of its tube. The third one was needed to be cleaned by wires or grinding machine.

Figure 63 The clean view of the journal bearing restrictor

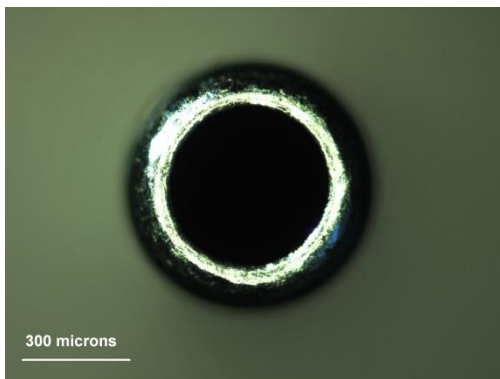
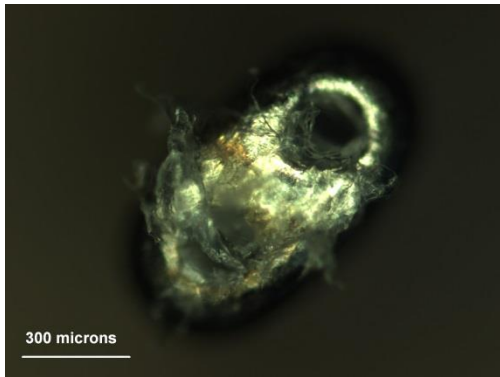


Figure 64 The clean view of the thrust bearing restrictor

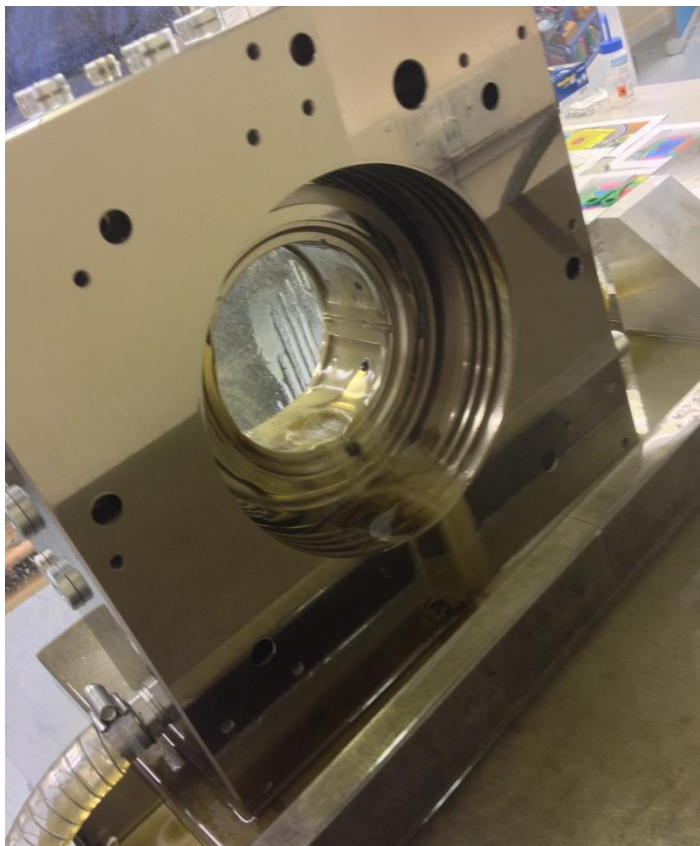


Figure 65 The burs on the top of an unclean thrust bearing restrictor tube



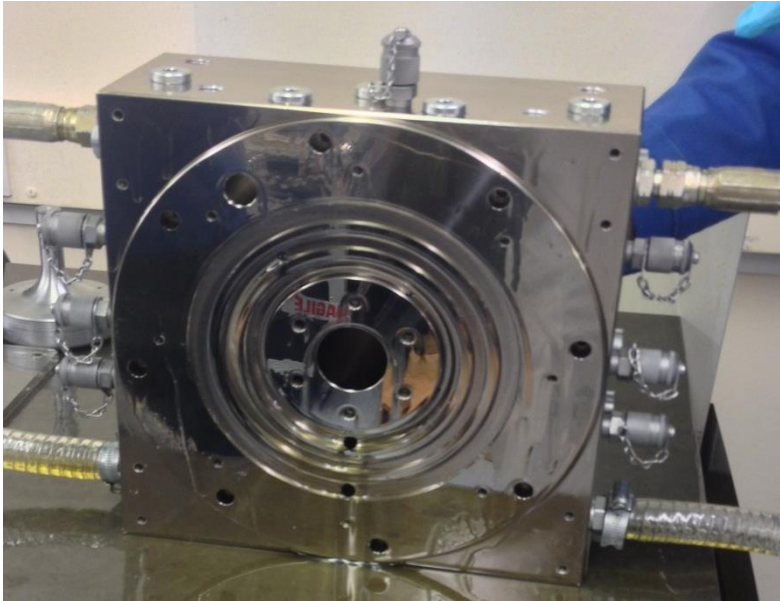
The pre-testing process is showed in *Figure 66 Testing before the bearing shaft being put on*. Make sure that there is some oil flow shooting out from every inflow holes through the restrictors in the bearing pockets. After one-hour operation, the system was considered to be self-flushed.

Figure 66 Testing before the bearing shaft being put on



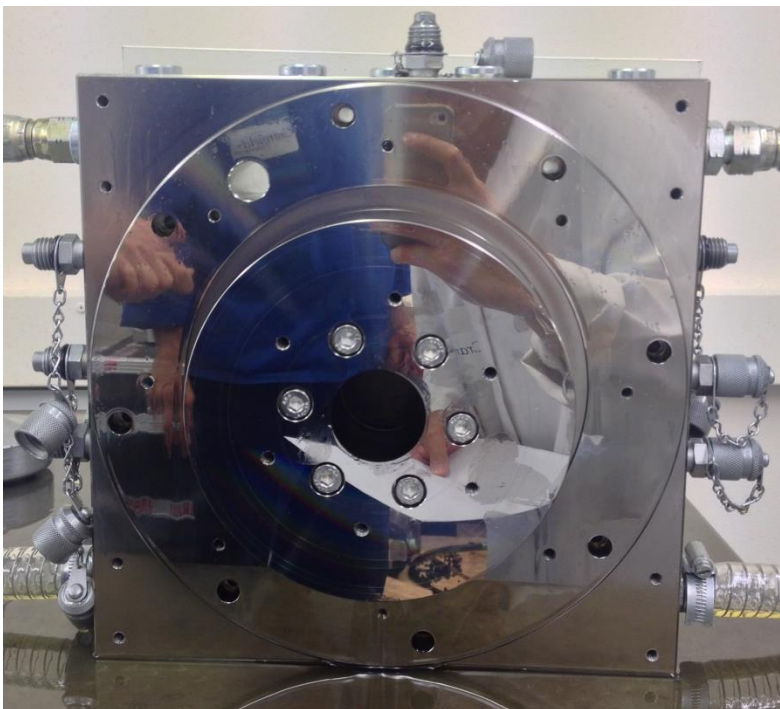
After the pre-testing process, the bearing shaft was put into the bearing housing. The bearing spindle shall be put into the housing firstly.

Figure 67 The bearing spindle being put into the housing



And then the thrust plate was bolted on the bearing spindle.

Figure 68 The bearing thrust plate being bolted on the bearing spindle



After the bearing shaft being put on the housing, the assembling process was finished. Then the pocket pressure was measured to check whether the restrictors worked well. According to the original design, the resistance ratio of

the journal bearings is 1 and the resistance ratio of the thrust bearings is 3. The pocket pressure can be calculated by the following equation:

The pocket pressure
$$P_{pocket} = \frac{P_{supply}}{1 + \xi}$$
 Equation 33

Then the pocket pressure of the journal bearing shall be 0.5 supply pressure and the pocket pressure of the thrust bearing shall be 0.25 supply pressure.

If the pocket pressure is not high enough, the dimensions of the orifice restrictors could be adjusted slightly to reduce the resistance ratio. The ways to reduce the resistance are either shortening the length of the needle or enlarging the diameter of the needle by designing new restrictors.

After finished the testing experiments, the hydrostatic system was disassembled to check the inside burs and attrition condition. The following two pictures are the debris remained in the system after being disassembled and the microscope image of the debris.

Figure 69 The debris inside the bearing housing

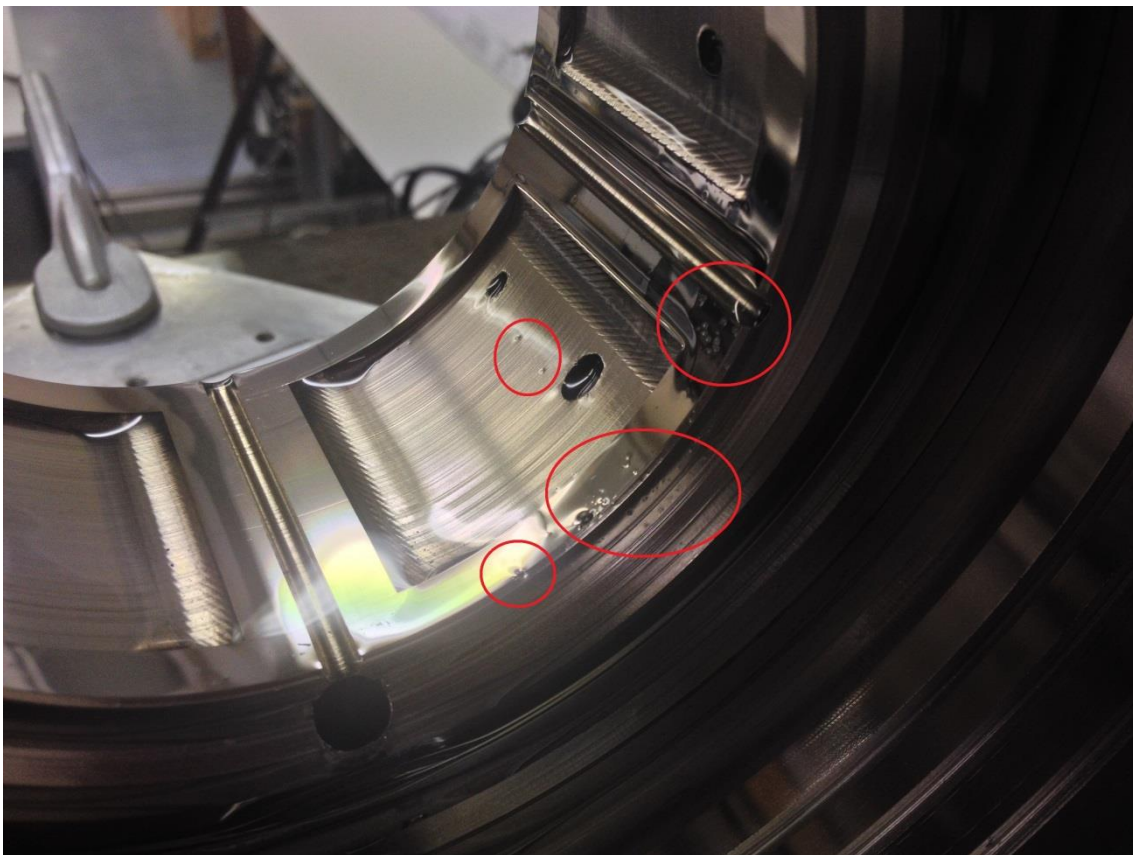
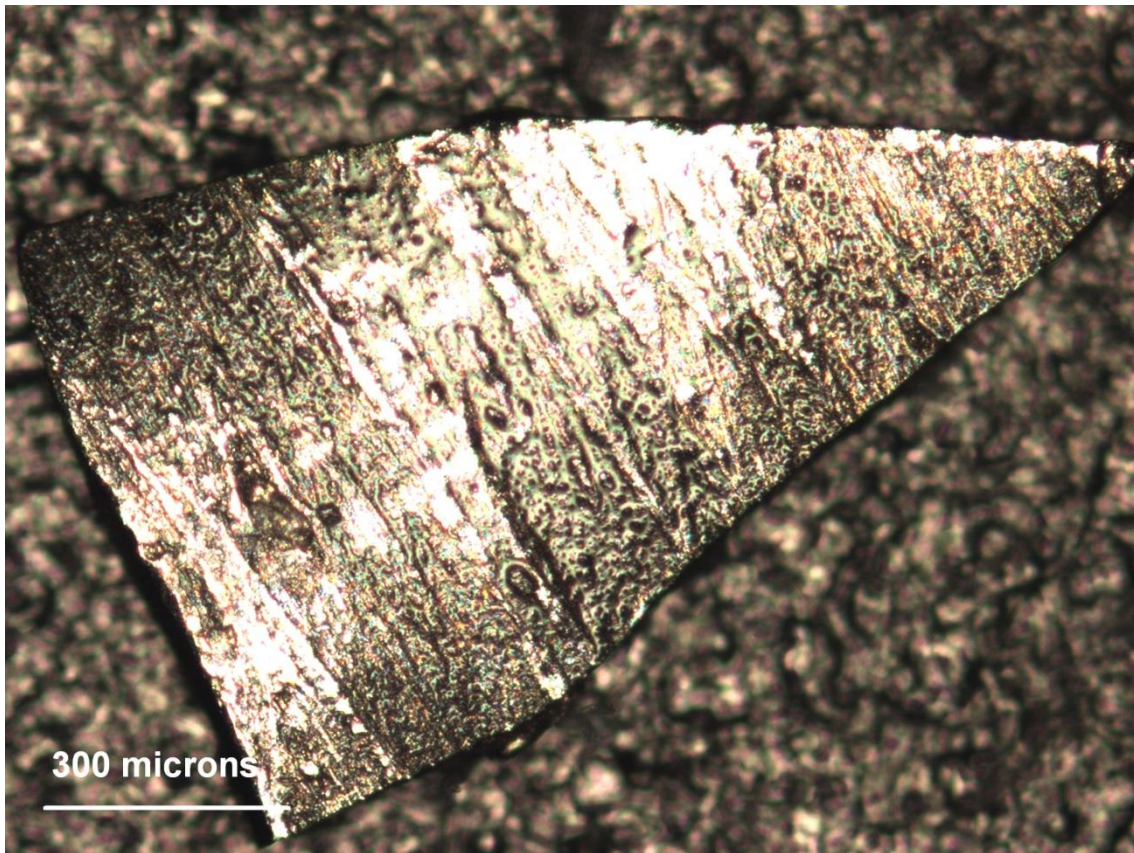
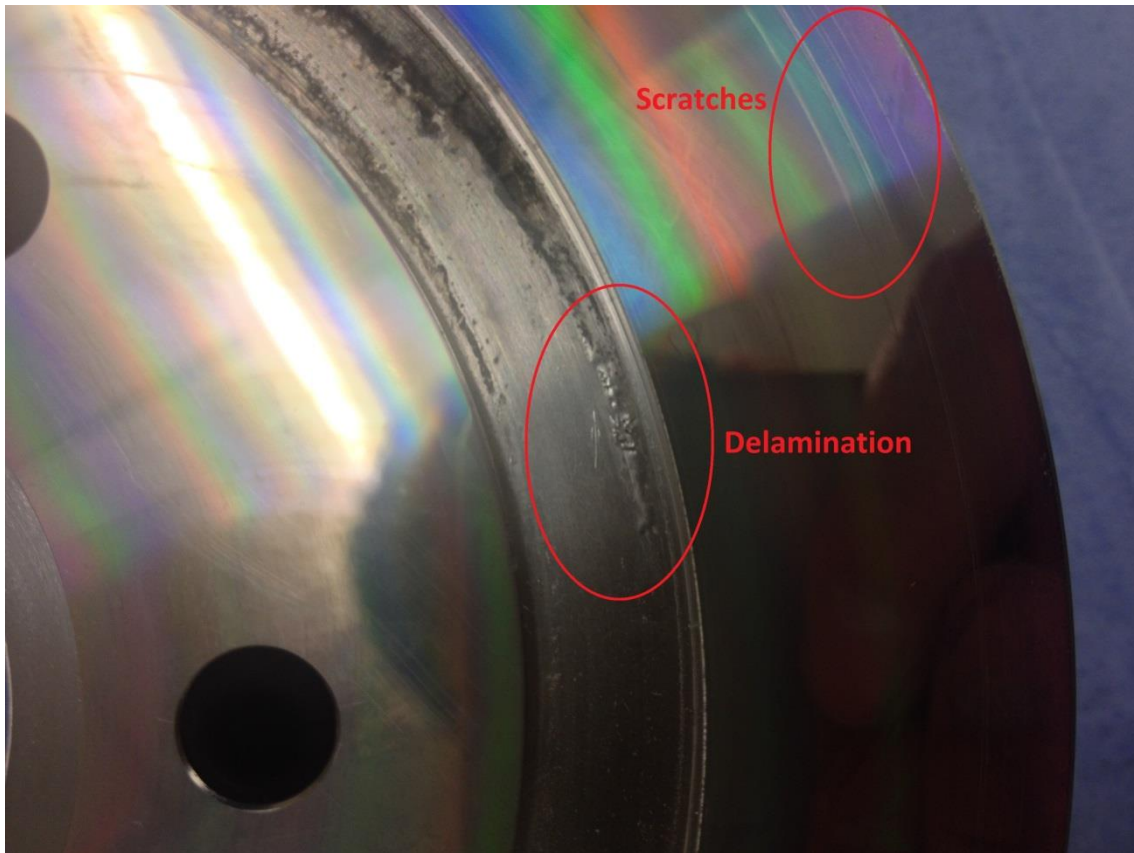


Figure 70 The microscope image of the coating debris inside the bearing housing



The debris above was about 1.2mm*0.9mm big. From its texture, it probably came from the coating inside the bearing housing. Since the design bearing gap was just about 30 μ m, such a large fragment would definitely cause extra attrition to the system. Its source might be the screw thread remaining of the coating or from the delamination of the nickel coating just as the following figure shows.

Figure 71 The delamination and scratches condition on the surface of the thrust plate



The depth of the scratches was measured by Taylor-Hobson Form Talysurf-120L and specifications were listed in the appendix.

Figure 72 Taylor-Hobson Form Talysurf-120L



The measuring results are showed in the following figures. The first figure indicates the surface roughness of it and the second figure shows the depths of the scratches.

Figure 73 The surface roughness of the surface of the thrust bearing pad

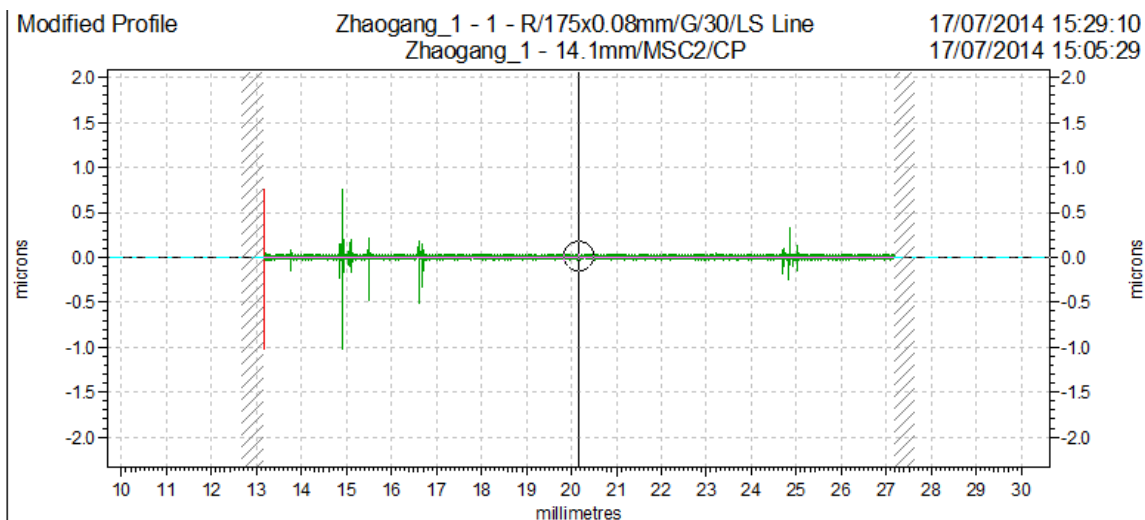
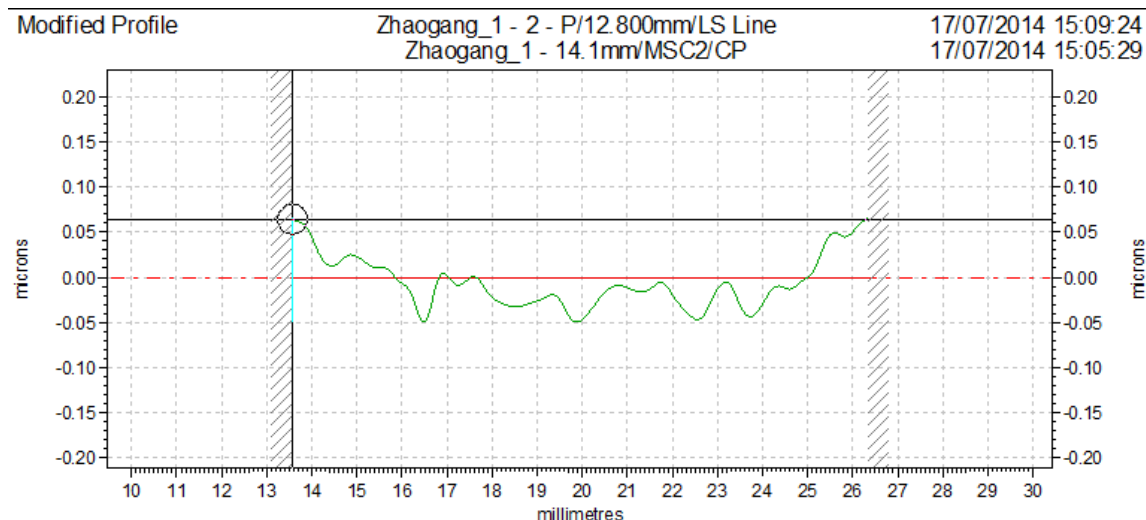


Figure 74 The depth of the scratches on the thrust bearing pad



From the above figure, the surface roughness was about $0.7\mu\text{m}$, and the depth of the scratches was about $0.1\mu\text{m}$. The scratches were not very serious compared with the bearing gap of about $30\mu\text{m}$ and the depth of the nickel coating of about $50\mu\text{m}$. But it would accelerate the degradation of the bearing surface and affect the bearing performance in a long term.

6.4.2 THE EXPERIMENT PROCESS

Under the testing process, the viscosity was 15cSt (0.0135Ns/m^2), the journal supply pressure was 60bar , the thrust supply pressure was 40bar , and the rotational speed was 0rpm . As mentioned in 6.2.2 *THE DIMENSIONS OF THE EXPERIMENTAL COMPONENTS*, the journal bearing clearance was $28.5\mu\text{m}$, the thrust bearing clearance was $29\mu\text{m}$. The bearing parameters calculations are listed in the following tables.

Table 40 The journal bearing parameters under the testing conditions

Number of pockets: $n=$	5	
Diameter of bearing: $d_B=$	0.099800	m
Length of bearing: $L_B=$	0.059000	m
Width of axial land: $c_a=$	0.065000	m
Width of circumferential land: $c_c=$	0.013000	m
Radial clearance: $h_{L(av)}=$	0.00002850	m

Depth of pocket: h_p =	0.002000	m
Supply Pressure: p_1 =	6000000	Pa
Rotational speed: N_d =	0	rev/min
Resistance ratio: ξ =	1	
Viscosity of oil: η =	15	cSt
Density of oil: ρ =	900	kg/m ³
Specific Heat capacity of oil: C_m =	2000	J/(kg*K)
Constant: k =	0.943000	
Bearing shape factor: Φ =	0.753099	
Bearing shape factor: E_a =	0.559322	
Bearing shape factor: E_c =	0.170315	
Outflow resistance: R_{od} =	7257.776767	10 ⁸ Ns/m ⁵
Inflow resistance: R_i =	7257.776767	10 ⁸ Ns/m ⁵
Ultimate load capacity: W_u =	18176.168029	N
Radial stiffness: S_i =	8.860691	10 ⁸ N/m
Flow rate: Q =	1.216	L/min
Pumping power: P_p =	123.694904	W
Friction power: P_f =	0.000000	W
Temperature rise: $\Delta t \approx$	3.333	° C

Table 41 The thrust bearing parameters under the testing conditions

Outer diameter of thrust pad: D_B =	0.176000	m
Outer diameter of annular pocket: D_P =	0.163000	m
Inner diameter of annular pocket: d_P =	0.133000	m
Inner diameter of thrust pad: d_B =	0.120000	m
Clearance at the lands of each thrust pad at no load: h_d =	0.00002900	m
Clearance at the pocket: h_P =	0.002000	m
Supply pressure: p_1 =	4000000	Pa
Speed of rotation: n =	0	rev/min
Resistance ratio: ξ =	3	
Viscosity of the fluid: η =	15	cSt
Density of oil: ρ =	900	kg/m ³

Specific Heat capacity of oil: C_m =	2000	J/(kg*K)
Ratio ξ_2/ξ_1 for a pair of opposed plane pads or rotary thrust bearings: Ξ =	1	
Ratio A_{V2}/A_{V1} for a pair of opposed plane pads or rotary thrust bearings: T =	1	
Virtual area of the thrust pad: $A_{V2}=A_{V1}$ =	0.009991	M^2
$R_{o(1)}$ =	8.116112	$10^{10}Ns/m^5$
$R_{o(2)}$ =	10.879197	$10^{10}Ns/m^5$
Outflow resistance: $R_{o(net)}$ =	4.648347	$10^{10}Ns/m^5$
Inflow resistance: R_i =	13.945041	$10^{10}Ns/m^5$
Ultimate thrust capacity: $T_{(net)}$ =	38367.29647	N
Stiffness: S_T = when $h_{(1)}=h_d$	15.504026	$10^8N/m$
Flow rate: Q =	1.291	L/min
Total Pumping power: P_p =	172.104196	W
Total Friction power: P_f =	0.000000	W
Temperature rise: $\Delta t \approx$	2.222222	K

The total flow rate of two bearing system was 2.507L/min, the temperature rise was 2.78 C, the total pumping power was 295.79W.

Under 60bar supply pressure, the journal resistance ratio 1 and the thrust resistance ratio 3, the bearing clearances at 30bar journal pocket pressure and 10 bar thrust pocket pressure were 31.45 μ m and 32.69 μ m respectively, the theoretical calculations considering the deflections of the journal bearings are listed in the following tables.

Table 42 The journal bearing parameters under the specified testing conditions

Number of pockets: n =	5	
Diameter of bearing: d_B =	0.099800	m
Length of bearing: L_B =	0.059000	m
Width of axial land: c_a =	0.065000	m
Width of circumferential land: c_c =	0.013000	m
Radial clearance: $h_{L(av)}$ =	0.00003145	m
Depth of pocket: h_p =	0.002000	m

Supply Pressure: $p_1=$	6000000	Pa
Rotational speed: $N_d=$	0	rev/min
Resistance ratio: $\xi =$	1	
Viscosity of oil: $\eta =$	15	cSt
Density of oil: $\rho =$	900	kg/m ³
Specific Heat capacity of oil: $C_m=$	2000	J/(kg*K)
Constant: $k=$	0.937096	
Bearing shape factor: $\Phi =$	0.753099	
Bearing shape factor: $E_a=$	0.559322	
Bearing shape factor: $E_c=$	0.170315	
Outflow resistance: $R_{od}=$	5399.995342	10 ⁸ Ns/m ⁵
Inflow resistance: $R_i=$	5399.995342	10 ⁸ Ns/m ⁵
Ultimate load capacity: $W_u=$	18176.168029	N
Radial stiffness: $S_l=$	8.029051	10 ⁸ N/m
Flow rate: $Q=$	1.663	L/min
Pumping power: $P_p=$	166.250143	W
Friction power: $P_f=$	0.000000	W
Temperature rise: $\Delta t \approx$	3.333	° C

Table 43 The thrust bearing parameters under the specified testing conditions

Outer diameter of thrust pad: $D_B=$	0.176000	m
Outer diameter of annular pocket: $D_P=$	0.163000	m
Inner diameter of annular pocket: $d_P=$	0.133000	m
Inner diameter of thrust pad: $d_B=$	0.120000	m
Clearance at the lands of each thrust pad at no load: $h_d=$	0.00003269	m
Clearance at the pocket: $h_P=$	0.002000	m
Supply pressure: $p_1=$	4000000	Pa
Speed of rotation: $n=$	0	rev/min
Resistance ratio: $\xi =$	3	
Viscosity of the fluid: $\eta =$	0.0135	Ns/m ²
Density of oil: $\rho =$	900	kg/m ³
Specific Heat capacity of oil: $C_m=$	2000	J/(kg*K)

Ratio ξ_2/ξ_1 for a pair of opposed plane pads or rotary thrust bearings: $\Xi =$	1	
Ratio A_{v2}/A_{v1} for a pair of opposed plane pads or rotary thrust bearings: $\Gamma =$	1	
Virtual area of the thrust pad: $A_{v2}=A_{v1}=$	0.009991	M^2
$R_{o(1)}=$	5.665750	$10^{10}Ns/m^5$
$R_{o(2)}=$	7.594623	$10^{10}Ns/m^5$
Outflow resistance: $R_{o(net)}=$	3.244949	$10^{10}Ns/m^5$
Inflow resistance: $R_i=$	9.734848	$10^{10}Ns/m^5$
Ultimate thrust capacity: $T_{(net)}=$	38367.296470	N
Stiffness: $S_T=$ when $h_{(1)}=h_d$	13.753533	$10^8N/m$
Flow rate: $Q=$	1.849	L/min
Total Pumping power: $P_p=$	246.536986	W
Total Friction power: $P_f=$	0.000000	W
Temperature rise: $\Delta t \approx$	2.222222	K

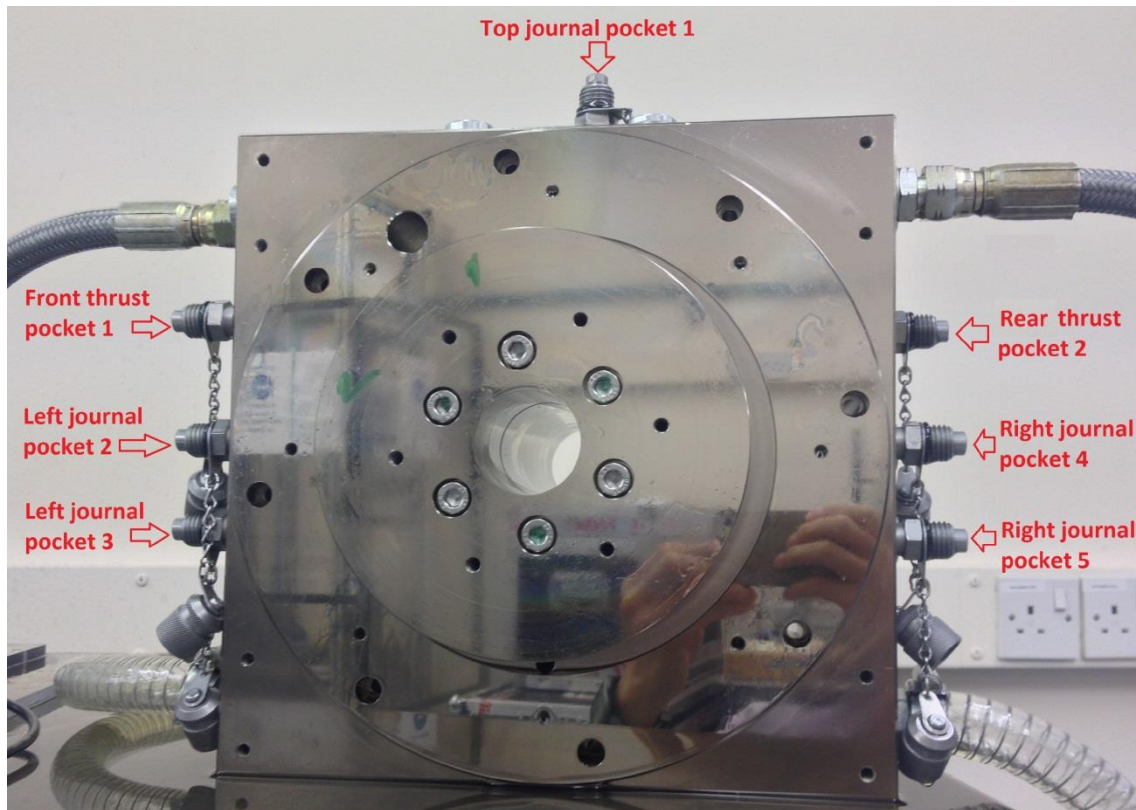
From the tables above, the stiffness for journal bearing was $802.9N/\mu m$, so the Δh under 3000N maximum load was $3.736\mu m$. The stiffness for thrust bearing was $1375.4N/\mu m$, so the Δh under 500N maximum load was $0.364\mu m$.

6.4.3 THE EXPERIMENT RESULTS

6.4.3.1 THE POCKET PRESSURE

There are 7 pockets within the bearing housing. As shown in the following figure, the seven pocket pressure measuring screws were on the top and two sides of the bearing housing: 2 for thrust pockets and 5 for journal pockets.

Figure 75 Seven pocket pressure measuring screws



The required journal pocket pressure is 30bar and the resistance ratio for the journal resistors is 1, so the supply pressure shall be adjusted as 60bar.

The required thrust pocket pressure is 10bar and the resistance ratio for the thrust resistors is 3, so the supply pressure shall be 40bar.

But there was only one pump to supply both the journal bearings and the thrust bearings. The supply pressure was 60bar. So a pressure regulating valve as well as a pressure gauge was put before the thrust bearing inlet pipe. The following two figures show the pipe connections and the schematic diagram of the oil supply system.

Figure 76 The pipes and connections for the hydraulic system

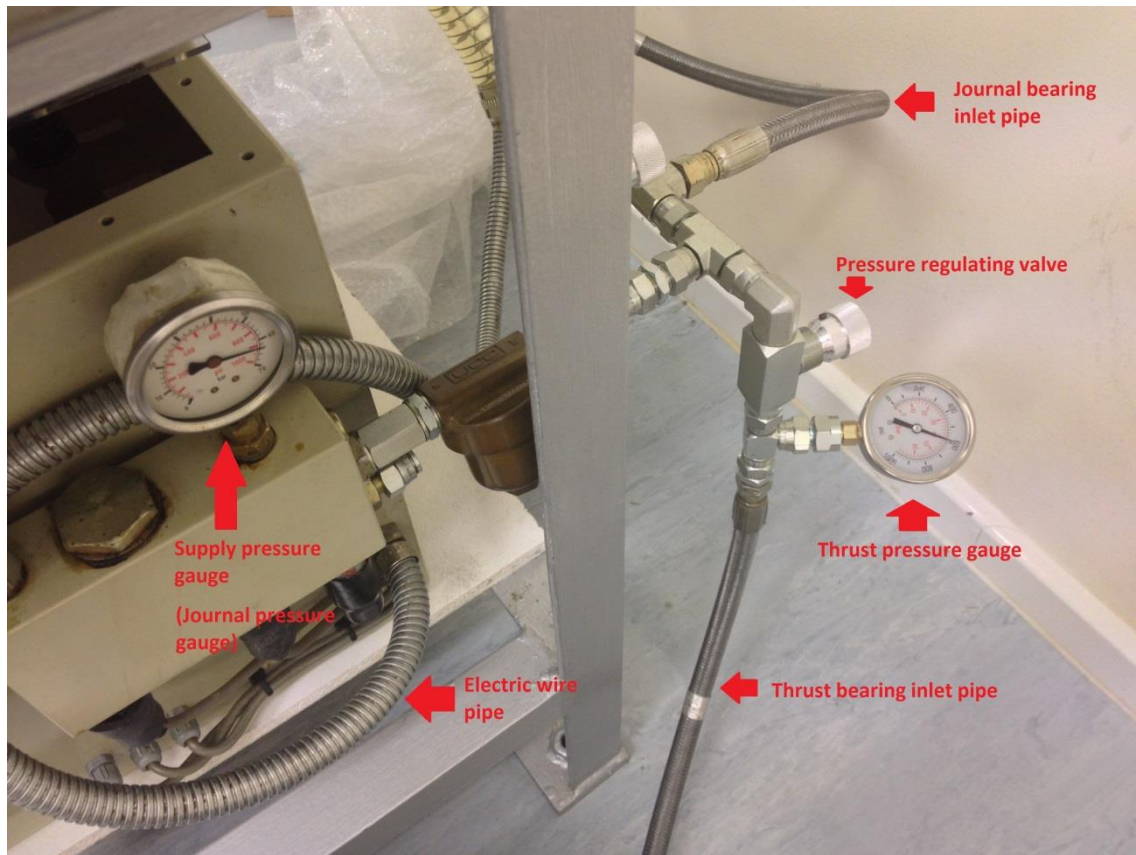
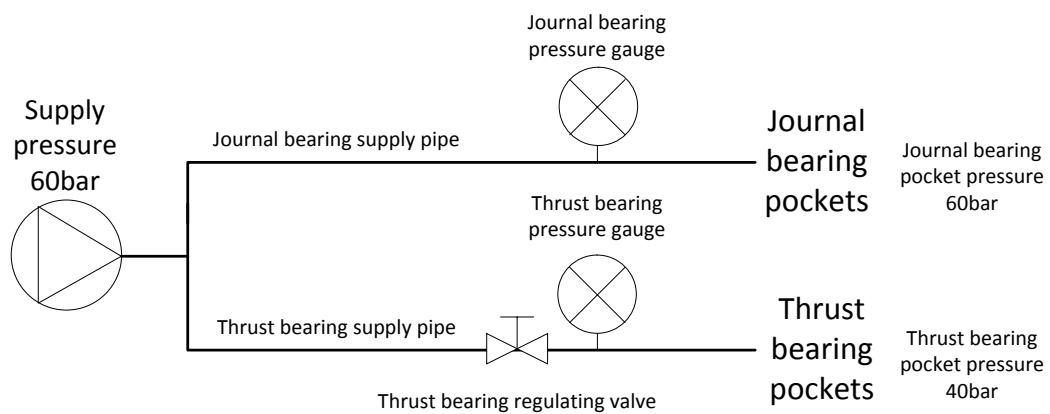


Figure 77 The schematic diagram of the oil supply system



By using a thrust bearing regulating valve, the thrust bearing supply pressure could be adjusted to 40bar. Under the new supply pressure combination of journal bearing supply pressure of 60bar and thrust bearing supply pressure of 40bar, new pocket pressures without any loading conditions are listed below:

$$P_{\text{thrust1}}=6\text{bar}$$

$$P_{\text{thrust2}}=7\text{bar}$$

$P_{\text{journal1}}=10\text{bar}$

$P_{\text{journal2}}=17.5\text{bar}$ $P_{\text{journal4}}=16\text{bar}$

$P_{\text{journal3}}=11\text{bar}$ $P_{\text{journal5}}=13\text{bar}$

The starting force to rotate the bearing spindle under this uneven journal pocket pressures was 0.1N as showed in the following figure.

Figure 78 The start rotating force of the bearing spindle under uneven journal bearing pocket pressures



According to the supply pressure and the resistance ratio, the pocket pressure shall be 10bar in thrust and 30bar in journal respectively. The actual pressures were all lower than the target pressures.

Although the bearing restrictors were nominally same as one specified type, the actual manufacturing process seemed not that ideal. Since the inner diameter of the tube was very small, about 0.3mm, and the inner diameter was strongly relevant to the resistance of the hydrostatic bearing restrictors. Any slight reduce or increase of the inner diameter could cause different resistance value. The inner diameter of the restrictor tube might vary slightly, which would finally lead to different resistance ratio of the journal bearing.

Another reason was that there was only one journal bearing inlet pipe and this pipe supplied all the five journal bearings. Five different journal restrictors had different distance to the supply point and the paths conducting the oil flow within

the housing were different from each other. The pressure drop in pipes was mainly caused by:

- Friction;
- Elevation difference;
- Changes of kinetic energy due to the shape of the paths;

The pressure drop in circular pipes could be calculated by the equation below:

Pressure drop equation $\Delta p = \lambda \times \frac{L}{D} \times \frac{\rho}{2} \times v$ Equation 34

Where λ is pipe friction coefficient, v is flow velocity.

Also according to Bernoulli's Equation below:

Bernoulli's Equation $p + \frac{1}{2} \rho V^2 + \rho gh = constant$ Equation 35

When the elevation h keeps constant, the higher the flow rate is, the lower the pressure will be. Ideally, each journal pocket has the same pocket pressure. But the actual condition was that the flow rate of each pocket was different due to different bearing gaps. The different outflow resistance of each journal pocket led to different pocket pressure.

In this case, the frictional force within the flow paths was the main source of the pressure drop. The paths' difference would lead to different actual supply pressure for each restrictor on the inlet side.

So swapping the nearer restrictor with a larger resistance restrictor and the farther restrictor with a smaller resistance restrictor might be a simple solution. The method was to keep swapping the restrictors of the highest pocket pressure and the lowest pocket pressure to adjust the five bearing pocket pressures until reaching an even condition.

After swapping the highest pressure journal restrictor and the lowest pressure journal restrictor, the pocket pressures changed to the data below:

$P_{thrust1}=7bar$ $P_{thrust2}=7bar$

$P_{journal1}=15bar$

$P_{\text{journal}2}=17\text{bar}$ $P_{\text{journal}4}=17\text{bar}$

$P_{\text{journal}3}=16\text{bar}$ $P_{\text{journal}5}=15\text{bar}$

The starting force to rotate the bearing spindle under this uneven journal pocket pressures was 0.05N as showed in the following g figure.

Figure 79 The start rotating force of the bearing spindle under even journal bearing pocket pressures



It was initially concluded that the even journal pocket pressure could lead to less internal frictional force to make the system more efficient.

The target pocket pressure is 30bar for journal bearings and 10bar for thrust bearings, the solution to attain higher pocket pressure was to either increase the motor power or change the shape of the restrictors to get the ideal resistance ratio.

Another solution was to supply each pocket separately with an independent close-loop-control pressure regulating valve to keep the pocket pressure on the target value. As a result, its cost would be much higher than the original design.

The journal bearing pocket pressure increased a lot after changing the journal restrictors to lower resistance, and by increasing thrust supplying pressure, the thrust bearing pocket pressure also increased. The improved value is showed in the following:

$P_{\text{thrust1}}=8\text{bar}$ $P_{\text{thrust2}}=8\text{bar}$

$P_{\text{journal1}}=27\text{bar}$

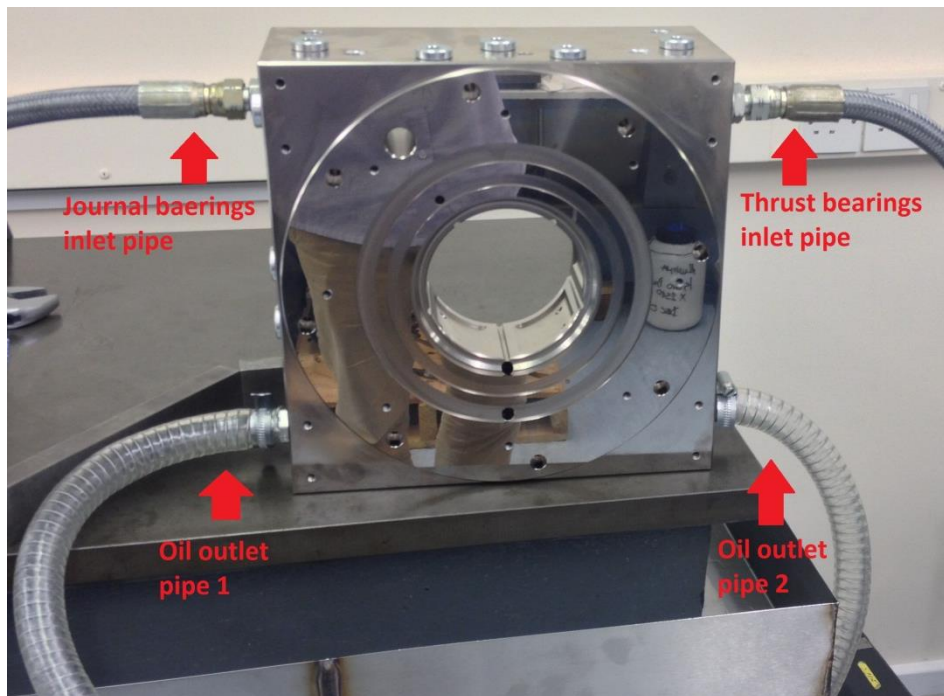
$P_{\text{journal2}}=25\text{bar}$ $P_{\text{journal4}}=25\text{bar}$

$P_{\text{journal3}}=27\text{bar}$ $P_{\text{journal5}}=25\text{bar}$

This pocket pressure distribution was almost close to the target pressure combination: $P_{\text{journal}}=30\text{bar}$ and $P_{\text{thrust}}=10\text{bar}$. Since the fuse in the plug of the inverter was 3A, when the working frequency of the plug reached 50Hz, the fuse blew and the system broke down. So the target supply pressure could not be realized by this set of inverter and motor.

6.4.3.2 THE FLOW RATE

There were two oil inlet pipes connected to the housing of the bearing system. Since these two pipes were high pressure pipes, the flow rate was not safe by being measured through high pressure pipes.



There were also two outlet pipes of the bearing system. Most of the oil from the bearing pockets flowed through these two pipes into the oil tank. However there was still some oil flowing through the bearing gap and drops to the workbench

surface, being collected by the sink under the workbench. The method to measure the total outflow was using a liquid container to collect the all three strands of the oil for 1 minute to see the volume (L/min).

Figure 80 The container used to measure the flow rate



The flow rate experiment at:

$$P_{\text{thrust1}}=6\text{bar}$$

$$P_{\text{thrust2}}=6\text{bar}$$

$$P_{\text{journal1}}=11.5\text{bar}$$

$$P_{\text{journal2}}=19\text{bar}$$

$$P_{\text{journal4}}=19\text{bar}$$

$$P_{\text{journal3}}=14.5\text{bar}$$

$$P_{\text{journal5}}=14.5\text{bar}$$

$$Q=1.6\text{L/min}$$

Changed the journal restrictors, the flow at:

$$P_{\text{thrust1}}=8\text{bar}$$

$$P_{\text{thrust2}}=8\text{bar}$$

$$P_{\text{journal1}}=27\text{bar}$$

$$P_{\text{journal2}}=25\text{bar}$$

$$P_{\text{journal4}}=25\text{bar}$$

$$P_{\text{journal3}}=27\text{bar}$$

$$P_{\text{journal5}}=25\text{bar}$$

$$Q=2.8\text{L/min}$$

The flow rate increased quite a lot due to the increased supply pressure.

According to the theoretical calculation at $P_{\text{thrust}}=10\text{bar}$ and $P_{\text{journal}}=30\text{bar}$:

Journal clearance was $28.5\mu\text{m}$, the deflection at 30bar was $2.952\mu\text{m}$, the $h'=31.452\mu\text{m}$, the total theoretical flow rate (30bar, 15cSt, 5 journal pockets) was 1.216L/min.

Thrust clearance was $29.0\mu\text{m}$, the deflection at 10bar was $3.691\mu\text{m}$, the $h'=32.691\mu\text{m}$, the total theoretical flow rate (10bar, 15cSt, 2 thrust pockets) was 1.849L/min.

The total flow rate of the system was 3.065L/min, which was quite near the second experimental data, 2.8L/min. If the pocket pressure could reach 30bar and 10bar ideally, the actual flow rate would probably be around 3L/min.

The increased flow rate at the same supply pressure also led to the higher pumping power of the motor. The temperature rise tests of the system would be illustrated in the following section.

6.4.3.3 THE AXIAL STIFFNESS

The axial stiffness could be measured when the bearing was lying on the workbench. The working load of the thrust bearing was 50KG. So 500N weights were used to do the tests.

Figure 81 Lying down the bearing housing to measure the axial stiffness

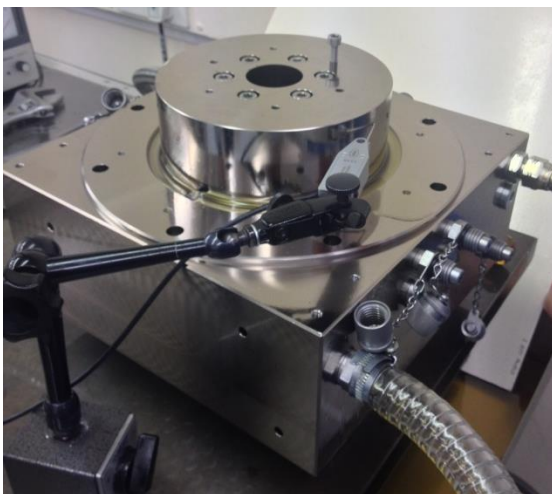


Figure 82 The sensor of the clock fixed on the top face of the bearing housing

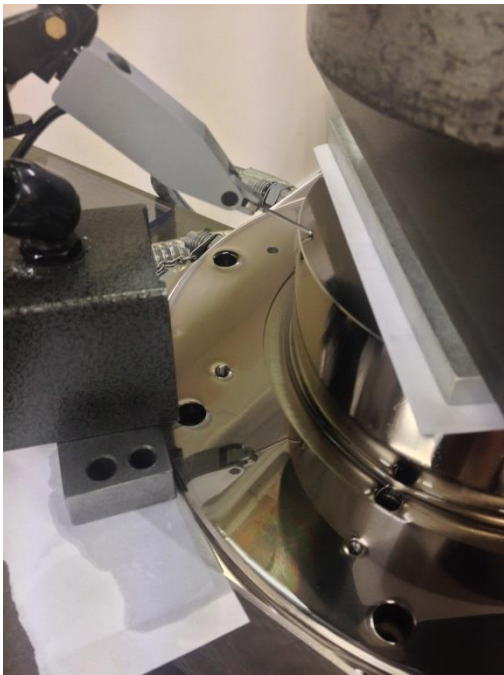
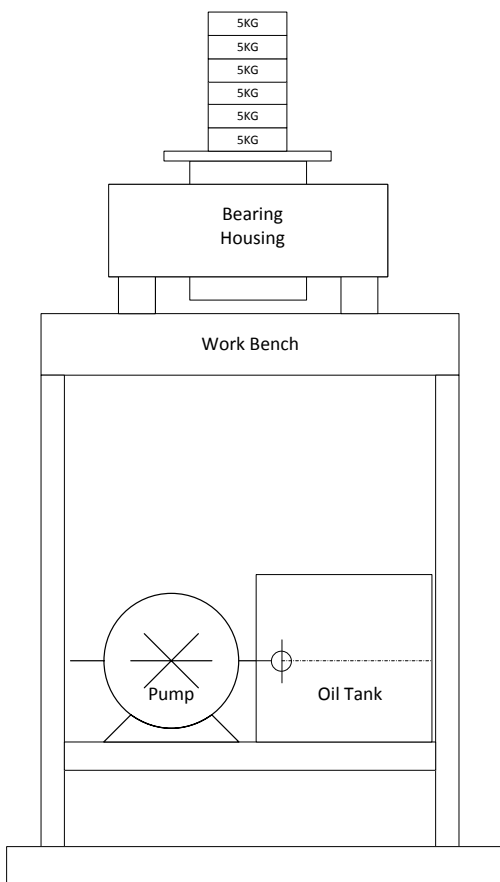


Figure 83 The schematic diagram of the axial stiffness testing system



The following tables and figures were the two sets of data of the experiments to measure the axial stiffness of the hydrostatic bearing system:

Table 44 The table of axial stiffness test 1 of the bearing system ($P_{journal1}=9bar$, $P_{journal2}=17bar$, $P_{journal3}=13bar$, $P_{journal4}=18bar$, $P_{journal5}=12bar$, $P_{thrustfront}=5bar$, $P_{thrustrear}=5bar$)

Weight (KG)	Displacement (μm)	Stiffness (N/ μm)
10.6	0.5	21.2
20.6	5	41.2
25.6	8	32
30.6	10	30.6
25.6	10	25.6
20.6	8	25.8
10.6	3	35.3
0	1	

Figure 84 The figure of axial stiffness test 1 of the bearing system ($P_{journal1}=9bar$, $P_{journal2}=17bar$, $P_{journal3}=13bar$, $P_{journal4}=18bar$, $P_{journal5}=12bar$, $P_{thrustfront}=5bar$, $P_{thrustrear}=5bar$)

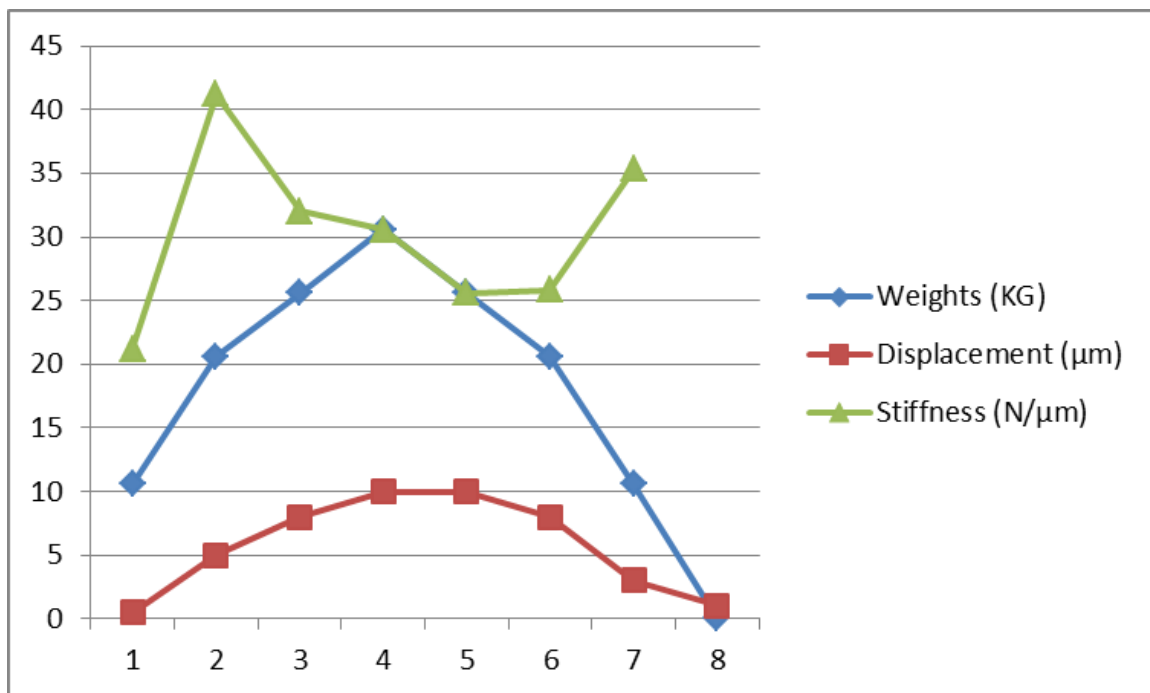
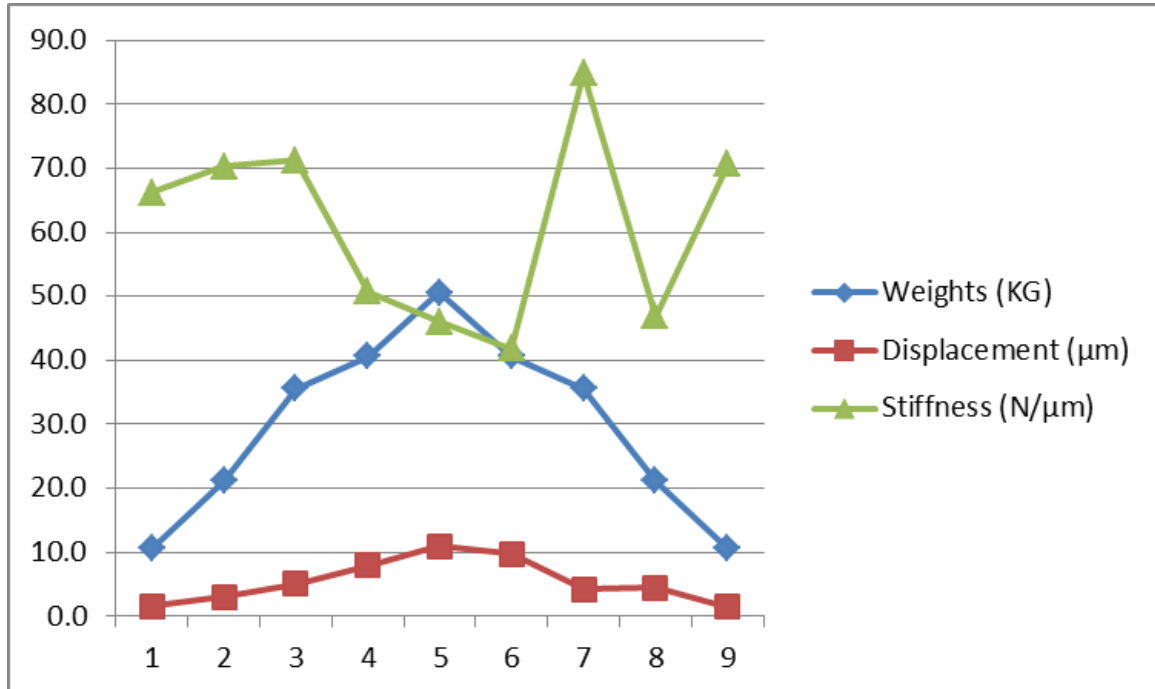


Table 45 The table of axial stiffness test 2 of the bearing system ($P_{journal1}=9bar$, $P_{journal2}=17bar$, $P_{journal3}=13bar$, $P_{journal4}=18bar$, $P_{journal5}=12bar$, $P_{thrustfront}=5bar$, $P_{thrustrear}=5bar$)

Weights (KG)	Displacement (μm)	Stiffness (N/ μm)
10.6	1.6	66.3
21.1	3.0	70.3
35.6	5.0	71.2
40.6	8.0	50.8
50.6	11.0	46.0
40.6	9.7	41.9
35.6	4.2	84.8
21.1	4.5	46.9
10.6	1.5	70.7

Table 46 The figure of axial stiffness test 2 of the bearing system ($P_{journal1}=9bar$, $P_{journal2}=17bar$, $P_{journal3}=13bar$, $P_{journal4}=18bar$, $P_{journal5}=12bar$, $P_{thrustfront}=5bar$, $P_{thrustrear}=5bar$)



During the loading and unloading process of the axial stiffness tests, the displacement data showed some consistency with the weights change. But the

axial stiffness displayed an irregular variation, which seemed to be irrelevant to the change of the weights.

The axial stiffness of the thrust bearings was about 30-60N/ μm .

According to the theoretical calculations, as $P_{\text{thrust pocket}}=5\text{bar}$, the axial stiffness was 187N/ μm , the testing result was about one-fourth of the theoretical result, which means the axial stiffness performance of the bearing was not very well according to the ideal design.

6.4.3.4 THE RADIAL STIFFNESS

To measure the radial stiffness of the hydrostatic bearing, some extra experimental tools shall be made. For example, the rod through the bearing spindle and symmetrical weights put on both sides of the rod shall all be prepared to do the tests.

Two screws were bolted on each side of the rod just as the following figure shows. Two aluminium plates were fixed on the bottom of the screws to put the weights on. The experiment configurations and schematic diagram are shown in the following figures.

Figure 85 The experimental tools used to measure the radial stiffness



Figure 86 The schematic diagram of the radial stiffness testing system

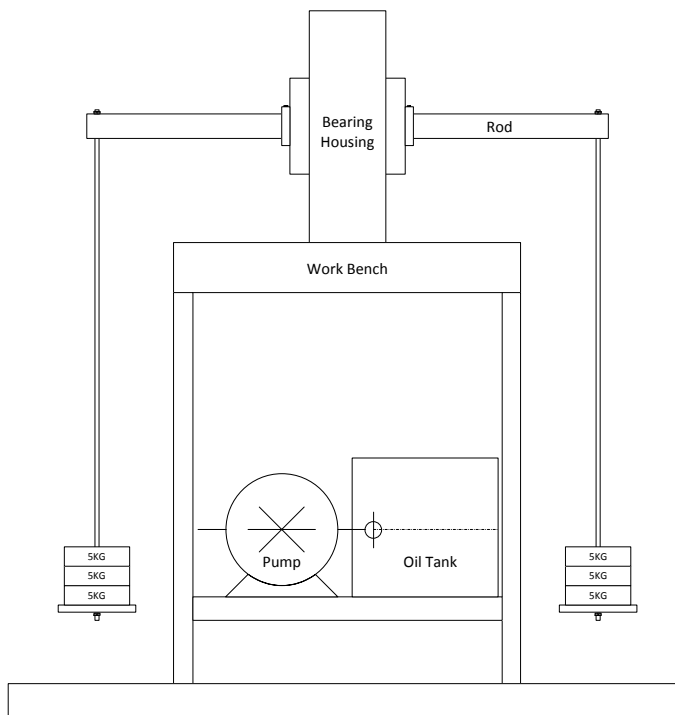


Figure 87 The weights used to load the system



Figure 88 Stack same weights on both sides of the rod at the same time

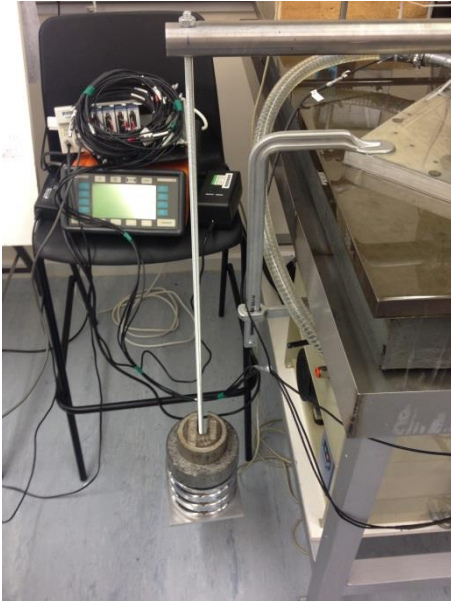


Table 47 Front thrust plate displacement measurement



Table 48 Rear thrust plate displacement measurement

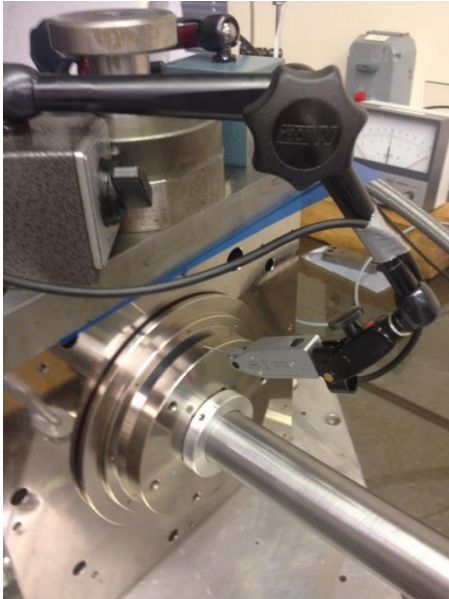


Table 49 Radial stiffness test 1

Weights (KG)	Front thrust plate displacement (μm)	Front stiffness ($\text{N}/\mu\text{m}$)	Rear thrust plate displacement (μm)	Rear stiffness ($\text{N}/\mu\text{m}$)
4.5	2.0	45.4	-1.0	-90.8
9.0	-0.5	-360.0	-0.5	-360.0
13.5	1.0	270.0	-3.0	-90.0
18.5	1.0	370.0	-3.0	-123.3
23.5	-3.0	-156.7	-4.0	-117.5
18.5	-3.0	-123.3	-3.0	-123.3
13.5	1.0	270.0	-4.0	-67.5
9.0	-4.0	-45.0	-4.0	-45.0
4.5	-3.0	-30.0	-4.0	-22.5
0.0	-2.0	0.0	-2.0	0.0

Figure 89 The figure of radial stiffness test 1

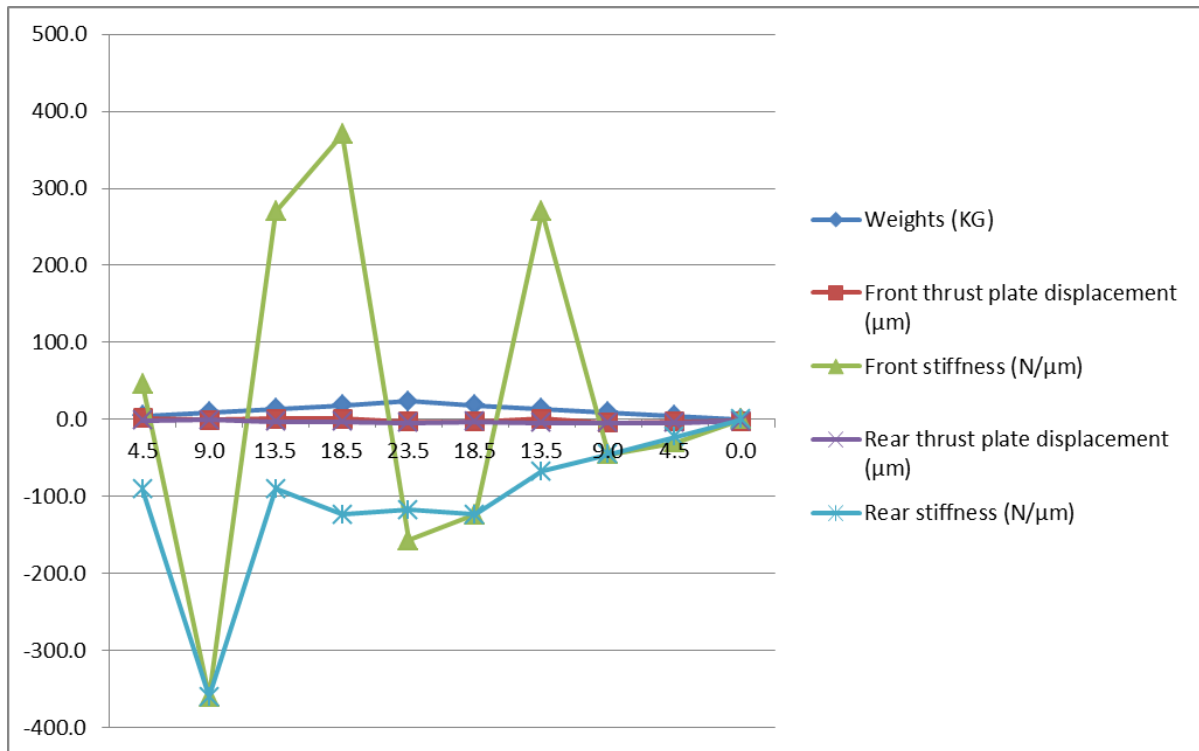


Table 50 Radial stiffness test 2

Weights (KG)	Front thrust plate displacement (µm)	Front stiffness (N/µm)	Rear thrust plate displacement (µm)	Rear stiffness (N/µm)
4.5	3.0	30.3	-1.0	-90.8
9.0	-2.5	-72.0	0.0	-270.0
13.5	3.0	90.0	-1.0	-370.0
18.5	-3.0	-123.3	-1.0	-370.0
23.5	-3.0	-156.7	-2.8	-167.9
18.5	-1.5	-246.7	-3.0	-123.3
13.5	2.0	135.0	-2.0	-135.0
9.0	-1.0	-180.0	-3.0	-60.0
4.5	1.5	60.0	-2.8	-32.1
0.0	1.8	0.0	1.0	0.0

Table 51 The figure of radial stiffness test 2

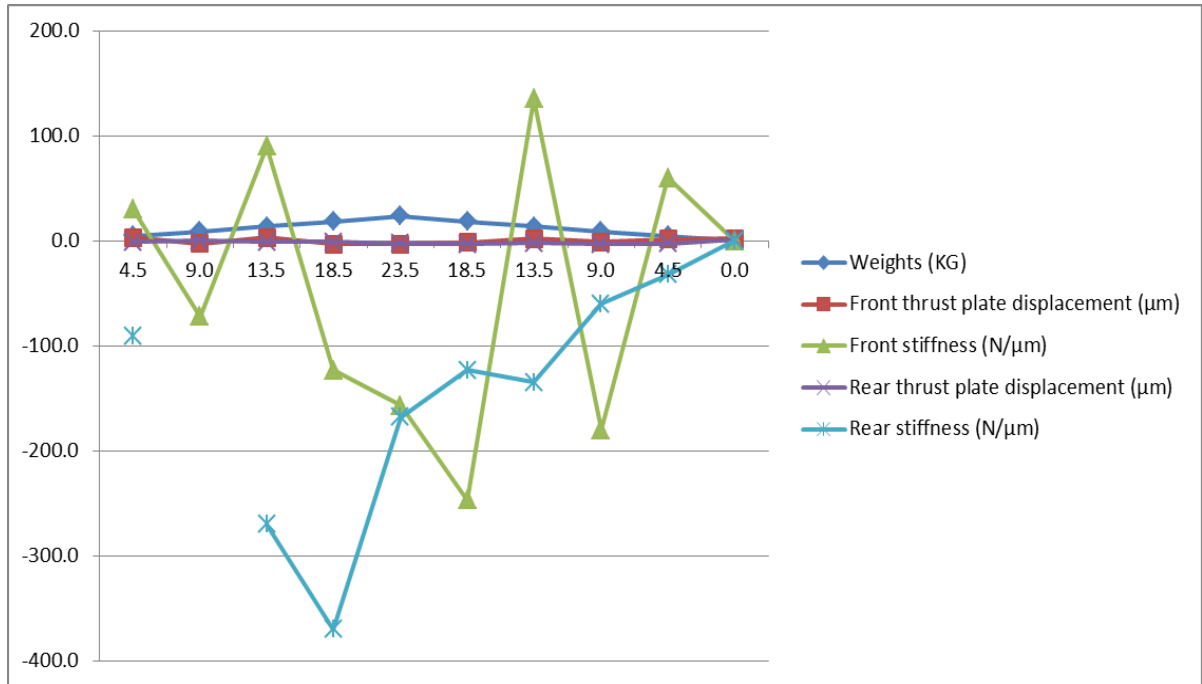
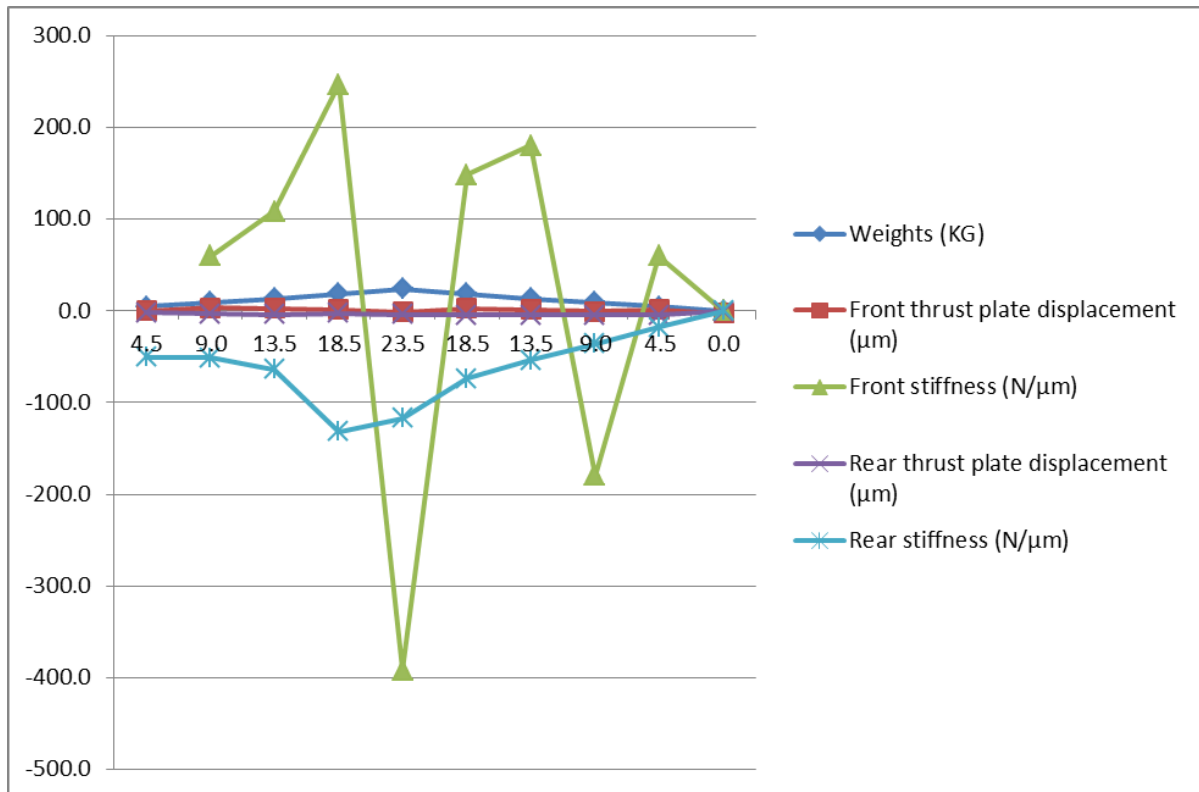


Table 52 Radial stiffness test 3

Weights (KG)	Front thrust plate displacement (µm)	Front stiffness (N/µm)	Rear thrust plate displacement (µm)	Rear stiffness (N/µm)
4.5	0.0		-1.8	-50.4
9.0	3.0	60.0	-3.5	-51.4
13.5	2.5	108.0	-4.2	-64.3
18.5	1.5	246.7	-2.8	-132.1
23.5	-1.2	-391.7	-4.0	-117.5
18.5	2.5	148.0	-5.0	-74.0
13.5	1.5	180.0	-5.0	-54.0
9.0	-1.0	-180.0	-5.0	-36.0
4.5	1.5	60.0	-5.0	-18.0
0.0	-3.0	0.0	-1.0	0.0

Table 53 The figure of radial stiffness test 3



The positive value of the displacement meant an upward movement of the edge of the thrust pad, which was an abnormal phenomenon. The normal result should be all negative values to indicate the downward movements of both edges of the opposite thrust pads.

From the data, the rear stiffness was always negative, which meant the displacement of the rear thrust plate was always downwards. But the movement of the front thrust plate was quite irregular. Its direction fluctuated with different weights. The poor tilting performance of the hydrostatic bearing system was probably the reason of it.

From all the data above, the average radial stiffness of the hydrostatic bearing system was about 100N/µm.

According to the theoretical calculations, as $P_{\text{journal pocket}}=27\text{bar}$, the axial stiffness was 361N/µm, the testing result was about one-third of the theoretical result, which meant the radial stiffness performance of the bearing was not very well according to the ideal design.

6.4.3.5 THE TEMPERATURE RISE

The energy used to increase the temperature mainly came from two sources: pumping power and frictional power. The over temperature rise would cause the malfunction of the bearing system.

To test the relationship between the pumping power and the temperature rise, the bearing spindle was set as a stationary status, i.e. $N=0\text{rpm}$. If only the pumping power was high enough to raise the oil temperature, then the cooling system was necessary before doing the rotational tests.

The following table was used to show the temperature rise due to the pumping power only within 60 minutes.

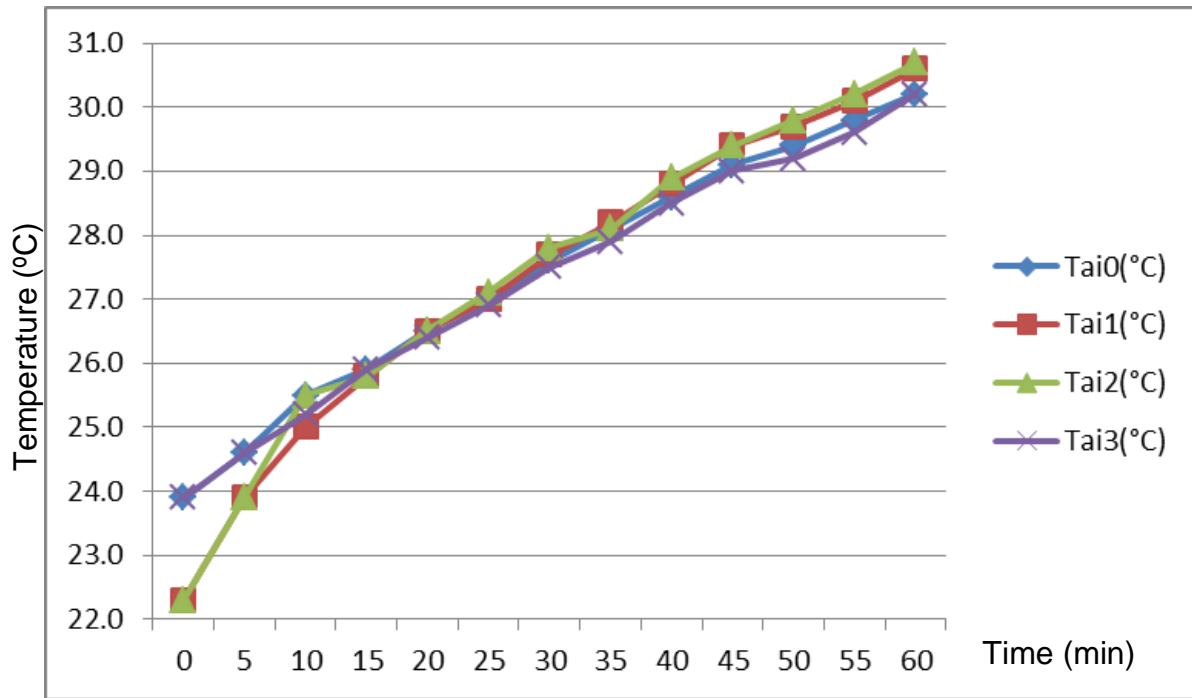
$P_{\text{journal supply}}=60\text{bar}$		$P_{\text{thrust supply}}=40\text{bar}$
$\eta=15\text{cSt}$	$N=0\text{rpm}$	$T_{\text{room}}=22.8^\circ\text{C}$
$P_{\text{thrust front}}=7\text{bar}$		$P_{\text{thrust rear}}=7\text{bar}$
$P_{\text{journal1}}=17\text{bar}$		
$P_{\text{journal2}}=20\text{bar}$		$P_{\text{journal4}}=17\text{bar}$
$P_{\text{journal3}}=15\text{bar}$		$P_{\text{journal5}}=20\text{bar}$

Table 54 The temperature rise condition under stationary pumping condition and lower pocket pressure

T(min)	$T_{\text{ai0}}(^{\circ}\text{C})$	$T_{\text{ai1}}(^{\circ}\text{C})$	$T_{\text{ai2}}(^{\circ}\text{C})$	$T_{\text{ai3}}(^{\circ}\text{C})$
0	23.9	22.3	22.3	23.9
10	24.6	23.9	23.9	24.6
15	25.5	25.0	25.5	25.2
20	25.9	25.8	25.8	25.9
25	26.5	26.5	26.5	26.4
30	27.0	27.0	27.1	26.9
35	27.6	27.7	27.8	27.5
40	28.1	28.2	28.1	27.9
45	28.6	28.8	28.9	28.5

50	29.1	29.4	29.4	29.0
55	29.4	29.7	29.8	29.2
60	29.8	30.1	30.2	29.6

Figure 90 The temperature rise condition under stationary pumping condition and lower pocket pressure



The theoretical temperature rises considering the deflection of the bearing surface at $P_{\text{journal pocket}}=18\text{bar}$ and $P_{\text{thrust pocket}}=7\text{bar}$ were:

$$\Delta T_{\text{thrust}}=1.6^{\circ}\text{C}$$

$$\Delta T_{\text{journal}}=2.0^{\circ}\text{C}$$

From the testing data, the temperature keeps rising. The temperature rise was below 3°C during the first 30 minutes. After the pump's continuous work, the temperature continuously rose and reached about 30°C in 60 minutes.

After changing five journal restrictors from high resistance to low resistance, the pocket pressure increased. The condition was listed below:

$$P_{\text{journal supply}}=60\text{bar}$$

$$P_{\text{thrust supply}}=40\text{bar}$$

$$\eta=15\text{cSt}$$

$$N=0\text{rpm}$$

$$T_{\text{room}}=22.8^{\circ}\text{C}$$

$P_{\text{thrust front}}=8\text{bar}$

$P_{\text{thrust rear}}=8\text{bar}$

$P_{\text{journal1}}=27\text{bar}$

$P_{\text{journal2}}=25\text{bar}$

$P_{\text{journal3}}=27\text{bar}$

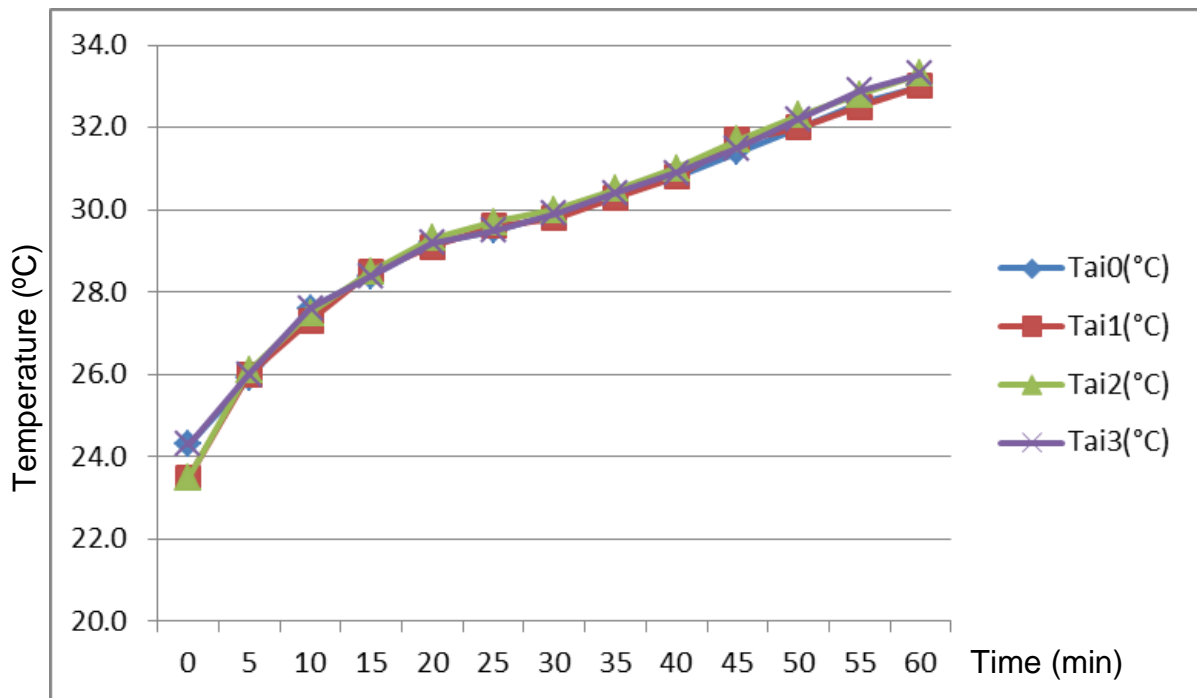
$P_{\text{journal4}}=25\text{bar}$

$P_{\text{journal5}}=25\text{bar}$

Table 55 The temperature rise condition under stationary pumping condition and higher pocket pressure

T(min)	$T_{\text{ai0}}(^{\circ}\text{C})$	$T_{\text{ai1}}(^{\circ}\text{C})$	$T_{\text{ai2}}(^{\circ}\text{C})$	$T_{\text{ai3}}(^{\circ}\text{C})$
0	24.3	23.5	23.5	24.3
5	25.9	26.0	26.1	26.0
10	27.6	27.3	27.5	27.6
15	28.4	28.5	28.5	28.4
20	29.2	29.1	29.3	29.2
25	29.5	29.6	29.7	29.5
30	29.9	29.8	30.0	29.9
35	30.4	30.3	30.5	30.4
40	30.8	30.8	31.0	30.9
45	31.4	31.7	31.7	31.5
50	32.0	32.0	32.3	32.2
55	32.6	32.5	32.8	32.9

Figure 91 The temperature rise condition under stationary pumping condition and higher pocket pressure



The theoretical temperature rose considering the deflection of the bearing surface at $P_{\text{journal pocket}}=26\text{bar}$ and $P_{\text{thrust pocket}}=8\text{bar}$ were:

$$\Delta T_{\text{thrust}}=1.8^{\circ}\text{C}$$

$$\Delta T_{\text{journal}}=2.9^{\circ}\text{C}$$

From the testing data, the temperature kept rising. The temperature rise was below 3°C during the first 30 minutes. After the pump's continuous work, the temperature continuously rose and reached about 33°C in 60 minutes.

Also from the data, the temperature rise at higher pocket pressure was larger than the temperature rise at lower pocket pressure. In a lower resistance hydrostatic bearing system, to maintain the same supply pressure meant the increase of the supply power because the flow rate increased a lot. Since it was a stationary system, all the energy raising the temperature came from the pumping power.

So, if the pumping power increases, the temperature rise will also increase. The highest temperature rise was about 10°C , which greatly beyond the required

temperature rise. So a chilling system was definitely needed to cool down the oil as well as a large oil tank was needed to maintain the oil at a lower temperature.

7 RESULTS AND DISCUSSION

According to experiment design, the target supply pressures were $P_{\text{thrust}}=10\text{bar}$ and $P_{\text{journal}}=30\text{bar}$. Adjusted the size of the restrictors, the optimum supply pressures were obtained as:

$$P_{\text{thrust1}}=8\text{bar} \quad P_{\text{thrust2}}=8\text{bar}$$

$$P_{\text{journal1}}=27\text{bar}$$

$$P_{\text{journal2}}=25\text{bar} \quad P_{\text{journal4}}=25\text{bar}$$

$$P_{\text{journal3}}=27\text{bar} \quad P_{\text{journal5}}=25\text{bar}$$

The fuse in the plug blew when the frequency of the inverter exceeded 50Hz, so the highest safe supply pressures under this condition were 60bar for the journal bearings and 40bar for the thrust bearings. The test results based on this combination of pocket pressures could be used to analyse the comparison between the theoretical calculations and actual experimental results.

The reasons of uneven journal bearing pocket pressures at the same supply pressure were probably the following two points:

1. The slight manufacturing difference, including the burrs remained within the tube or the different straightness of the hypodermic needles from different bearing restrictors, led to the different resistance ratio of the bearing restrictors;
2. Different oil conducting paths of each bearing pocket led to different pressure drop through different paths. Because of the manufacturing technique of drilling the holes inside the bearing housing to make the oil paths, the angles of two straight drills would cause the oil flow lose its kinetic energy when flowing through the angle and will lead to the extra pressure drop through the oil path. Different shapes of the oil paths would have different influences on the pressure drop of each journal bearing pockets.

According to the reasons listed above, the simply solution was to swapping the restrictors of the highest pocket pressure and the lowest pocket pressure and repeat this procedure until all the journal pocket pressures equal to each other. And another advanced solution might be using the 3D-printing technology to manufacture the oil path inside the bearing housing more smooth, which means not any sharp drill angles on the oil paths. By using the 3D-printing technology, each oil path of the five journal bearing pockets will have the same and minimum pressure drop condition by designing each path smoothly and separately.

The flow rate at higher pocket pressures was 2.8L/min, and the theoretical flow rate was 3.1L/min. So the experimental results were quite accord with the theoretical results. The close values probably meant the actual bearing gap was quite close to the design bearing gap. From the last measurement by the CMM machine, the final bearing gap was 24.955 μm , which quite accorded with the target bearing gap of about 25 μm . So the diamond turning process complied quite well with the design requirement.

The experimental axial stiffness, 30-60N/ μm , was about one-fourth of the theoretical value, 187N/ μm , and the radial stiffness, 80-100N/ μm , was about one-third of the theoretical value, 361N/ μm . The error between the theoretical values and actual values were quite large mainly due to the poor tilting performance of the bearing system. The single pocket thrust plate was easy for manufacturing which also meant lower cost, but it had relatively lower tilting stiffness compared with the multi-pockets design. If a high tilting stiffness was needed, the hydrostatic bearing system should be designed to meet the specific demand. In this R2R manufacturing system, since a couple of symmetrical hydrostatic bearings are used to put the 300KG drum roll on, most of the load comes from the gravity of the drum with its direction towards the ground, there is almost no tilting force or torque on the hydrostatic bearing shaft. And the total gravity force is distributed evenly on the two bearing spindles without too much irregular motions. So in this research project, the tilting stiffness is not regarded as the important working parameter for the bearing system. On the other side,

the radial stiffness to balance the gravitational force on the spindle is one of the crucial properties of the hydrostatic bearing system.

The experimental temperature rise just under the static condition, i.e. no rotational speed, continued to rise before turning off the pump. After one hour operation time, the oil temperature rise within the system was about 10°C. According to the analysis before, the temperature rise over 3°C was not well recommended, so a cooling system was definitely required to lower the temperature of the hydrostatic bearing system. The temperature control was beneficial not only to the accuracy of the bearing spindle, but also to the life cycle of the hydrostatic bearing system in a long term as well.

According to *Figure 71 The delamination and scratches condition on the surface of the thrust plate*, after short operational tests, the scratches on the surface were just about 0.1µm, and it probably came from the friction between the remained burs and the bearing surfaces. The delamination conditions showed in the figure were quite obvious that the burs drop easily at high rotational speed and cause the extra attrition between the surfaces of the hydrostatic bearings. The depth of the scratches was quite small that it could almost be considered as no extra attrition during the normal operational process. But the quality of the nickel-based electroless coating was definitely needed to be improved to eliminate the delamination degradation phenomenon and strengthen the surface mechanical properties such as hardness. If the coating is cheap and perfect, the new R2R hydrostatic bearing system might be economically successful and will definitely have a broad application.

8 CONCLUSIONS AND FURTHER WORKS

Measured performance in terms of lubricant temperature rise, flow rate was in close agreement with the predictions from the theoretical calculations.

Axial stiffness and radial stiffness were measured by amplifiers by adding symmetrical weights on both sides of the system. Since the fluctuation of the values of both axial stiffness and radial stiffness were quite large, the reasons of the deviation of the stiffness were needed to be further analysed by both theoretical analysis and experimental testing works. The reasons might be due to the design features as well as the manufacturing accuracy.

The tilt stiffness of the bearing system was not satisfied, so the rotational tests were not recommended to proceed due to the irregular rotational movement will cause some extra attrition to the surface of the bearing spindle. The low tilt stiffness could not prevent the contact of the surfaces by the force of the irregular rotational torque. So the 300rpm test shall be performed when the tilt stiffness is improved in the future. And a cooling system is needed to protect the system from the overheat condition.

The equations in the book (Stansfield, 1970, Hydrostatic bearings for machine tools and similar applications) only use some basic parameters of the hydrostatic bearing systems, such as the radial clearance, the dimensions of the shaft and the pocket, the viscosity of the lubricant, the rotational speed, the supply pressure, the density of the oil, the specific heat capacity of the oil, etc., and some advanced parameters were not included into the calculation process, such as centripetal acceleration when one bearing surface is rotated in a very high speed for an externally pressurized thrust bearing (Srinivasan, 2013a).

All the equations were based on the assumption that all the flow within the hydrostatic bearing systems is laminar, so some complex static and dynamic conditions inside the bearing systems during the operational process were not been analysed in the initial review report. All the typical parameters of the hydrostatic system, such as outflow resistance, inflow resistance, ultimate load capacity, radial stiffness, flow, pumping power, frictional power, and

temperature rise, were calculated without a velocity dependency. The geometry of the hydrostatic bearing pockets and their restrictors were optimized by using the time continuous pressure distribution at the bearing pocket, the laminar flow behaviour and the constant velocity of the bearing (Srinivasan, 2013a). The dynamic effects of the flow at high velocities within the pockets and the space between the shaft and the bearing were not considered.

The best hydrostatic bearing design has higher load capacity, higher stiffness, lower flow rate, lower energy consumption, and lower manufacturing cost. In the next step, hydrostatic bearings experiments will probably be designed to real-time monitor the pocket pressure, flow rate, temperature change of the system.

The environmental conditions, such as temperature of the environment, dust and dirt in the surrounding air, moisture and corrosive conditions, can also affect a bearing's performance adversely. Both mechanical and environmental factors may affect the choice of a bearing and its performance. The more complex the system is, the more important it is to consider all of its real operational conditions, and then select the most suitable bearing type and its features as well the proper lubricant type (Srinivasan, 2013b).

APPENDICES

Appendix A THE CODES FOR AUTOMATIC CALCULATION EXCEL SPREADSHEET

A.1 CODES FOR HYDROSTATIC JOURNAL BEARINGS

Table A-1 Codes for hydrostatic journal bearings

Parameters	Codes to calculate the parameters
Number of pockets: n =	=B3
Diameter of bearing: d_B =	=B4
Length of bearing: L_B =	=B5
Width of axial land: c_a =	=B6
Width of circumferential land: c_c =	=B7
Radial clearance: $h_{L(av)}$ =	=B8
Depth of pocket: h_p =	=B9
Supply Pressure: p_1 =	=B10
Rotational speed: N_d =	=B11
Resistance ratio: ξ =	=B12
Viscosity of oil: η =	=B13
Density of oil: ρ =	=B14
Specific Heat capacity of oil: C_m =	=B15
Constant: k =	=1-4*B8/B9
Bearing shape factor: Φ =	=B5/(3.14*B4/4)
Bearing shape factor: E_a =	=(B5-2*B7)/B5
Bearing shape factor: E_c =	=1-B6/(3.14*B4/4)
Outflow resistance: R_{od} =	=0.75*B3*B13*B17*(1-B18)/B8/B8/B8/POWER(10,8)
Inflow resistance: R_i =	=B20*B12 =1.47*B12*B17*(1-B19)*(1+B18)*B10*B4*B4/(B12*(B12+0.4)*B17*B17*B18*(1-B18)+0.642*(B12+0.207)*(B12+6.02)*(1-B19))
Ultimate load capacity: W_u =	
Radial stiffness: S_l =	=1.5*B12*B17*(1+B18)*B10*B4*B4/(B8*(1+B12)*(1+B12)*(1+(0.5*B12*B17*B17*B18*(1

	$-B18)/((1+B12)*(1-B19)))/POWER(10,8)$
Flow: Q=	$=1.33*B10*B8*B8*B8/(B13*B17*(1+B12)*(1-B18))*POWER(10,6)$
Pumping power: $P_p=$	$=1.33*B10*B10*B8*B8*B8/(B17*B13*(1+B12)*(1-B18))$
Frictional power: $P_f=$	$=0.00677*B17*B13*POWER(B4,4)*POWER(B11,2)*(1-B16*B18*B19)*(1+0.25*B16*B18*(1-B19)*(B3-4)/(1-B16*B18*B19))/B8$
Temperature rise: $\Delta t \approx$	$=(B10+B26/(B24*POWER(10,-6)))/(B14*B15)$

A.2 CODES FOR HYDROSTATIC THRUST BEARINGS

Table A-2 Codes for hydrostatic thrust bearings

Parameters	Codes to calculate the parameters
Outer diameter of thrust pad: D_B	=B3
Outer diameter of annular pocket: D_P	=B4
Inner diameter of annular pocket: d_P	=B5
Inner diameter of thrust pad: d_B	=B6
Clearance at the lands of each thrust pad at no load: h_d	=B7
Clearance at the pocket: h_p	=B8
Supply pressure: p_1	=B9
Speed of rotation: n	=B10
Resistance ratio: ξ	=B11
Viscosity of the fluid: η	=B12
Density of oil: ρ	=B13
Specific Heat capacity of oil: C_m	=B14
Ratio ξ_2/ξ_1 for a pair of opposed plane pads or rotary thrust bearings: Ξ	=B16
Ratio A_{v2}/A_{v1} for a pair of opposed plane pads or rotary thrust bearings: T	=B17
Virtual area of the thrust pad: $A_{v2}=A_{v1}$	$=3.14*(B3*B3-B4*B4)/LN(B3/B4)/8-3.14*(B5*B5-B6*B6)/LN(B5/B6)/8$
$R_{o(1)}$	$=6*B12*LN(B3/B4)/3.14/B7/B7/B7*POWER(10,-10)$
$R_{o(2)}$	$=6*B12*LN(B5/B6)/3.14/B7/B7/B7*POWER(10,-10)$
Outflow resistance: $R_{o(net)}$	$=B20*B21/(B20+B21)$
Inflow resistance: R_i	$=B11*B22$
Ultimate thrust capacity: $T_{(net)}$	$=B9*POWER(10,6)*B19*(1-B17/(1+8*B16*B11))$
Stiffness: S_T (when $h_{(1)}=h_d$)	$=B9*POWER(10,6)*B19/B7*(3*B11/((1+B11)*(1+B11))+3*B16*B17*B11/((1+B16*B11)*$

	$(1+B16*B11))) * POWER(10,-8)$
Flow: Q=	$=B9*POWER(10,6)/(B22*POWER(10,10)*(1+B11))*POWER(10,6)$
Total Pumping power: P _p =	$=B9*POWER(10,6)*B26*POWER(10,-6)^2$
	$=2*(1.078*POWER(10,-3)*B12*B10*B10*(POWER(B3,4)-POWER(B4,4))/B7+1.078*POWER(10,-3)*B12*B10*B10*(POWER(B4,4)-POWER(B5,4))/B8+1.078*POWER(10,-3)*B12*B10*B10*(POWER(B5,4)-POWER(B6,4))/B7)$
Total Frictional power: P _f =	
Temperature rise: Δt ≈	$= (B9*POWER(10,6)+B28/(B26*POWER(10,-6)))/(B13*B14)$

Appendix B THE TABLES OF MATERIALS TO BE TURNED BY DIAMOND

B.1 THE MATERIALS READILY MACHINABLE BY DIAMOND TURNING

Table B-1 The materials readily machinable by diamond turning (Gerchman, 1986)

Plastics

- Acetal
- Acrylic
- Nylon
- Polycarbonate
- Polypropylene
- Polystyrene
- Zeonex

Metals

- Aluminum and aluminium alloys
- Brass
- Copper
- Gold
- Electroless nickel plating on other materials
- Silver
- Tin
- Zinc

Infrared crystals

- Cadmium sulfide
 - Cadmium telluride
 - Calcium fluoride
 - Cesium iodide
 - Gallium arsenide
 - Germanium
 - Lithium niobate
 - Potassium bromide
 - Potassium dihydrogen phosphate (KDP)
 - Silicon
 - Sodium chloride
 - Tellurium dioxide
 - Zinc selenide
 - Zinc sulfide
-

B.2 THE MATERIALS NOT READILY MACHINABLE BY DIAMOND TURNING

Table B-2 The materials not readily machinable by diamond turning (Gerchman, 1986)

-
- Silicon-based glasses and ceramics
 - Ferrous materials (steel, iron)
 - Beryllium
 - Titanium
 - Molybdenum
 - Nickel (except for electroless nickel plating)
-

Appendix C THE SPECIFICATIONS FOR SJ100 INVERTER

Figure C-1 The specifications for HITACHI SJ100 inverter

Item		200V Class Specifications				
SJ100 inverters, 200V models	CE version	002NFE	004NFE	005NFE	007NFE	011NFE
	UL version	002NFU	004NFU	—	007NFU	—
Applicable motor size *2	kW	0.2	0.4	0.55	0.75	1.1
	HP	1/4	1/2	3/4	1	1.5
Rated capacity (kVA) *12	230V	0.6	1.0	1.1	1.5	1.9
	240V	0.6	1.0	1.2	1.6	2.0
Rated input voltage		1-phase: 200 to 240V +5/-10%, 50/60 Hz \pm 5%, 3-phase: 200 to 240V +5/-10%, 50/60 Hz \pm 5%, (037LFU, 055LFU, and 075LFU 3phase only)				
Rated input current (A)	1-phase	3.5	5.8	6.7	9.0	11.2
	3-phase	2.0	3.4	3.9	5.2	6.5
Rated output voltage *3		3-phase: 200 to 240V (corresponding to input voltage)				
Rated output current (A)		1.6	2.6	3.0	4.0	5.0
Efficiency at 100% rated output (%)		90.5	92.8	93.6	94.1	95.4
Watt loss, approximate (W)	at 70% output	15	21	25	31	38
	at 100% output	19	29	32	41	51
Starting torque *6		200% or more				
Dynamic braking approx. % torque, short time stop *7	without resistor, from 50 / 60 Hz	100%: \leq 50Hz 50%: \leq 60Hz			70%: \leq 50Hz 50%: \leq 60Hz	
	with resistor	150%				
DC braking		Variable operating frequency, time, and braking force				
Weight	kg	0.7	0.85	0.85	1.3	1.3
	lb	1.54	1.87	1.87	2.87	2.87

Appendix D THE SPECIFICATIONS FOR ABB M2AA 090 L-4 MOTOR

Figure D-1 The specifications for the ABB M2AA 090 L-4 motor

General purpose aluminum motors Technical data for totally enclosed squirrel cage three phase motors



IP 55 – IC 411 – Insulation class F, temperature rise class B

Output kW	Motor type	Product code	Speed r/min	Efficiency		Power factor cos φ	Current		Torque			
				Full load 100%	3/4 load 75%		I_N	I_s	T_N	T_s	T_{max}	
			400 V 50 Hz				Basic design					
0.09	M2VA 56 A	3GVA 051 001-***A	2820	59.8	53.3	0.69	0.32	3.9	0.31	2.9	2.7	
0.12	M2VA 56 B	3GVA 051 002-***A	2840	67.2	63.8	0.64	0.41	4.1	0.41	3.2	2.8	
0.18	M2VA 63 A	3GVA 061 001-***C	2820	73.7	70.6	0.64	0.56	4.2	0.62	3.5	3.1	
0.25	M2VA 63 B	3GVA 061 002-***C	2810	77.5	75.8	0.71	0.66	4.5	0.87	3.6	3.3	
0.37	M2VA 71 A	3GVA 071 001-***C	2840	77.1	76.5	0.72	1	5.5	1.25	3.8	3.9	
0.55	M2VA 71 B	3GVA 071 002-***C	2830	79.2	78.2	0.76	1.35	5.7	1.86	3.6	3.7	
0.75	M2VA 80 A	3GVA 081 001-***B	2870	81.2	79.3	0.75	1.8	6.2	2.49	2.9	3.6	
1.1	M2VA 80 B	3GVA 081 002-***B	2850	81.4	79.5	0.78	2.5	6.1	3.69	2.3	3.5	
1.5	M2AA 90 S	3GAA 091 001-***E	2870	80.1	76.2	0.82	3.35	5.5	5	2.4	3.0	
2.2	M2AA 90 L	3GAA 091 002-***E	2885	83.6	83.9	0.87	4.37	6.0	7.5	2.5	3.0	
3	M2AA 100 L	3GAA 101 001-***E	2900	86.0	84.1	0.88	5.95	7.5	10	2.7	3.6	
4	M2AA 112 M	3GAA 111 001-***A	2850	86.0	86.0	0.91	7.4	7.5	13.4	2.8	3.0	
5.5	M2AA 132 SA	3GAA 131 001-***A	2855	86.0	86.0	0.88	10.5	6.8	18.3	2.7	3.5	
7.5	M2AA 132 SB	3GAA 131 002-***A	2855	87.0	87.0	0.90	13.9	7.2	25	3.2	3.8	
11	¹⁾ M2AA 160 MA	3GAA 161 111-***A	2915	88.4	88.9	0.89	20.5	6.2	36	2.1	2.5	
15	¹⁾ M2AA 160 M	3GAA 161 112-***A	2900	89.5	89.9	0.90	27	6.1	49.4	2.4	2.6	
18.5	¹⁾ M2AA 160 L	3GAA 161 113-***A	2915	90.2	90.5	0.91	32.5	6.8	61	2.6	3.0	
22	¹⁾ M2AA 180 M	3GAA 181 111-***A	2925	91.2	91.3	0.89	39	7.9	72	2.8	3.2	
30	¹⁾ M2AA 200 LA	3GAA 201 011-***A	2945	92.0	92.0	0.88	53	7.9	97	3.0	3.7	
37	¹⁾²⁾ M2AA 200 L	3GAA 201 012-***A	2945	92.8	92.9	0.89	65	8.2	120	3.1	3.6	
45	M2AA 225 M	3GAA 221 011-***A	2940	93.0	93.0	0.88	80	7.7	146	2.8	3.0	
55	¹⁾ M2AA 250 M	3GAA 251 011-***A	2960	93.5	93.8	0.90	95	7.3	177	2.8	3.0	

¹⁾Temperature rise class F for 380 V 50 Hz.

²⁾Temperature rise class F for 415 V 50 Hz.

The bullets in the product code indicate choice of mounting arrangement, voltage and frequency, generation code (see ordering information page).

Appendix E THE SPECIFICATIONS FOR MILLIMAR 1200 IC COMPACT AMPLIFIER

Figure E-1 The specifications for Millimar 1200 IC compact amplifier

Millimar 1200 IC compact amplifier
M



1200 IC/MZ

IP40

Features

- Compact housing
- Battery powered for portable usage in the workshop
- Large analog display with 2 tolerance markers
- Quick and reliable display of the measured value
- Switchable measuring direction
- One inductive probe can be connected
- Fine adjustment due to the large range zero setter
- Battery operation with the commercially available round R14 batteries
- Testing button for batteries
- Supplied with: Mains adapter
- Used with "Mahr" - M type Inductive Probes.

Technical Data

	1200 IC	1200 IC/MZ
Measuring range	± 3 µm / 0.1 µm	± .0001" / .000002"
Resolution	± 10 µm / 0.2 µm ± 30 µm / 1 µm ± 100 µm / 2 µm ± 300 µm / 10 µm	± .0003" / .00001" ± .001" / .00002" ± .003" / .0001" ± .01" / .0002"
Scale length		120 mm / 4.724"
Response time		350 ms
Probe input		1
Single meas. combinations		+A, -A
Range of zero adjustment: 5 and 100 µm		1 Large range setter
Deviation spread referring to measuring range		≤ 2.5%
Protection class acc. to DIN		IP40
Working temperature range		+ 10... + 40° C / + 50... + 104° F
Power supply		mains adapter, 9V = -5 VA
Power consumption		approx. 0.1 W
Dimensions		137 x 157 x 80 mm / 5.394" x 6.181" x 3.149"
Weight		1 kg / 2.205 lbs
Order no.	5312000	5312009

Accessories

	Order-no.
Battery , R 14 battery 1.5 V, (6 are required)	3004424
Mains Adapter 100-240V~, 50-60Hz	3017926*

Not for use with EHE or Pantograph style gage heads
For appropriate Inductive probes please [click here](#)

* Included in scope of supply

Appendix F THE SPECIFICATIONS FOR NI 9217 RTD ANALOG INPUT C SERIES MODULE

The following specifications are typical for the range -40°C to 70°C unless otherwise noted. All voltages are relative to COM unless otherwise noted.

All specifications given in $^{\circ}\text{C}$ are specific to 100Ω platinum RTDs.

Input Characteristics

Table F-1 The specifications for NI 9217 RTD Analog input C series module

Number of channels	4 Analog input channels
ADC resolution	24 bits
Type of ADC	Delta-sigma
Sampling mode	Scanned
Measurement range	
Temperature	-200 to 850°C
Resistance	0 to 400Ω
Common-mode range	
COM-to-earth ground	$\pm 250 V_{\text{rms}}$
Channel-to-COM	50 mV
Conversion time	
High-resolution mode	200 ms per channel 800 ms total for all channels
High-speed mode	2.5 ms per channel 10 ms total for all channels
Noise	
High-resolution mode	0.003 $^{\circ}\text{C}$
High-speed mode	0.02 $^{\circ}\text{C}$
Excitation current	1 mA per channel
Noise rejection	
Normal mode (50/60 Hz)	
High-resolution mode	85 dB min
High-speed mode	None

Temperature accuracy (including noise), 4-wire mode

Measured Value	Typical (25 °C)	Maximum (–40 to 70 °C)
-200 to 150 °C	0.15 °C	0.35 °C
150 to 850 °C	0.20 °C	1.0 °C

Temperature accuracy (including noise), 3-wire mode

Measured Value	Typical (25 °C)	Maximum (–40 to 70 °C)
-200 to 150 °C	0.20 °C	0.50 °C
150 to 850 °C	0.30 °C	1.0 °C

Appendix G THE SPECIFICATIONS FOR HAAKE PHOENIX II SYSTEMS

Figure G-1 Specifications for HAAKE Phoenix II systems

Specifications and Accessories

Cryostats



Optional accessories	Order-No.
Universal hose nozzle for tubing of 3 to 6 mm i. Ø	001-3718
Reservoir drain valve	333-0499
Trolley for P1-C75P, P2-C75P	333-0678
External analog box	333-0685
230V Power supply for analog box	333-0705
Software ThermStar95plus	091-2950
Pt100 sensors TT	333-0429
Pt100 sensors ST	333-0428
Pt100 sensors HT	333-0423
Additional heater for C75P	333-0741
Additional heater for CT90L/W	333-0745
Additional heater for CT50L/W	333-0749
Additional pump	333-0746

Technical specification acc. to DIN 12876		P1-C75P	P2-C75P	P2-CT80L	P2-CT50L	P2-CT50W	P2-CT90L	P2-CT90W	
Working temperature range	°C	-75..100	-75..100	-80..100	-50..100	-50..100	-90..100	-90..100	
Temperature accuracy	+/-K	0.02	0.02	0.1	0.1	0.1	0.1	0.1	
Heater capacity	kW	1.0	1.0	1.0	2.0	3.0	2.0	2.0	
Cooling	at 20°C / 0°C	W	280/220	280/220	800/750	2500/1750	5000/3000	1650/1500	1900/1700
	at -20°C / -40°C	W	180/130	18 /130	700/600	1100/300	1900/800	1300/1150	1500/1300
	at -60°C / -80°C	W	50/-	50/-	500/50	-	-	600/170	700/200
Pump: Pressure / Flow rate max.	mbar/l/	560/24	560/24	560/24	560/24	560/24	560/24	560/24	
	min	380/22	380/22	380/22	380/22	380/22	380/22	380/22	
Bath opening: WxLxD	cm	13x10x20	13x10x20	22x14x20	22x27x20	22x27x20	22x15x20	22x15x20	
Bath volume	l	6	6	12	24	24	15	15	
Overall dimensions: WxLxH	cm	40x51x77	40x51x77	42x66x102	50x75x109	50x75x109	50x90x109	50x90x109	
Net weight	kg	68	68	107	125	180	190	185	
Total wattage	VA	2500	2500	2500	3300	5800	5300	5300	
Order-No. for 230V / 50Hz for 220V / 60Hz for 380V / 3Ph / 50Hz for 220V / 3Ph / 60Hz		440-0751	441-0751	441-0801	-	-	-	-	
		440-0759	441-0759	441-0809	-	-	-	-	
		-	-	-	446-0503	447-0503	448-0903	449-0903	
		-	-	-	446-0504	447-0504	448-0904	449-0904	

HAAKE Phoenix II P2 circulators are also available with a Profibus interface on special request. Please do not forget to order the correct hoses and bath liquids for your external application.

Appendix H THE SPECIFICATIONS FOR LEMO FGG.00 TEMPERATURE MEASURING CONNECTOR

Table H-1 The specifications for LEMO FGG.00 temperature measuring connector

Manufacturer	LEMO
Product Category	B-Series Plugs and Receptacles
Product Type	Connectors
Series	00
Shell Style	Plug
Number of Contacts	4
Mounting Style	Cable
Termination Style	Solder
Current Rating	2 A
Brand	LEMO
Contact Plating	Copper, Nickel, Gold
Shell Plating	Chrome
Factory Pack Quantity	150
Voltage Rating	700

Appendix I THE SPECIFICATIONS FOR TAYLOR-HOBSON FORM TALYSURF-120L

Table I-1 The specifications for Taylor-Hobson form Talysurf-120L

Traverse Length	120mm
Traverse Speed	10mm/sec maximum
Measuring Speeds	1mm and 0.5mm/sec $\pm 5\%$
Return Speed	up to 5mm/sec
Gauge Type	Phase Grating Interferometer, 1mN force nominal
Measuring Range	10mm
Resolution	12.8nm @ 10mm range
Range to Resolution Ratio	780,000:1
Straightness Accuracy	0.5 μ m over 120mm traverse 0.2 μ m over any 20mm traverse
Data Resolution	0.25 μ m
Dimensions (LxDxH)	396 x 127 x 195mm
Weight	11.5kg

REFERENCE

- "Hydrostatic bearing design : J. P. O'Donoghue and W. B. Rowe, *Tribology*, 2 (1) (1969) 25–71; 68 figs., 4 tables, 10 refs.", (1969), *Wear*, vol. 13, no. 2, pp. 137.
- "Electroless nickle composite coatings", (1997), *Metal Finishing*, vol. 95, no. 3, pp. 26.
- Benga, G. C. and Abrao, A. M. (2003), "Turning of hardened 100Cr6 bearing steel with ceramic and PCBN cutting tools", *Journal of Materials Processing Technology*, vol. 143–144, no. 0, pp. 237-241.
- Chen, D., Bonis, M., Zhang, F. and Dong, S. (2011), "Thermal error of a hydrostatic spindle", *Precision Engineering*, vol. 35, no. 3, pp. 512-520.
- Chen, D., Fan, J. and Zhang, F. (2012), "Dynamic and static characteristics of a hydrostatic spindle for machine tools", *Journal of Manufacturing Systems*, vol. 31, no. 1, pp. 26-33.
- Cheng, F., Jiang, S. and Liang, J. (2013), "Cavitation erosion resistance of microarc oxidation coating on aluminium alloy", *Applied Surface Science*, vol. 280, no. 0, pp. 287-296.
- Cheng, K. and Rowe, W. B. (1995), "A selection strategy for the design of externally pressurized journal bearings", *Tribology International*, vol. 28, no. 7, pp. 465-474.
- Cheng, K. and Shore, P. (2010), "Special issue on design of ultraprecision and micro machine tools and their key enabling technologies", *International Journal of Machine Tools and Manufacture*, vol. 50, no. 4, pp. 309.
- De Pellegrin, D. V. and Hargreaves, D. J. (2012), "An isoviscous, isothermal model investigating the influence of hydrostatic recesses on a spring-supported tilting pad thrust bearing", *Tribology International*, vol. 51, no. 0, pp. 25-35.
- Dumbrava, M. A. (1985), "Review of principles and methods applied to the optimum calculation and design of externally-pressurized bearings: Part 1: Low/moderate speed bearings", *Tribology International*, vol. 18, no. 3, pp. 149-156.
- El-Sherbiny, M., Salem, F. and El-Hefnawy, N. (1984a), "Optimum design of hydrostatic journal bearings Part I: Maximum load capacity", *Tribology International*, vol. 17, no. 3, pp. 155-161.

- El-Sherbiny, M., Salem, F. and El-Hefnawy, N. (1984b), "Optimum design of hydrostatic journal bearings Part II. Minimum power", *Tribology International*, vol. 17, no. 3, pp. 162-166.
- Evans, C. and Bryan, J. B. (1991), "Cryogenic Diamond Turning of Stainless Steel", *CIRP Annals - Manufacturing Technology*, vol. 40, no. 1, pp. 571-575.
- Forman, B. R., Gilles, H. L. and Faul, M. (2000), "Thermally induced bond failure of electroless nickel/IVD aluminum coatings deposited on steel", *Surface and Coatings Technology*, vol. 123, no. 2–3, pp. 106-111.
- Gerchman, M. C. (1986), "SPECIFICATIONS AND MANUFACTURING CONSIDERATIONS OF DIAMOND MACHINED OPTICAL COMPONENTS.", *Proceedings of SPIE - The International Society for Optical Engineering*, Vol. 607, pp. 36.
- Gu, L., Chen, X., Fan, X., Liu, Y., Zou, B., Wang, Y. and Cao, X. (2011), "Improvement of thermal shock resistance for thermal barrier coating on aluminum alloy with various electroless interlayers", *Surface and Coatings Technology*, vol. 206, no. 1, pp. 29-36.
- Guo, Y. B. and Yen, D. W. (2004), "Hard turning versus grinding—the effect of process-induced residual stress on rolling contact", *Wear*, vol. 256, no. 3–4, pp. 393-399.
- Ha, T., Lee, Y. and Kim, C. (2002), "Leakage and rotordynamic analysis of a high pressure floating ring seal in the turbo pump unit of a liquid rocket engine", *Tribology International*, vol. 35, no. 3, pp. 153-161.
- HINO, M., MURAKAMI, K., MITOOKA, Y., MURAOKA, K. and KANADANI, T. (2009), "Effects of zincate treatment on adhesion of electroless Ni-P coating onto various aluminum alloys", *Transactions of Nonferrous Metals Society of China*, vol. 19, no. 4, pp. 814-818.
- Kagnaya, T., Lambert, L., Lazard, M., Boher, C. and Cutard, T. (2014), "Investigation and FEA-based simulation of tool wear geometry and metal oxide effect on cutting process variables", *Simulation Modelling Practice and Theory*, vol. 42, no. 0, pp. 84-97.
- Kazama, T. and Yamaguchi, A. (1993), "Optimum design of bearing and seal parts for hydraulic equipment", *Wear*, vol. 161, no. 1–2, pp. 161-171.
- Kher, A. K. and Cowley, A. (1970), "An experimental investigation into the temperature effects in hydrostatic journal bearings", *Tribology*, vol. 3, no. 3, pp. 165-167.

- König, W., Berktold, A. and Koch, K. -. (1993), "Turning versus Grinding – A Comparison of Surface Integrity Aspects and Attainable Accuracies", *CIRP Annals - Manufacturing Technology*, vol. 42, no. 1, pp. 39-43.
- Lebeck, A. O. (1988), "Contacting mechanical seal design using a simplified hydrostatic model", *Tribology International*, vol. 21, no. 1, pp. 2-14.
- Loxham, J. and Hemp, J. (1964), "The application of hydrostatic bearings to high precision machine tools", *Production Engineer*, vol. 43, no. 11, pp. 556-568.
- Manojkumar, P. A., Gandhi, A. S., Kamaraj, M. and Tyagi, A. K. (2014), "Sliding wear behaviour of alumina coatings prepared from mechanically milled powders", *Wear*, vol. 313, no. 1–2, pp. 11-18.
- Martin, J. K. (2004a), "Measured stiffness and displacement coefficients of a stationary rotor hydrostatic bearing", *Tribology International*, vol. 37, no. 10, pp. 809-816.
- Martin, J. K. (2004b), "Measured stiffness and displacement coefficients of a stationary rotor hydrostatic bearing", *Tribology International*, vol. 37, no. 10, pp. 809-816.
- Mayr, J., Jedrzejewski, J., Uhlmann, E., Alkan Donmez, M., Knapp, W., Härtig, F., Wendt, K., Moriwaki, T., Shore, P., Schmitt, R., Brecher, C., Würz, T. and Wegener, K. (2012), "Thermal issues in machine tools", *CIRP Annals - Manufacturing Technology*, vol. 61, no. 2, pp. 771-791.
- Mekid, S. (2000), "High precision linear slide. Part I: design and construction", *International Journal of Machine Tools and Manufacture*, vol. 40, no. 7, pp. 1039-1050.
- Moore, H. D. (1969), "Lubricating grease: Laboratory tests and their significance", *Tribology*, vol. 2, no. 1, pp. 11-17.
- O'Donoghue, J. P. and Rowe, W. B. (1968), "Hydrostatic journal bearing (exact procedure)", *Tribology*, vol. 1, no. 4, pp. 230-236.
- Osman, T. A., Safar, Z. S. and Mokhtar, M. O. A. (1991), "Design of annular recess hydrostatic thrust bearing under dynamic loading", *Tribology International*, vol. 24, no. 3, pp. 137-141.
- Poli, M. (1975), "Dynamic behaviour of externally pressurized hydrostatic pads fed by throttling valves", *Wear*, vol. 31, no. 2, pp. 193-211.
- Prabhu, T. J. and Ganesan, N. (1984), "Finite element application to the study of hydrostatic thrust bearings", *Wear*, vol. 97, no. 2, pp. 139-154.

- Rowe, W. B. and Stout, K. J. (1972), "Viscosity variation in hydrostatic bearings", *Tribology*, vol. 5, no. 6, pp. 262-264.
- Rudnik, E. and Jucha, T. (2013), "Electroless and electrolytic deposition of Co–SiC composite coatings on aluminum", *Surface and Coatings Technology*, vol. 232, no. 0, pp. 389-395.
- Safar, Z. S. (1980), "Performance characteristics for the hydrostatic thrust bearing of a saw blade", *Tribology International*, vol. 13, no. 2, pp. 79-83.
- Saxena, V., Rani, R. U. and Sharma, A. K. (2006), "Studies on ultra high solar absorber black electroless nickel coatings on aluminum alloys for space application", *Surface and Coatings Technology*, vol. 201, no. 3–4, pp. 855-862.
- SHAO, J., DAI, C., ZHANG, Y., YU, X., XU, X. and WANG, Y. (2011), "The effect of oil cavity depth on temperature field in heavy hydrostatic thrust bearing", *Journal of Hydrodynamics, Ser.B*, vol. 23, no. 5, pp. 676-680.
- Sharma, S. C., Jain, S. C. and Bharuka, D. K. (2002), "Influence of recess shape on the performance of a capillary compensated circular thrust pad hydrostatic bearing", *Tribology International*, vol. 35, no. 6, pp. 347-356.
- Silva Mamede, N. F., Pinho Ramos, A. and Faria, D. M. V. (2013), "Experimental and parametric 3D nonlinear finite element analysis on punching of flat slabs with orthogonal reinforcement", *Engineering Structures*, vol. 48, no. 0, pp. 442-457.
- Sinhasan, R., Sharma, S. C. and Jain, S. C. (1989), "Performance characteristics of an externally pressurized capillary-compensated flexible journal bearing", *Tribology International*, vol. 22, no. 4, pp. 283-293.
- Sood, R., Guo, C. and Malkin, S. (2000), "Turning of Hardened Steels", *Journal of Manufacturing Processes*, vol. 2, no. 3, pp. 187-193.
- Srinivasan, V. (2013a), "Analysis of Dynamic Load Characteristics on Hydrostatic Bearing with Variable Viscosity and Temperature using Simulation Technique", *Indian Journal of Science and Technology*, vol. 6, no. 6, pp. 4797-4803.
- Srinivasan, V. (2013b), "Analysis of Static and Dynamic Load on Hydrostatic Bearing with Variable Viscosity and Pressure", *Indian Journal of Science and Technology*, vol. 6, no. 6.
- Stansfield, F. M. (1970), *Hydrostatic bearings for machine tools and similar applications*, Machinery Publishing.

Sudagar, J., Lian, J. and Sha, W. (2013), "Electroless nickel, alloy, composite and nano coatings – A critical review", *Journal of Alloys and Compounds*, vol. 571, no. 0, pp. 183-204.

ZHANG, Y., FAN, L., LI, R., DAI, C. and YU, X. (2013), "Simulation and experimental analysis of supporting characteristics of multiple oil pad hydrostatic bearing disk", *Journal of Hydrodynamics, Ser.B*, vol. 25, no. 2, pp. 236-241.